LITHIUM-7 PROBLEM IN SOLAR-LIKE STARS

WAN AISHAH BT WAN HARUN

FACULTY OF SCIENCE
UNIVERSITI MALAYA
KUALA LUMPUR

2022

LITHIUM-7 PROBLEM IN SOLAR-LIKE STARS

WAN AISHAH BT WAN HARUN

DISSERTATION SUBMITTED IN FULFILMENT OF THE REQUIREMENTS FOR THE DEGREE OF MASTER OF SCIENCE

DEPARTMENT OF PHYSICS
FACULTY OF SCIENCE
UNIVERSITI MALAYA
KUALA LUMPUR

2022

UNIVERSITI MALAYA

ORIGINAL LITERARY WORK DECLARATION

Name of Candidate: **WAN AISHAH BT WAN HARUN**

Registration/Matric No.:**17043034/1**

Name of Degree: **MASTER OF SCIENCE**

Title of Project Dissertation ("this Work"):

LITHIUM-7 PROBLEM IN SOLAR-LIKE STARS

Field of Study:

THEORETICAL PHYSICS

I do solemnly and sincerely declare that:

(1) I am the sole author/writer of this Work;
(2) This work is original;
(3) Any use of any work in which copyright exists was done by way of fair dealing and for permitted purposes and any excerpt or extract from, or reference to or reproduction of any copyright work has been disclosed expressly and sufficiently and the title of the Work and its authorship have been acknowledged in this Work;
(4) I do not have any actual knowledge nor do I ought reasonably to know that the making of this work constitutes an infringement of any copyright work;
(5) I hereby assign all and every rights in the copyright to this Work to the University of Malaya ("UM"), who henceforth shall be owner of the copyright in this Work and that any reproduction or use in any form or by any means whatsoever is prohibited without the written consent of UM having been first had and obtained;
(6) I am fully aware that if in the course of making this Work I have infringed any copyright whether intentionally or otherwise, I may be subject to legal action or any other action as may be determined by UM.

Date: 22/3/2022

Candidate's Signature

Subscribed and solemnly declared before,

Witness's Signature Date: 22/3/2022

Name:
Designation:

LITHIUM-7 PROBLEM IN SOLAR-LIKE STARS

ABSTRACT

Although ^{7}Li is a stable isotope, the element is fragile to an extreme temperature higher than 10^{6} K. Therefore, ^{7}Li content in a star can only survive in the region of the convection zone, where it can be observed by using high-resolution spectral line analysis. However, many theoretical predictions have shown that lithium abundance in the Sun should be higher by 2 dex than the observed photospheric value. Other similar missing lithium is found in some stars, which contributes to the lithium problem in general. Therefore, this thesis aims to analyze the mechanisms that may lead to the higher mixing of lithium burning. We first calibrate the solar model by using MESA code to implement past solutions suggested from the literature. We verified that the existing solutions are indeed failed to explain the discrepancy. Hence, we enhanced the convection mixing process to induce more lithium burning of the surface. The computation showed that the higher convection parameter α = 2.4 could effectively deplete another one dex of lithium. While the increase by a factor three of the gravitational settling, can only enhance the lithium by 0.1 dex. Interestingly, we successfully reproduced the observed lithium content when we had adopted a higher rotational velocity kick-off of 46 km/s. However, the result is ambiguous as we can not explain how the initially applied rotation can be spun down to the present solar rate. We found that lithium mixing below the convection base is highly dependent on the opacity of the solar mixture. Finally, we had predetermined the initial lithium abundance at ZAMS to be 1.42 dex in which can represent today's photospheric lithium value.

Keywords: Lithium problem, convection, gravitational settling, MESA, rotation.

MASALAH LITHIUM-7 PADA BINTANG SEPERTI MATAHARI

ABSTRAK

Isotop ^{7}Li ialah unsur yang stabil tetapi mudah terbakar pada suhu yang lebih tinggi dari 10^{6} kelvin. Maka, kandungan ^{7}Li ini hanya didapati di kawasan perolakan permukaan bintang dan boleh dicerap melalui kaedah analisis garis spektra beresolusi tinggi. Namun, kebanyakan ramalan teori memberi kandungan ^{7}Li matahari adalah 2 dex lebih tinggi dari nilai fotosfera yang dicerap. Masalah kekurangan ^{7}Li ini juga telah didapati pada bintang-bintang lain dan akhirnya mewujudkan satu masalah yang umum. Maka, tesis ini bertujuan untuk membuat analisa mekanisma yang dapat mendorong peningkatan percampuran pembakaran lithium tersebut. Awalnya, kami membina model seakan matahari menggunakan kod evolusi MESA bagi mengadaptasi semula cadangan penyelesaian lepas dari sastera. Kami mengesahkan cadangan lepas tidak berupaya menerangkan perbezaan kandungan ^{7}Li ini. Maka, kami telah meningkatkan proses percampuran perolakan yang berlaku di dalam bintang bagi mendorong kenaikan pembakaran lithium yang berada di permukaan. Hasil komputasi menunjukkan parameter perolakan lebih tinggi, α = 2.4 boleh mengurangkan kandungan ^{7}Li sebanyak 1 dex. Manakala, hanya 0.1 dex yang berjaya dikurangkan sekiranya kami mengenakan tiga kali kenaikan pengendapan graviti. Yang menariknya, kami berjaya menghasilkan semula kandungan lithium tercerap apabila menggunakan nilai putaran kelajuan awal yang lebih tinggi iaitu 46 km/s. Tetapi, keputusan ini adalah taksa kerana tidak boleh menerangkan bagaimana putaran awal boleh dikurangkan ke nilai kadar matahari sekarang. Hasil kajian juga mendapati bahawa kandungan percampuran lithium di bawah tapak perolakan berkadar terus dengan kelegapan campuran matahari. Akhirnya kami menemukan kandungan awal lithium di ZAMS adalah 1.42 dex bagi mewakili nilai fotosfera.

ACKNOWLEDGEMENTS

First, I would like to thank my thesis advisor Prof Hasan Abu Karim, from the science faculty, Universiti Malaya. The door to Professor Hasan's office was always open whenever I was struggling with my research project or had a question about my research or writing. He was the one who initially steered me in the direction of stellar evolution theory when I originally wanted to pursue general astronomy. This has caused a significant shift in my field of study and enlightened my perspective on theoretical astrophysics. I would also like to acknowledge Dr. Norhazlisa, my co-advisor from the same faculty of Universiti Malaya. She also helped me understand my field by sharing her wisdom and knowledge in stellar evolution and nuclear physics. Both of them were there when I needed them and greatly supported me whenever I felt hopeless and sometimes off-track during my project. For that, I can not be more than thankful to Allah for blessing me with two passionate advisors. I express my gratitude towards the Department of Physics and the Universiti Malaya for giving me the space and opportunity to learn here compassionately. A special thanks to my family. I must express my profound gratitude to my parents, who have raised me to believe that a core principle in life is never to stop acquiring knowledge. Working full-time as a teacher, being a mother, and learning is a struggle to juggle. Hence to my dear husband, Mr. Zulhilmi Fadzil, I am gratefully indebted to all sacrifices you have made so that I can finish my degree. Your love and support for me were what sustained me thus far. To my beloved son, YahyaAyyash, I would like to thank you for just being there with so much love and hugs. To my dear parents Mrs. Fathiah and Mr. Wan Harun. May Allah grant you love, good health, and always in His blessing. The pillar and the strength of my life. May Allah protect you and bless you with His gift, love, good health, and happiness forever.

TABLE OF CONTENTS

LIST OF FIGURES

LIST OF TABLES

LIST OF SYMBOLS AND ABBREVIATIONS

∇_{ad} : Adiabatic temperature gradient

γ : Adiabatic index

X_i : Abundance for species i

u : Cell-centered velocity

Ω_{crit} : Critical angular velocity

f_{ov} : Convective overshoot parameter

w_i : Convection velocity

$D_{coefficient}$: Coefficient of diffusion mixing

$T_{\rm eff}$: Effective temperature

$\rm F_i$: Flux across cell face i

$\alpha_{\rm mlt}$: Mixing length of MLT

β : Gas pressure

Z : Metal mass fraction

l : Mixing length

Y : Helium mass fraction

X : Hydrogen mass fraction

δt : Numerical time step

$H_{\rm p}$: Pressure scale height

M_i : Stellar mass

$M_\odot$: Solar mass

Ω_{sur} : Surface angular velocity

v : Linear velocity

$L_\odot$: Solar Luminosity

$[Z/H]$: Metallicity

LIST OF SYMBOLS AND ABBREVIATIONS

L_n : Radiant power emitted by nuclear burning

∇_{rad} : Radiative temperature gradient

R_{cz} : Radius of convection zone

$R_\odot$: Solar radius

$\tau_\odot$: Solar age (4.57x10^9 Year)

BBNS : Big Bang Nucleosynthesis

D_{DSI} : Coefficient of Dynamical Shear Instability

D_{SHI} : Coefficient of Solberg-Hoil Instability

D_{SSI} : Coefficient of Secular Shear Instability

D_{ECS} : Coefficient of Sweet circulation Instability

D_{GSF} : Coefficient of Goldreich-Schubert-Fricke

EOS : Equation Of State

GCR : Galactic Cosmic Ray

ISM : Interstellar Medium

Rot. : Rotational

Diff. : Diffusion

MS : Main Sequence

PP Chain : Proton-Proton Chain

PMS : Pre-Main Sequence

SSM : Standard Solar Model

NSSM : Non-Standard Solar Model

TAMS : Terminal-Age Main Sequence

ZAMS : Zero-Age Main Sequence

LIST OF APPENDICES

CHAPTER 1: INTRODUCTION

In the last thirty years, the observation of surface lithium abundances in most stars has been significantly lower compared to the predicted value. However, there is no concrete solution so far to explain the issue (Asplund et al., 2009; Baraffe et al., 2017; Caballero Navarro et al., 2020; Dantona & Mazzitelli, 1984; Ghezzi et al., 2010; Pace et al., 2012; Ramirez et al., 2012; Swenson & Faulkner, 1992). It is essential to solve the discrepancy as lithium can be an excellent tracer to describe the physical processes occurring in the deep stellar interior. Therefore, this thesis aims to study the history of the lithium depletion problem and analyze the various effects of internal mixing mechanisms that can impose such a lithium destruction trend.

The detailed patterns of metallicity abundances in stars reveal traces of its enrichment over different timescale in our universe. Stars will evolve over time and enrich their core with heavier elements such as metals. Eventually, stars will die following the metal deposits for the birth of new stars and their interstellar medium. Hence, it is understood why older stars Population II and Populations III formed at early times will carry no metal or at least very low metallicity ranging [Z/H] = -3 to [Z/H] = -1 (Karlsson et al., 2013). Yet younger stars which are considered metal-rich are categorized in Population I . This initial [Z/H] constraint and some other major parameters discussed later in this thesis are crucial to how theory predicts the evolution of lithium abundance in different stars population. The source of lithium abundance is obtainable from three different mechanisms in the universe, one is originated from the Primordial Big Bang Nucleosynthesis (PBBN), the second is through spallation interaction between Galactic Cosmic Rays (GCR) with Interstellar Medium (ISM) and the last one is from the stellar nucleosynthesis via PPII branch of the proton-proton cycles (Ćiprijanović, 2016).

During Big Bang Nucleosynthesis, ^{7}Li was produced in the first few minutes of the evolution of the universe together with ^{2}H, ^{3}He, and ^{4}He, which are believed to be constituted in the early stars. However, chemical comparison between theoretical prediction and observational data are only at odd for ^{7}Li abundance. The predicted result ^{7}Li from Standard Big Bang Nucleosynthesis (SSBN) and cosmic baryon density of cosmic microwave background (CMB), is a factor of three times higher than the observed data in metal-poor- halo stars, which the so-called spite-plateau found by Spite and Spite (1981). The main speculation to explain the discrepancy is from the fact that lithium is an element that burns when it is exposed to a temperature above 10^{6} K. Hence it was postulated when a protostar with primordial abundances evolves in an increasing temperature, its convective zone also gradually rises to the stellar surface and burns most of its lithium during the process. Therefore, ^{7}Li will mostly be destroyed in the pre-main sequence (PMS) stage and a smaller amount will remain in the cooler outer layer. Nevertheless, an additional ^{7}Li abundance is continuously produced over stellar nucleosynthesis afterward when the protosolar temperature is high enough to reach nuclear fusion reaction and this protostar is transitioned to the main sequence star. It follows that this ^{7}Li abundance formed in this production including some of the ^{6}Li produced through GCR induced spallation reaction, can only survive at the base of the convection zone and above where the region is much cooler.

There are increasing number of observations made to determine photospheric lithium abundance by using optical high-resolution spectroscopy. Work by Sestito et al. (2003) had confirmed that lithium depletion occurs primarily during the PMS based on the observations of stars later than type-G of young Cluster and T Tauri Stars. Their work was verified by early works such as Swenson and Faulkner (1992) and many others. However much recent work by Ramirez et al. (2012), Cunming et al. (2012) and Balachandran et

al. (1999) have disagreed with the postulation and observational data. Ramirezs work based on the analysis of the mass-metallicity correlation particularly in HIP 13402 and HIP 30034 had shown that these young stars which were a few million years in age still contain high lithium abundance (^{7}Li > 2.8 dex) which means that their surface lithium abundance has not yet been depleted during the PMS. They proposed that the lithium depletion on the stars should take place in the internal processes during the main sequence stage or sub-giant phase. Although, they had acknowledged that they might encounter errors in determining the age of the stars to conclude such a trend. Nevertheless, both observation results are still debatable, and no more further speculations were made by both groups. Later in this thesis, further discussion on depletion at these different stages will be included in our work when models to determine stellar abundances have been established.

During the main sequence stage, the lithium problem is still a mystery in many ways. The current observations made by Sousa et al. (2011) show that the lithium abundance on the Sun's surface is 140 times way too low compared to its protosolar value. Asplund et al. (2009) also have confirmed with their work in the evaluation of solar compositions that photospheric lithium abundance is 2 dex smaller than the meteoric counterpart, A(Li) = 1.05±0.10 dex vs. A($Li_{meteorite}$) = 3.26±0.05 dex. Furthermore, the comparison made between the Sun and its virtually identical stars in the solar-age M67 cluster has shown a common problem. The fraction of 40 percent of the star members have about lithium abundance comparable to the Sun whereas the remaining fraction in the upper envelope of M67 has 10 times more lithium (Pasquini et al., 1994). Pasquini et al. (1994) suggested that the depletion is not entirely dependent on a star's age and even its stellar mass. Even the rate of lithium depletion during the main sequence stage is not decreasing consistently with the increasing age for stars and this indicates that lithium depletion is not a continuous process where it cannot just simply be described by the stars effective temperature. In

summary, we have presented lithium problems that occur from different originated sources (BBNS, GCR, stellar nucleosynthesis). However, in this thesis, we will only focus on the lithium depletion on the stellar evolution through nucleosynthesis for solar-like stars. The lithium abundance from here on will be referred to as the ^{7}Li isotope because ^{6}Li (from GCR) has a very short life and decays spontaneously. We speculate that there must be astrophysical justifiable answers to somehow explain the missing lithium particularly due to the stars internal mixing processes.

Hence in this work, we will start the Chapter 2 with a brief overview of the production ^{7}Li via PPII branching of the proton-proton chains. This information will give us a better insight into the stability of the element and how they were formed and survived in a star. Furthermore, we will examine the PP-branching ratios to determine how significant ^{7}Li production in the solar abundance. We will then address the methods used by various literature to obtain the solar chemical compositions and therefore, present our reasons for recommending a specific table compilation of abundance in this work. These solar abundances will be one of the main parameters for our constructed standard solar model (SSM). Finally, we will conclude the chapter by reviewing the lithium problem in the past and solutions that have been proposed so far.

In Chapter 3, we first discuss the stellar structure and evolution of solar-like stars. Then we will run MESA evolution code to produce our standard solar model that fits with the helioseismology result. This fitted solar model will adopt some standard internal diffusion transport mechanisms such as convection, overshooting, atomic chemical diffusion, and gravitational settling. The effects of these transport mechanisms on the evolution of ^{7}Li and other solar abundances will be investigated. Furthermore, we must replicate methods proposed in the past to validate our work. This implies that the implementation of solar surface rotation and magnetic field dynamo will be included in our stellar models to

find some answers to the unexplained ^{7}Li depletion. Finally, Chapter 3 is concluded by addressing the change in the evolution of ^{7}Li abundance during the later age of the main sequence to look for any trace of ^{7}Li plateau that was mentioned by A. Boesgaard and Tripicco (1986).

There was a promising work by Gruyters et al. (2016) which showed that the stars in M30 are greatly affected by atomic diffusion and ad-hoc additional mixing below the surface convection zone. Thus, it is highly believed that the extra mixing processes can cause more lithium burning in the stellar interior compared to the model adopting standard transport mechanisms process. So in Chapter 4, we attempt to solve the lithium depletion problem by looking at the additional mixing caused by the enhanced overshooting starting from Pre-Main Sequence until the current age. Then, we will promote higher lithium mixing by increasing the gravitational field sinking to the abundances on solar surface. The higher gravitational settling is expected to increase the diffusion of ^{7}Li towards the interior. Besides, increasing solar's surface rotation rate is also another popular method to transport abundance efficiently due to the impact of angular momentum. A new initial solar rotation rate will be adopted here.

Assuming that the lithium problem comes from the sensitivity of opacity determined by the initial metallicity z fraction and chemical composition. Hence we will simulate the evolution of ^{7}Li abundance using different solar mixtures suggested from various literature together with their respective initial mass fraction and metallicity. Furthermore, most stellar evolution codes including MESA incorporate initial solar abundance with a combined mixture of photospheric observation and *CI Condrite* data within the same table. This suggests that remodeling stellar evolution solely using photospheric data in its solar composition table will produce a different ^{7}Li abundance result. Same constraints from our previous fitted solar model calibration will be consistently adopted in the studies.

Finally, the focus is to search for an answer from a different perspective. Under the assumptions of all transport mechanisms and internal processes calculation of stellar evolution are correct and sound, then the possibility of error is within the primordial lithium data used in the computation. There are many plausible ways that the higher initial lithium adopted so far by using the *CI Chondrite* measurement is not an accurate initial lithium content in the Sun. Hence our work will predetermine the initial mass fraction ^{7}Li that will match the ^{7}Li observation. Then, the thesis is concluded in Chapter 5 with our points of view and suggestions for any future work.

1.1 Problem statements

1. The rate of lithium depletion during the Main Sequence (MS) stage is not decreasing consistently with the increasing age for all-stars and this indicates that lithium depletion is not a continuous process where it cannot just be described by the effective temperature or even its stellar mass.
2. There is a certain stage of a star evolution that might undergo major lithium depletion. So, does the rate of lithium burning has a higher possibility to take place during the main sequence stage (or even sub-giant phase) compared to its early star formation?
3. It has been postulated that several chemical transport mechanisms can efficiently transport the surface lithium abundance towards the solar interior.
4. Another interesting problem that arises is whether the lithium abundance production has any co-relation with solar mixtures adopted by a different chemical composition table and its respective opacity.

1.2 Objectives

1. To study the history of the lithium depletion problem in the Sun and other similar solar-like stars.
2. To reproduce and analyze the various effects of internal mixing mechanisms that had been proposed in the past to solve the lithium depletion problem.
3. To enhance the lithium mixing beyond the convection zone instability to investigate further lithium burning which may impose such a lithium destruction trend.
4. To investigate the correlation between lithium depletion problem and the role of solar opacity based on different solar chemical compositions.
5. To predetermine the initial lithium content that will match the observed lithium value today.

CHAPTER 2: LITHIUM-7 PRODUCTION IN SOLAR-LIKE STARS AND THE DEPLETION PROBLEMS

2.1 Introduction

A star forms when interstellar cloud gaseous with growing kinetic energy and angular momentum collapsed under the influence of gravitational contraction. The gravitational energy will transform into thermal energy and cause hydrogen to be fully ionized. Hence when internal pressure rises and the cloud gaseous reaches hydrostatic equilibrium, it will halt any further collapse. If the protostar's core temperature is sufficiently high, about 14×10^6 K, it will then induce a reaction known as thermonuclear fusion.

2.2 The Production of ^{7}Li

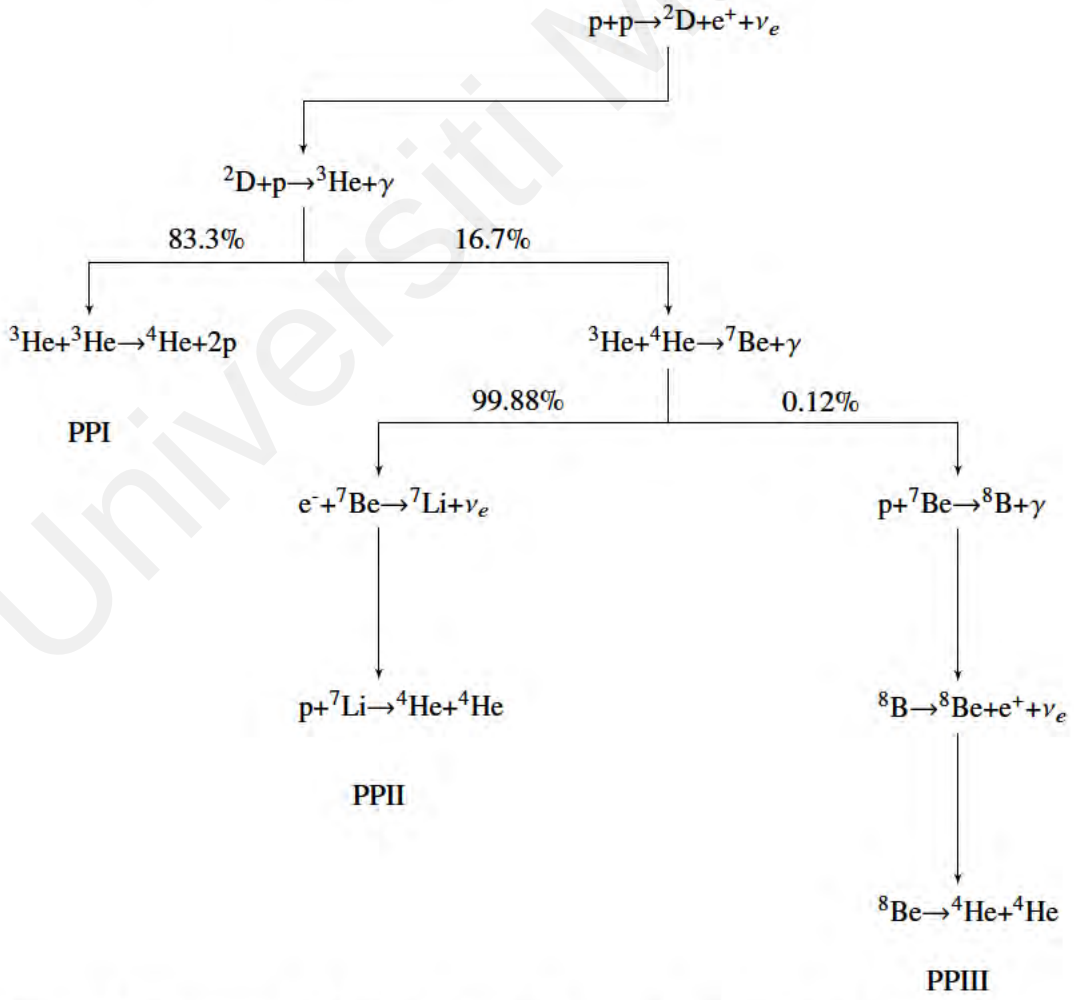

Figure 2.1: Sequence of nuclear fusion reactions defining the Proton-Proton (PP) Chain.

For low mass stars like our Sun, the thermonuclear fusion is activated when two hydrogen nuclei are fused to form a deuteron nucleus along with the release of enormous amounts of energy. This high nuclear energy will provide the force in the outward direction to balance out the gravitational contraction and support the star's size during its transition into the Main Sequence. Figure 2.1 shows how the first fusion process triggers a sequence of chain reactions called the Proton-Proton (PP) Chain. In detail, the deuteron produced in the initial reaction continue to fuse with another hydrogen to form a ^{3}He nucleus (PPI). Then the PPI branch reaction completes when ^{3}He fused with another ^{3}He with the branching ratio of 83.3%. The remaining 16.7% goes to the chances of ^{3}He fuses with ^{4}He to produce a ^{7}Be nucleus.

The significant fraction of ^{7}Be production in the star's internal structure will continue to decay by electron capture. The beta-decay usually will take 52.9 days under standard laboratory conditions. However, based on the work carried out in a red giant model No VII by Sandage and Schwarzschild (1952), they showed that ^{7}Be half-life lies about $50 - 100$ years at a temperature greater than $1{\times}10^{6}$ K. At this extreme temperature, electrons of the nuclei are completely stripped off. Only some small fractions have been able to retain the K shell electron. Meanwhile, the probability of electron-capture transition is directly proportional to the square of the electron wave function at the surface of ^{7}Be nucleus (Blatt et al., 1953). Hence, the half-life of ^{7}Be is lengthened enormously. Detailed analysis on the electron capture rate of ^{7}Be in the high-density solar plasma can be found in Bahcall and Moeller (1969).

The mean lifetime of ^{7}Be is long enough for ^{7}Be to be circulated in the radiative currents until a substantial amount reaches the outer cooler region and capturing electron in the process producing a stable ^{7}Li isotope. The abundance of ^{7}Li can remain above the base of the convection zone until eventually some will be pulled back to the hotter center of the star

and destroyed by proton capture, completing the PPII branch. The 'pulling' mechanisms are perhaps due to the diffusion transports by convection and the gravitational settling, overshooting of angular momentum by the surface's rotation, and perhaps many more nature of the circulation currents we might not understand yet. On the other hand, the equilibrium ^{7}Li abundance built on the star surface over time can be observed via high resolution stellar spectroscopic measurement.

Finally, the third branch, PPIII in the PP Chain will occur at a much higher temperature in the core with the lowest percentage of branch termination. At the cooler region in the convection zone, the reaction is unusual and negligible importance as the temperature is too low for any ^{7}Be nucleus to capture any proton.

Table 2.1: Average energy released in the PP chain.

Reaction	Q value (MeV)
PPI	
$p + p \rightarrow d + e^{+} + \nu$	1.442
$d + p \rightarrow {}^{3}He + \gamma$	5.493
$^{3}He + {}^{3}He \rightarrow {}^{4}He + 2p$	12.859
PPII	
$^{3}He + {}^{4}He \rightarrow {}^{7}Be + \gamma$	1.586
$^{7}Be + e^{-} \rightarrow {}^{7}Li + \nu$	0.861
$^{7}Li + p \rightarrow {}^{4}He + {}^{4}He$	17.347
PPIII	
$^{7}Be + p \rightarrow {}^{8}B + \gamma$	0.135
$^{8}B \rightarrow 2{}^{4}He + e^{+} + \nu$	18.074

The energy, Q generated by the PP Chain for each reaction classified in the corresponding branches is summarized in Table 2.1. Note that the PP Chain gives out 98% of thermal energy available in the Sun while the remaining is obtainable from the CNO cycle. Both the PP Chain and the CNO cycle are set off simultaneously in hydrogen-dominated stars. Based on the data, the beta-decay of ^{7}Li emits significant energy per reaction following

the PPII branch. However, considering that the ^{7}Li nuclei are stable isotopes that produce in a small fractional abundance ^{7}Li/H $\approx 10^{-9} - 10^{-15}$, the reaction ^{7}Li(p,$\alpha$)$\alpha$ has a low cross-section per pair, leaving the energy released via PPI to be dominant compared to PPII or PPII, as referred to earlier in the reaction branching ratio.

2.3 The Determination of ^{7}Li Abundance

The determination of stars' photospheric abundances is of profound importance as it gives us access to the elemental and isotopic composition of a star and how they relate to the formation and evolution of the placed galaxy. Abundances of different species are obtainable by using analysis on the high-resolution spectral lines formation, and it has been widely proven as a reliable tool to conduct many astronomical types of research. Prior studies generally confirm that all observed solar abundances are in good agreement with any prediction made by solar modeling except for ^{7}Li abundance (Asplund et al., 2009). There is also another method used to measure the abundances in which, by using mass spectroscopy of meteorites in terrestrial laboratories directly. A rare meteor, so-called *CI Carbonaceous Chondrites* found on earth, can be used to determine primordial solar abundances as it has been postulated they were not altered much since 4.5 million years ago.

Even though the mass spectroscopy method is valuable, six of the elements H, He, C, N, O, and Ne are considered volatile and highly depleted in time. Hence, it is impossible to predict solar primordial abundances solely using the *Chondrites*. With this knowledge, helioseismology studies have widely incorporated both methods to promote the solar chemical composition table. The helioseismology data is used to determine the present-day solar abundances, whereas the *Chondrites* measurement represents the predicted primordial solar abundances (except for the volatile elements).

Several authors have posited great solar compositions during the past, and some are within our interest which they are Asplund et al. (2009), hereafter AGS09, Asplund et al. (2005), hereafter AGS05, Grevesse & Sauval (1998), hereafter GS98, and the Grevesse & Noels (1993), hereafter GN93. However, a comparison made between all compilations by Serenelli et al. (2009) yielded to a conclusion that models adopting AGS09 and AGS05 have failed to agree with the helioseismology data for the radius of the convection zone, ($R_{cz} = 0.713 R_{\odot}$) and sound speed profile. Serenelli et al. (2009) used a modified version of the GARSTEC code for the solar modeling and suggested a better revision on the solar radiative opacities to compensate for the disagreement made by the AGS09 and AGS05 compilations. Despite the revision on the AGSS09, their proposed model (AGSS09ph) has also been conflicted with determined solar properties. Table 2.2 and Figure 2.2 are summaries of the revision made on the problem with solar models.

Besides, it has been recommended a few years earlier by Basu and Antia (2013) that even different stellar evolution code (Yale Stellar Evolution Code, YREC) they used has continued to have the best match with helioseismology with GS98 abundances. Thus in this literature, we will include our chosen present-day solar chemical composition table GS98 for references. Table 2.3 has clearly shown that every photospheric abundance of the chemical elements here are in good agreement with their meteorites abundances except for a wide gap for lithium. Despite the discrepancy, the table will be used consistently in our constructed solar-type star models except later when we want to study the effect of adopting different compilations of initial mass fraction to the evolution of lithium abundance.

Table 2.2: The comparison between different chemical compilation implemented in models and their respective solar properties (Serenelli et al., 2009).

Model	GS98	AGS05	AGS09	AGSS09ph
$(Z/X)_{surf}$	0.0229	0.0165	0.0178	0.0181
Z_{surf}	0.017	0.0126	0.0134	0.0136
Y_{surf}	0.2423	0.2292	0.2314	0.2349
$(R/R_{\odot})_{cz}$	0.713	0.728	0.724	0.722
<Δc/c>	0.0010	0.0049	0.0038	0.0031
$< \Delta\rho/\rho >$	0.0011	0.0048	0.0040	0.0033
Z_{ini}	0.0187	0.0139	0.0149	0.0151
α_{mlt}	2.15	2.10	2.09	2.12

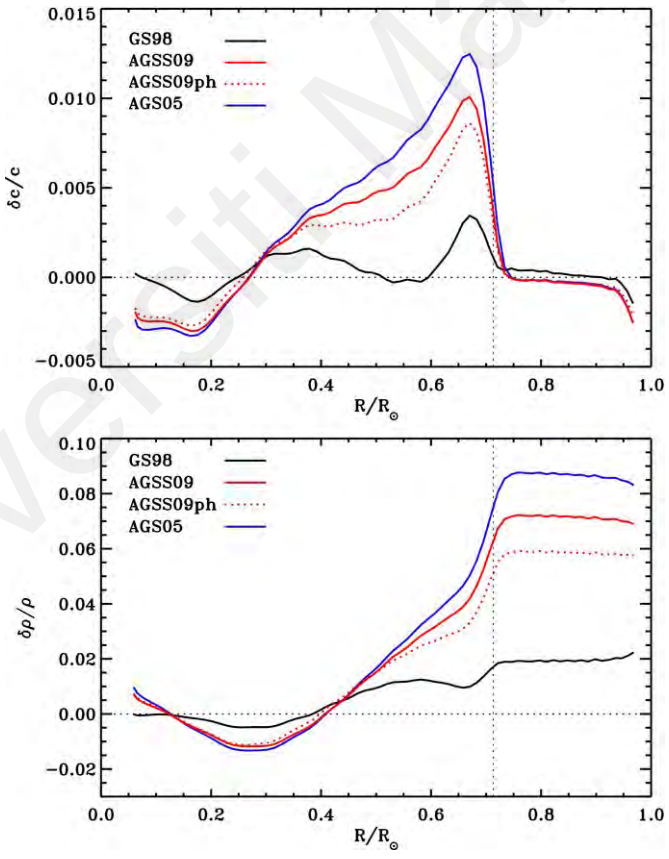

Figure 2.2: Comparison of relative sound speed δc/c and density $\delta\ \rho/\rho$ in the solar models using chemical abundances compilations from various authors. The helioseismology result was taken from Basu et al. (2009). The standard solar model computed by adopting GS98 was found to be an excellent match with the experimental data. Figure has been kindly supplied by Serenelli et al. (2009) with AGSS09ph is his proposed revised model.

Table 2.3: Present-day solar chemical composition in the unit of dex provided by Grevesse and Sauval (1998) for solar photosphere and in meteorites (*C1 Chondrites*).

Element	Photosphere	Metcorites	Ph-Met	EL	Photosphere	Meteorites	Ph-Met
01 H	12.00	-	-	42 Mo	1.92±0.05	1.97±0.02	-0.05
02 He	10.93±0.004	-	-	44 Ru	1.84±0.07	1.83±0.04	+0.01
03 Li	1.10±0.10	3.31±0.04	-2.21	45 Rh	1.12±0.12	1.10±0.04	+0.02
04 Be	1.40±0.09	1.42±0.04	0.02	46 Pd	1.69±0.04	1.70±10.04	-0.01
05 B	(2.55±0.30)	2.79±0.05	(-0.24)	47 Ag	(0.94±0.25)	1.24±0.04	(-0.30)
06 C	8.52±10.06	-	-	48 Cd	1.77±0.11	1.76±0.04	+0.01
07 N	7.92±0.06	-	-	49 In	(1.66±0.15)	0.82±0.04	(+0.84)
08 o	8.83±0.06	-	-	50 Sn	2.0±(0.3)	2.14±10.04	-0.14
09 F	[4.56±0.3]		+0.08	51 Sb	1.0	1.03±0.07	-0.03
10 Ne	[8.08±0.06]	-	-	52 Te	-	2.24 ±0.04	-
II Na	6.33±0.03	6.32±0.02	+0.01	531	-	1.51±0.08	-
12 Mg	7.58±10.05	7.58±0.01	0.00	54 Xe	-	2.17±0.08	-
13 Al	6.47±0.07	6.49±0.01	-0.02	55 Cs	-	1.13±0.02	-
14 Si	7.55±0.05	7.56±0.01	-0.01	56 Ba	2.13±0.05	2.22±0.02	-0.09
15 P	5.45±(0.04)	5.56±0.06	-0,11	57 La	1.17±0.07	1.22±0.02	-0.05
16 S	7.33±10.11	7.20±0.06	+0.13	58 Ce	1.58±10.09	1.63±0.02	-0.05
17 CI	[5.5±10.3]	5.28±0.06	0.22	59 Pr	0.71±0.08	0.80±0.02	-0.09
18 Ar	[6.40±0.06]	-	-	60 Nd	1.50±0.06	1.49±0.02	+0.01
19 K	5.12±0.13	5.13±0.02	-0.01	62 Sm	1.01±0.06	0.98±0.02	+0.03
20 Ca	6.36±0.02	6.35±10.01	+0.01	03 Eu	0.51±10.08	0.55±0.02	-0.04
21 Sc	3.17±0.10	3.10±0.01	+0.07	64 Gd	1.12±0.04	1.09±0.02	+0.03
22 Ti	5.02±0.06	4.94±0.02	+0.08	65 Tb	(-0.1±0.3)	0.35±0.02	(-0.45)
23 V	4.00±10.02	4.02±10.02	-0.02	66 Dy	1.14±10.08	1.17±10.02	-0.03
24 Cr	5.67±0.03	5.69±0.01	-0.02	67 Ho	(0.26±0.16)	0.51±0.02	(-0.25)
25 Mn	5.39±10.03	5.53±0.01	-0.14	68 Er	0.93±0.06	0.97±0.02	-0.04
26 Fe	7.50±0.05	7.50±0.01	0.00	69 Tm	(0.00±0.15)	0.15 ±0.02	(-0.15)
27 Co	4.92±0.04	4.91±0.01	+0.01	70 Yb	1.08±(0.15)	0.96±0.02	+0.12
28 Ni	6.25±0.04	6.25±0.01	0.00	71 Lu	0.06±0.10	0.13±0.02	-0.07
29 Cu	4.21±0.04	4.29±0.04	-0.08	72 Hf	0.8±(0.08)	0.75±0.02	+0.13
30 Zn	4.60±0.08	4.67±0.04	-0.07	73 Ta	-	0.13±10.02	-
31 Ga	2.88±(0.10)	3.13±10.02	-0.25	74 W	(1.11±0.15)	0.69±0.03	(+0.42)
32 Ge	3.41±10.14	3.63±0.04	-0.22	75 Re	-	0.28±0.03	-
33 As	-	2.37±0.02	-	76 Os	1.45±0.10	1.39±0.02	+0.06
34 Se	-	3.41±0.03	-	77 Ir	1.35±(0.10)	1.37±0.02	-0.02
35 Br	-	2.63±0.04	-	78 Pr	1.8±0.3	1.69±0.04	+0.11
36 Kr	-	3.31±0.08	-	79 Au	(1.01±0.15)	0.85±0.04	(+0.16)
37 Rb	2.60±(0.15)	2.41±0.02	+0.19	80 Hg	-	1.13±0.08	-
38 Sr	2.97±0.07	2.92±0.02	+0.05	81 T1	(0.9±0.2)	0.83±0.04	(+0.07)
39 Y	2.24±0.03	2.23±20.02	+0.01	82 Pb	1.95±0.08	2.06±0.04	-0.11
40 Zz	2.60±10.02	2.61±10.02	-0.01	83 Bi	-	0.71±0.04	-
41 Nb	1.42±0.06	1.40±0.02	+0.02	90 Th	-	0.09±0.02	-

Normally in the stellar evolution model, abundances are expressed in relative abundance ratios compared to hydrogen. However, in solar photospheric observation derived from the spectroscopic analysis, they are usually given in logarithmic-12,

$$A(X) = 12 + \log[N_X/N_H]. \tag{2.1}$$

where N_X is the element abundance, N_H is the hydrogen abundance and by definition, hydrogen abundance in logarithmic-12 scale is $A(^1H) = 12$ dex. The unit term dex is frequently used in the astronomical literature to designate decadic logarithmic units, where 1 dex hold for a factor of 10 ($= 10^1$) (Lodders, 2019). Meanwhile the abundances from the *CI Carbonaceous Chondrites* are set to cosmochemical scale relative to 10^6 silicon atoms. Then both scales are equalized by re-normalizing photospheric (or meteorite) abundances with a scaling factor derived from any refractory element that serves link between the two scales such as Si, Mg, Ti, or Ca (Holweger, 2001). Any implication of statistical error from the conversion of abundance to astronomical scale will not be discussed here. Our highlight here, is to address the presented lithium abundance in Table 2.3. For decades, no concrete explanation as to why the solar photospheric, A(Li) had depleted about a factor of 2 dex in magnitude compared to its meteorites corresponds.

2.4 History of Lithium Problem

To date, most of the existing literature has confirmed that the lithium abundance in our solar surface is too low compared to the prediction made by the *CI Carbonaceous Chondrites* (Asplund, 2005; Asplund et al., 2009; Grevesse & Sauval, 1998). Many researchers have tried to address the massive depletion issue and still staring at a blank wall. Our knowledge of the mixing processes in the solar interior is based mainly on very limited data. Hence the current solution is to probe other stars with similar solar age and metallicity in the open clusters. Perhaps we may encounter a relationship between the lithium problem with the existing solar-like conditions.

2.4.1 Lithium and Metallicity

One may convey an initial assumption that a star with higher metallicity might contain more pristine lithium abundance. Hence if the entire lithium content would not have burnt in the PMS process, there must be a direct dependency between these two. However, based on the high resolution spectroscopic from large sample solar-like stars in M67 and Hyades, the assumption was far-fetched. López-Valdivia et al. (2015) had cataloged 52 objects G0-G3 type stars with similar solar mass and metallicity, [Z/H] = ±0.32 on the MS and derived their atmospheric parameters and lithium abundances. The work had included 671 dwarfs to subgiant objects of M67 from Ramirez et al. (2012) as a reference to determine the lithium abundance correlation with the effective temperature. The result of the lithium abundance distribution is reported with some bizarre findings. Ramirez et al. (2012) highlighted that lithium is less abundant in cooler, less massive stars with larger convective envelopes. Whereas hotter stars appeared at much higher lithium abundance creating an empty region called 'lithium desert' with no stars. Although lithium desert was first proposed by Chen et al. (2001), however, López-Valdivia et al. (2015), on his contrary analysis, points out that one of his star BD+473218 was found to be in the empty

region, suggesting more data is needed to endorse Ramirez's and Chen's conclusion. Despite the minor conflict, these three pieces of literature have agreed with the same postulation in which the solar-type stars with low-metallicity or higher metallicity do not pose any significant changes to the lithium abundance. Figure 2.3 has shown that some low-metallicity solar-like stars contained higher lithium than some with high-metallicity. This finding is interesting as it has opposed our initial prediction of a direct proportion between lithium-metallicity correlation.

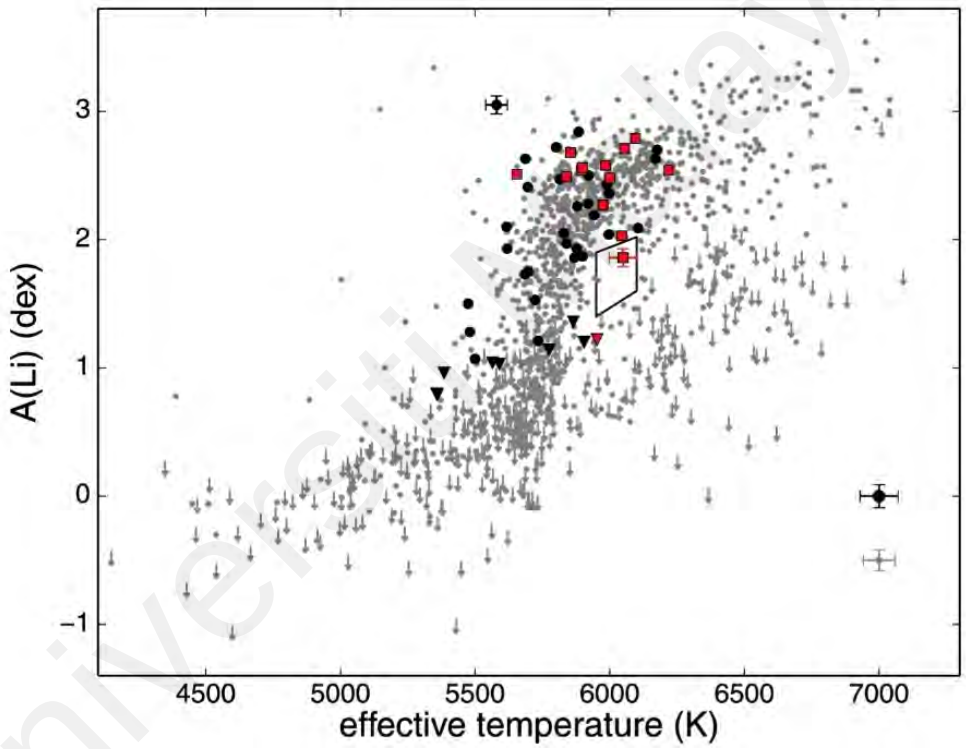

Figure 2.3: Distribution of lithium abundance as a function of effective temperature for observed stars. The black filled circles indicate low-metalicity stars with [Z/H] < 0.16 dex, while red squares show metal-rich stars and downward triangles mark 3σ upper limits. Grey dots and downward arrows represent (Ramirez et al., 2012) work on lithium and the upper limits. The polygon shows the so-called lithium desert. The bottom right is the average errors (López-Valdivia et al., 2015).

2.4.2 Lithium and Mass of Solar Twins

Based on Figure 2.4, the solar twin stars within (0.85 $M_{\odot}$ - 1.1 $M_{\odot}$) range had shown a wide ^{7}Li dispersion. The correlation between lithium abundance and stellar mass is not clearly apparent. More studies from different groups yield the same determination. (Bouvier, 2008; Carlos, Marília et al., 2016; Israelian et al., 2004)

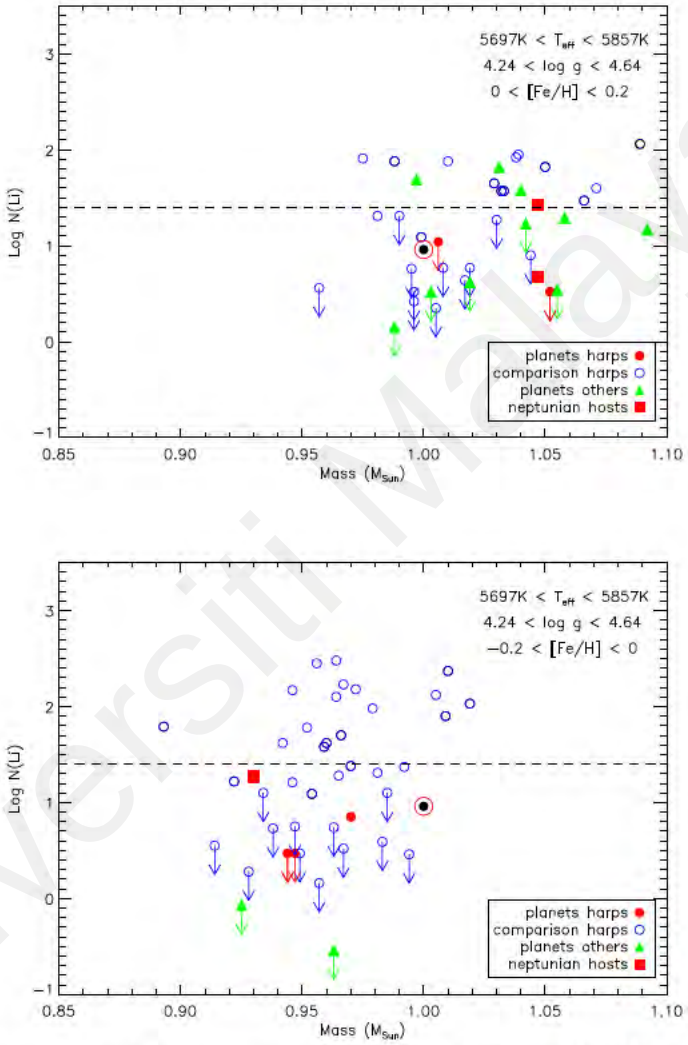

Figure 2.4: Lithium abundances vs mass for solar twins at [Fe/H] < 0 (top panel) and solar twins at [Fe/H] > 0 (lower panel).The symbols used here are for planet host stars (red filled circles) and *'single'* stars (blue open circles) from HARPS together with other planet hosts (green triangles). Squares are stars that only host Neptunian- or Super-Earth-type planets (Delgado Mena et al., 2014).

2.4.3 Lithium and Age of Stars

Ramirez et al. (2012) presented in their work that there are no young stars age < 2 Gyr at the lower side of the lithium desert. The result suggests that the mechanism which depletes surface lithium in the objects occur at the MS or subgiant phases and not the PMS. Besides, lithium abundance becomes plateau after a certain temperature (600 to 700K). Another early work by A. Boesgaard and Tripicco (1986) also supports the figures and presented that the depletion becomes ineffective beyond an age of $1 - 2$ Gyr for the majority of the stars, leading to a lithium plateau at old age for which was found in observations of F-late stars. Furthermore, we include recent evidence by Delgado Mena et al. (2014) on lithium abundances of 326 main sequence solar twin stars. The solar twin stars which are in $T_{\rm eff}$ = $T_{\odot} \pm 80$ K, $\log g = \log g_{\odot} \pm 0.2$ and [Z/H] = $[\mathrm{Z/H}]_{\odot} \pm 0.2$ were taken mainly from the HARPS sample. It turns out that their finding shown in Figure 2.5 reveals that there is no tight correlation between lithium abundance and their age except for very young ages. They claimed they would find young stars with low lithium abundance as well as old stars with higher abundance. One of the evaluations made by Pace et al. (2012) had also arrived at the same conclusion. Therefore, it is agreed that the depletion of lithium abundance does not depend on mass, age, or metallicity.

2.4.4 Lithium and Planet-Hosting Stars

Debate on the relationship between lithium abundance and planet-hosting stars has emerged for years (Garcia Lopez & Perez de Taoro, 1998; King et al., 1997; Cochran et al., 1997; Ryan, 2000; Deliyannis et al., 2000; Santos et al., 2004a; Gonzalez & Laws, 2000; Takeda et al., 2007; Israelian et al., 2004; Takeda & Kawanomoto, 2005; Luck & Heiter, 2006; Chen & Zhao, 2006; Gonzalez, 2008). In theory, the solar-analog planet-hosting stars may have different rotational star formation history and more significant angular

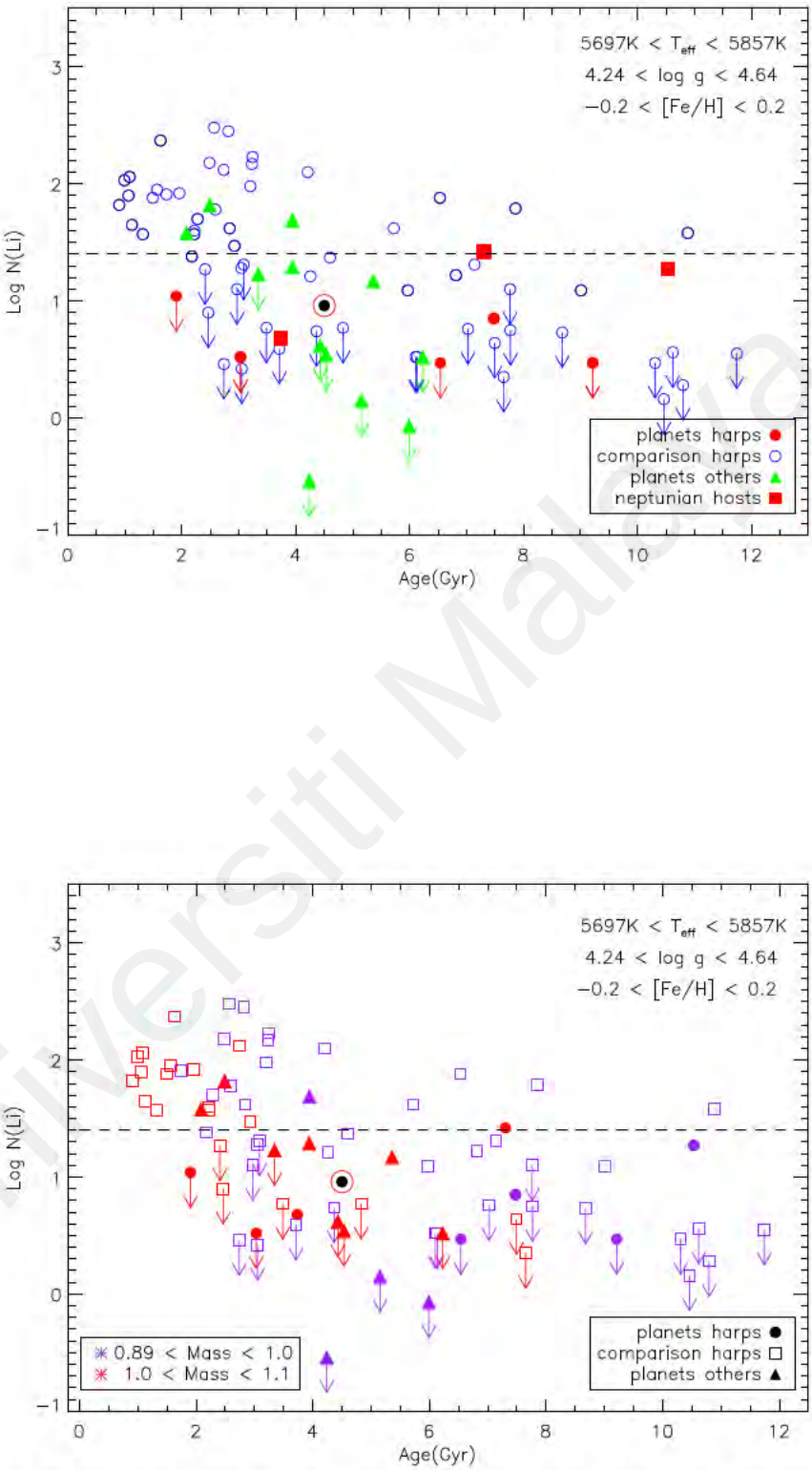

Figure 2.5: Lithium abundances vs. age for solar twins on the top panel and on the lower panel is the colors version denoting different solar mass ranges in the same sample. Symbols as in Figure 2.4 (Delgado Mena et al., 2014).

momentum transferred than stars with no detected planet. Hence the presence of planets in the system may increase the amount of mixing and deepen the convective zone to cause more lithium burning (Bouvier, 2008). Some observational works by Baumann et al. (2010); Chen and Zhao (2006); Pinsonneault (2009); Sousa et al. (2011); Stanley et al. (1998) reported supporting the idea of enhanced lithium depletion in planet-hosting stars. However, these several findings have been contradicted with observations made by Carlos, Marília et al. (2016); Delgado Mena et al. (2014); Ryan (2000); Sousa et al. (2011), which they claimed no such trend was found. At this stage of comparison, we found that the sample of the observed stars in Carlos, Marília et al. (2016); Ryan (2000); Sousa et al. (2011) are too small to confirm their conclusion.

2.4.5 Boesgaard Lithium Gap

Another unexplained lithium problem has emerged in intermediate-age and old open clusters. A. Boesgaard and Tripicco (1986) show there was an abrupt drop of lithium among the F stars, the so-called *Boesgaard Lithium Gap*, which is linked to stars' effective temperature. The *Boesgaard Lithium gap* is severe lithium depletion found during the main sequence stage of Population I F-stars in the narrow range of effective temperature, T_{eff} = 6600 - 6700 K. Then surprisingly, some of the stars contain normal expected lithium abundance between T_{eff} = 6550 - 6000 K before the abundance suddenly drops again at cooler temperatures. Many different theoretical explanations have been proposed with each of these mostly are mechanisms based on astrophysical solutions. In conclusion, many more studies have been published on lithium problem history, and these various phenomena are indeed what motivate researchers in this field.

2.5 Solutions In The Past

2.5.1 Convection and Overshooting

One of the earliest methods attempted in the past was a suggestion to include overshoot mixing below the bottom of the convective envelope (Baraffe et al., 2017; Grossman, 1992; Grossman et al., 1993; Xiong & Chen, 1992; Xiong & Deng, 2001; Zhang et al., 2019). The convection and convection-overshooting can be regarded as a diffusion mixing process that leads to two major consequences for stars. The impacts are that the mechanisms will modify the temperature gradient in the overshoot region and lower its value. Therefore, surface chemical compositions, including ^{7}Li may be modified.

Many researchers have widely incorporated the 30 years of extensive studies on the convection and convection-overshooting into stars' primary mixing process. However, there is still uncertainty whether to treat the convection as a local or non-local problem. Maeder (1975); Roxburgh (1978); Shaviv and Salpeter (1973); Xiong and Chen (1992) are some examples which doubtlessly implementing the non-local phenomena. They believe the overshooting region depends sensitively on the properties of the adjacent convective region. Whereas Bohm-Vitense and Nelson (1976); Spiegel (1963), and many other authors treated the convection with local mixing-length theory. Despite the never-ending disagreement, most stellar evolution codes today have implemented local-mixing which follows overshooting distance parameterized by $\alpha_{\rm mlt} = l/H_{\rm p}$ suggested by Maeder & Meynet (1988); Cox and Giuli (1968); Henyey, Vardya, and Bodenheimer (1965). In working principle, the code will determine the distance of convective overshooting by calibrating the free parameter, $\alpha_{\rm mlt}$ to reproduce the observed star luminosity and its bottom radius of convection zone without needing any non-local solution (Stothers, 1991; Stothers & Chin, 1992). Nevertheless, will convection and convection-overshooting are able to explain the lithium depletion issue?

Shaviv & Salpeter (1973); Maeder (1975); Roxburgh (1978); Bressanet et al. (1981); Langer (1986) have presented that when the boundary of convective zone instability is determined, then the neighbor's shell at the bottom of the convection zone can be related to its inertia and momentum transfer, including the equation of continuity. Therefore, elements or abundances from the base of the convective layer will overshoot and be carried beyond the boundary defined. Those masses on the surface penetrate deeper and increase the rate of nuclear reaction and certainly affect energy generation. Schaller et al. (1992) had successfully calibrated 65 stellar clusters, which are consistent with their respective observable data until the terminal age of the main sequence (TAMS) by applying the convective process with an overshoot distance of one-fifth of the pressure scale height. Although they have demonstrated that model with overshooting seems be able to solve most problems in stellar evolution, particularly the discontinuity in temperature change ∇_{rad} at the zone between convective and radiative burning region, however, many other groups such as Choi et al. (2016); Dantona and Mazzitelli (1984); Paczynski (1977) presented models with the inclusion of convection with or without overshooting have failed to match the same lithium abundance of any observed stars in young cluster or in present solar during the main sequence period. On the other hand, implementation of the same process during the pre-main sequence stage has caused an over-depletion and destroyed most of its protosolar lithium abundance (Dantona & Mazzitelli, 1984). Therefore, it is clear that even though convection is essential to the chemical mixing transport, we need to search for other options to explain the lithium problem.

2.5.2 Atomic Diffusion

Another popular proposal for solving the lithium problem is by adopting atomic diffusion and transportation of gravity waves as the mixing processes. Christensen-Dalsgaard, Proffitt, and Thompson (1993); Morel and Thévenin (2002) reported that model with diffusion

and no turbulence significantly improves the agreement between theory and observations. Perhaps the effect of this diffusion mechanism could also be the reason for major lithium depletion at the base of the convection zone. Proffitt and Michaud (1991) had shown that atomic diffusion decreases the helium abundance of the Sun's surface by roughly 10% below its original values. They also predicted the decrement of heavy metal by some small amount. Later on, many groups working with models computed with atomic diffusion implied such case of higher ^{7}Li burning, but they claimed the mechanism is still incapable of causing major depletion as inferred (Kovets et al., 1994; Montalban, 1994; Baglin et al., 1985; Zhang & Li, 2012; Chaboyer et al., 2001). For example, Kovets et al. (1994) had reported that the lithium depletion in their model with diffusion was enhanced by 1.08 dex. However, they were still unable to fully explain the other missing two dex of ^{7}Li.

2.5.3 Solar Rotation and Magnetic Field Dynamo

Some authors have introduced another solution linked to the increased efficiency of diffusion and convection in the convective boundary. Ventura et al. (1998a), D′Antona, Ventura & Mazzitelli (2000), Pinsonneault (2009) suggested a solution to include solar rotation to induced meridional circulation currents and generate both structural evolution and angular momentum loss from magnetized winds. The small rate of surface rotational may not cause significant disturbance on the surface abundance but the generated shears instabilities by plasma can drive mild turbulence and also induced a magnetic field into the solar surrounding.

Spruit (2002), in his work justified that the induced magnetic field due to differential rotation within the convection zone layer, lead to modification of fluid displacement. Many observational works have been done to study the rotation and magnetic field relations to the evolution of lithium in search for correlations between these two parameters (Skumanich, 1972; Rebolo & Beckman, 1988; King et al., 2000; Clarke et al., 2004; Bouvier, 2008;

Bouvier et al., 2016). However, none of the works are sufficient to conclude such ^{7}Li depletion trend. Perhaps, more data are needed to deduce the exact map of deep or surface solar rotation structure, especially in its early years right after Zero Age Main Sequence (ZAMS). Currently, researchers have only relied on the past one hundred years of sunspot observations to determine our magnetic solar activity cycle.

2.5.4 Planetary-Linked Solar Model

New postulation with the planetary linked has emerged in recent years, claiming solar-like stars with similar stellar properties but different lithium content are tied to the conditions in its initial phase of star formation. During the star's early hydrodynamic stage, the rotation rate can be considered related to the mass accretion rate. Hence, the expected initial rate of rotation has a strong relationship with the presence of protoplanetary disk (Pinsonneault, 2009).

However, one concern about the findings of affiliation between lithium abundance and planetary companion was that there is no exact rotational history of the star due to star-disc interaction in the past that researchers can use to remodel. Perhaps a higher initial rotational rate should be calibrated differently for stars with companion planets which could enhance stellar wind leading to higher mass loss, induced magnetic field, and lithium over-mixing.

In a nutshell, these past attempts have not succeeded in explaining lithium depletion thoroughly. Hence in the next section, we will construct stellar models and discuss the treatments suggested above to test the significance of changing solar transport mechanisms to the lithium problem. Then we will further explore the possibility of enhancing the lithium mixing beyond the convective zone to search for an answer.

CHAPTER 3: STRUCTURE AND EVOLUTION OF SOLAR-TYPE MODELS

3.1 Stellar Evolution and Structure

In order to construct our stellar model using a computational program, we first present the principle processes controlling our stellar structure. Generally, stars are assumed to be spherical symmetry so that we may express their stellar properties with a set of one-dimensional (1D) equations rather than a full set of three-dimensional (3D) equations. Then, for a star to achieve hydrostatic equilibrium in a quasi-static state, the star has to balance the outward pressure gradient force with the inwardly directed force from gravitation as below,

$$\frac{dP}{dr} = \rho(r)g = -\frac{\rho(r)GM(r)}{r^2}. \tag{3.1}$$

where $g = GM(r)/r^2$ is the local gravitational acceleration induced by all the mass, $M(r)$ is the mass of the star, and $\rho(r)$ is the mass per unit volume locally. These functions with respect to the radius r are defined as the distance outward from the center. Then, one can relate the density ρ(r), with the conservation of mass of a star

$$\frac{dM(r)}{dr} = 4\pi r^2 \rho(r). \tag{3.2}$$

The third important equation in the interior of stellar structure is based on the conservation of energy, given by

$$\frac{dL(r)}{dr} = 4\pi\rho(r)r^2\varepsilon(r). \tag{3.3}$$

where $\varepsilon(r)$ represents the rate of nuclear energy generated per mass per unit time and $L(r)$ is the total rate at which energy passes through a spherical shell.

The last essential equation involved in the stellar structure is the equation for energy transport. If we postulate that the energy is transported only via the emission and absorption of photons via black-body radiation, then emitted flux is directly proportional to the surface area of the emitting object, Stefan Boltzmann constant, $\sigma \propto T^4$. Then net flux of radiation may therefore be represented as the spatial gradient of temperature in the equation,

$$\frac{dT(r)}{dr} = -\frac{1}{4\pi r^2 \sigma} L(r). \tag{3.4}$$

where the $T(r)$ indicates the star's temperature. Therefore, when the temperature at the core is higher than at the surface, the heat (energy) will flow from the center to the outer, principally by radiation. On the other hand, there will be a region further from the star's center where it is not dense enough for the radiative energy transfer. The region known as the convective, will move energy photons by individual layer cells. The depth of the convective region is modeled by the mixing length theory in which the assumed mixing length parameter, $\alpha_{\rm mlt}$ represents the local size of elements relative to the pressure scale height, $H_{\rm p}$. The energy carried through the layers would be adiabatic, where the pressure is allowed to change, but no energy is lost to the surrounding. Hence, we express a new corresponding equation for the temperature gradient in the convective region,

$$\frac{dT(r)}{dr} = (1 - \frac{1}{\gamma})\frac{T dP}{P dr}. \tag{3.5}$$

where γ is the adiabatic index. We now have five equations from (3.1) to (3.5), which are known as the stellar structure equations. We then consider applying the following boundary conditions which are at the center, $M(r) = 0$

$$r = 0, \quad L(r) = 0, \tag{3.6}$$

and at the surface, $M(r) = M$

$$\rho(r) = 0, \quad T = \left(\frac{L}{8\pi R^2 \sigma})\right)^{\frac{1}{4}}. \tag{3.7}$$

These four boundary conditions will define the location in the star's radius, where temperature would provide the correct luminosity. We may now are able to solve them computationally and include the distribution of all chemical compositions with the mass, $X_i(M)$. Note that r is the independent variable, and $M(r), L(r), T(r), \rho(r)$, and $X_i(r)$ are being the dependent parameters with time derivatives.

3.2 MESA Evolution Code

Stellar evolution models will be computed by using Modules for Experiments in Stellar Astrophysics (MESA) code developed by Paxton et al. (2010b, 2015). The code has been tested as robust, efficient, thread-safe libraries for most applications in computational stellar astrophysics. Our computational work in this thesis will adopt the MESA version 10398 released in March 2018. Although there are few available updated versions, the several new options added, such as the treatments for the late stage of the white dwarf, are not crucial to our research areas.

3.2.1 Microphysics Module

The stellar model is initially set up to evolve a fully homogeneous of one solar mass starting from PMS stage until the present solar age $\tau_\odot = 4.57{\times}10^9$ years. The initial assumption made was the protostar is a fully convective symmetrical sphere where all abundances can be treated as constant on the Hayashi line. Once the star progresses to the ZAM stage, we standardize the nuclear reaction rate calculation using the JINA REACLIB database, including 12 prime isotopes and 40 reactions in the network. Then, we use the

MESA interpolation tool to access the pressure, internal energy, entropy, and a variety of derivatives quantities from the equation of state, (EOS) OPAL tables. Besides, the SCVH tables will be included in the interpolation to add cover for the lower temperature of the EOS.

For the opacity module in the MESA, we implement a table generated by Opacity Project (OP) complimented with Ferguson et al., (2005) for the case of temperature lower than 10 000 K. The reason was, OP opacity has been demonstrated to give a 2.5% finer result compared to OPAL opacity when fit with helioseismology observation (Bahcall et al., 2005). Furthermore, we include solar abundance composition by Grevesse and Sauval (1998) as our standard mixture based on its reliability to produce a similar helioseismology hydrogen abundance when tested using the MESA code. The result has been consistent with the literature in which the lower metallicity, Z in the latest AGSS09 mixture, had failed to match the observed data using other computational codes. Finally, another important input is to consider the atmospheric boundary treatment. We adopt atmosphere tables for photosphere described in MESA Paper I (Paxton et al. 2011) that provides cover for -4 $< \log(Z/Z_{\odot}) < 0.5$ and $T_{\rm eff}$ = 2000 to 50 000 K in step size of 250 K.

These microphysical constraints are implemented together with the standard macrophysical processes to model the changes of abundance on the stars' surface particularly ^{7}Li at different stages of star evolution. No mass loss and no solar rotation were adopted during the initial set up. Summary of input parameters and respective literature are shown in Table 3.1

Table 3.1: Summary of input data for solar model calibration.

Parameters	Adopted Values	References
Initial Solar Compositions	Z_{ini} = 0.02 , Y_{ini} = 0.2782	Grevesse and Sauval (1998)
EOS	OPAL EOS, SCVH	Rogers & Nayfonav (2008), Saumon et al. (1995)
Opacity	Opacity project (OP)	Seaton et al. (2005), Ferguson et al. (2005)
Reaction rate	JINA REACLIB	Cyburt et al. (2010)
Diffusion	Diffusion for 12 species	Thoul et al. (1993)
Rotation	No rotation	-
Convection	mixing length,$\alpha_{\rm mlt}$ = 1.92	Local mixing by Cox and Giuli (1968)
Overshooting	f_{ov} = 0.014	-
Magnetic effect	No magnetic field	-
Mass loss	No mass loss	-

3.2.2 Macrophysics Input

3.2.2.1 Convection And Convection-Overshooting

The MESA implements the mixing length theory, (MLT) module by treating the elements flow in the unstable convective mixing region as a diffusive process. The method as described by Cox and Giuli (1968), also assumes high optical depths and no radiative losses. Then, the convective mixing will be computed in time-dependent models with a diffusion coefficient, D_{conv} derived by Böhm-Vitense (1958) and Herwig et al. (1997),

$$D_{conv} = \frac{1}{3}\alpha^{\frac{2}{3}} H_{\rm p}[\frac{c}{\kappa\rho} g\beta(1-\beta)\nabla_{ad}(\nabla_{rad} - \nabla_{ad})]. \tag{3.8}$$

where $H_{\rm p}$ is the pressure scale height, κ is the opacity, α the mixing length free parameter quantity measuring the degree of eddy stretching in the z-direction, c the speed of light, ρ the density, g the gravitational acceleration, ∇_{rad}, and ∇_{ad} are the radiative and adiabatic temperature gradient respectively, and β is the gas pressure fraction. Here, we define a fully radiative region when coefficient, D_{conv} has dropped below than 10^{-2} cm/s^2. Nevertheless, there are adjacent shells right next to the convective region, which are accounted for the hydrodynamical mixing instabilities called the overshoot mixing. Hence, when MESA star

has finished MLT module computation, it continues to set the overshoot mixing diffusion coefficient,D_{ov} derived by Freytag et al. (1996),

$$D_{ov} = D_{conv,0} e^{\frac{-2z}{f H_{\mathrm{p},0}}} \tag{3.9}$$

$$H_{\mathrm{P},0} = \frac{l}{\alpha}. \tag{3.10}$$

where $D_{conv,0}$ is the MLT coefficient at the location of the user-defined, which closer to the Schwarzschild boundary determined by its criterion $\nabla_{rad} > \nabla_{ad}$, $H_{\mathrm{p},0}$ is the pressure scale height at the location, z is the distance in the radiative layer away from the location, and l is the mixing length scale to portray the fluid motion. However, f is an adjustable parameter that describes the efficiency of the extra diffusive mixing, which implies that the larger f will enhance the extra partial mixing further beneath the convective layer (Herwig, 2000).

Finally, MESA used mesh splitting shell k, to compute the changes of abundances of the star structure starting at the star's center towards the increasing surface. Each shell has the same average mass with its own variables of density ρ_k, temperature T_k, and mass fraction vector $x_{i,k}$ whereas boundary variables mass m_k, radius r_k, luminosity L_r, and velocity v_k are predetermined. Then, all the variables including the calculation of nuclear energy ϵ, opacity κ, and mass of species $F_{i,k}$ flowing across face k, are evaluated at time $t + \delta t$ with increase in time δt. We present the calculation of mass fraction $x_{i,k}$ for each species i due to the combined effects of convection and overshooting mixing as below (Paxton et al., 2015),

$$X_{i,k}(t+\delta t) - X_{i,k}(t) = dX_{burn} + dX_{mix}. \tag{3.11}$$

$$= \frac{dX_{i,k}}{dt}\delta t + (F_{i,k+1} - F_{i,k})\frac{\delta t}{dm_k}. \tag{3.12}$$

where $\frac{dX_{i,k}}{dt}$ is the rate of change from nuclear reactions computed by JINA Reaclib database and the mass of species, $F_{i,k}$ is defined by,

$$F_{i,k} = (X_{i,k} - X_{i,k-1})\frac{\sigma_k}{dm_k}. \tag{3.13}$$

where, $\sigma_k = D(4\pi r^2\rho)^2$ is the Lagrangian diffusion coefficient determined from Equation (3.8) and Equation (3.9). MESA solved this σ_k at the beginning of timestep and was held constant during the implicit solver iterations for improving numerical convergence.

3.2.2.2 Microscopic Atomic Diffusion and Gravitational Settling

Apart from the convection and overshooting as the main mixing processes, the microscopic diffusion and gravitational settling of elements can be an effective mechanism to modify stellar abundances. However, the inclusion of the atomic diffusion in stellar models does affect not only the abundances but also the mean molecular weight and the radiative opacity of the solar's radiative region. Elements like helium and heavy metals will tend to be diffused towards the center of the Sun due to gravitation while the hydrogen will be levitated. Hence the luminosity and neutrino fluxes between diffusion and non-diffusion models will be slightly varied for low-mass stars (Thoul et al., 1993).

Nevertheless, models with $M_i > 1.4\ M_\odot$ with this diffusion treatment has been predicted to cause an over-depletion of helium and worsen the stellar properties. Morel and Thévenin (2002) show that the problem arises from disappearing outer of the convection zone and a concomitant steepening of the temperature and pressure gradient. Therefore, our implementation of the atomic diffusion to our masses of solar-type (0.9 $M_\odot$ - 1.2 $M_\odot$),

is within such warrant in this thesis. The atomic diffusion implemented in MESA was based on implicit solution by Thoul et al. (1994) following the unmodified Burgers equation (Burgers, 1969). Then, we opted a MESA control which computes the transport of material by allocating all 12 species in the net reaction into 12 separate classes to be treated individually. Afterwards, diffusion velocities, w_i of each class will be determined using the semi-implicit, finite difference scheme described by Iben & MacDonald (1985).

To understand how MESA implement the process in its routine, we will present each species of particle s, as a distribution function $F_s(x, v, t)$ normalized to unit intergral, a mean number density n_s, an ionic charge $q_s \equiv Z_s e$, and a mass m_s. Temperature and overall hydrostatic equilibrium conditions are assumed to be constant and uniform for all species. Then, Burgers (1994) shows the diffusion velocity, $\mathbf{w_s}$ is just the relative difference of mean velocity of the fluid as a whole $\mathbf{u}$, and the mean species velocity $\mathbf{u_s}$,

$$\mathbf{w_s} = \mathbf{u_s} - \mathbf{u} \qquad \mathbf{u_s} = \frac{1}{n_s} \int d\xi \xi_i F_s(x, v, t) \qquad \mathbf{u} = \frac{1}{\rho} \sum \rho_s \mathbf{u_s}. \tag{3.14}$$

Additionally, it is crucial to define residual heat flow vectors r_{si}, to include the effects of thermal diffusion.

$$r_{si} = (\frac{m_s}{2 n_s k_B T} \int d^3\xi (\xi_s - u_i) |\xi - \mathbf{u}|^2 F_s) - \frac{5 \mathbf{w_{si}}}{2}. \tag{3.15}$$

The term i and j are used to represent spatial components of vectors whereas the function ξ_s is related to the diffusion velocity $\mathbf{w_s}$ through,

$$\xi_s(r) = \mathbf{w_s}(r) \rho(r) / T^{\frac{5}{2}}(r). \tag{3.16}$$

Then Burgers (1969) derives the collision integrals ($S_t^{(l)}$) and cross-sections ($\sum_{st}^{(l,j)}$) based

on fully ionized plasma from the Boltzmann equation to acquire these two equations

$$S_t^{(l)}) = 2\pi \int_{\infty}^{0} (1 - cosX_{st}) b \; db. \tag{3.17}$$

$$\sum_{st}^{(l,j)} = \frac{4\pi}{\pi^{\frac{3}{2}}} \int_{\infty}^{0} e^{(\frac{-v^2}{\alpha_{st}^2})(\frac{v^{2j+3}}{\alpha_{st}^2} S_{st}^{(l)})} dv. \tag{3.18}$$

where $\alpha_{st}^2 = 2k_B T/\mu_{st}$ and v represents the relative velocity of colliding particles. The angle deviation ξ_{st} is a function of both v and the impact parameter b that depends on the two particles interaction. The resistance coefficient K_{st}, in terms of collision integral and some dimensionless coefficients $z_{st}, z''_{st}, z'''_{st}$ are introduced and defined as the following constraints

$$\begin{aligned} K_{st} = K_{ts} &= \frac{2}{3} n_s n_t \mu_{st} \alpha_{st} \sum_{st}^{(11)} \\ \sum_{st}^{(12)} / \sum_{st}^{(11)} &= \frac{5}{2}(1 - z_{st}) \\ \sum_{st}^{(13)} / \sum_{st}^{(11)} &= \frac{25}{4} - \frac{25}{2} z_{st} + \frac{5}{2} z'_{st} \\ \sum_{st}^{(22)} / \sum_{st}^{(11)} &= z_{st} \\ \sum_{st}^{(23)} / \sum_{st}^{(11)} &= z'''_{st}. \end{aligned} \tag{3.19}$$

Now,the basic Burgers' diffusion equation for the plasma species, s with partial pressure P_s,mass density ρ_s,charge density ρ_{es}, number density n_s can be simplified as shown below,

$$\nabla p_s - \rho_s \mathbf{g} - \rho_{es} \mathbf{E} = \sum_{t \neq s} K_{st}(w_t - w_s) + \sum_{t \neq s} K_{st} z_{st} \frac{m_t \mathbf{r}_s - m_s \mathbf{r}_t}{m_s + m_t}. \tag{3.20}$$

For total number of plasma species s, the Equation (3.20) must be solved together with the $2S + 2$ unknowns which are diffusion velocities $\mathbf{w_s}$, S heat flow vectors (r_s), the electric field $\mathbf{E}$, and the gravitational acceleration $\mathbf{g}$. Thoul et al. (1994) had solved new resistance coefficients based on the collision integrals in Equation (3.20) and introduce an expression in Equation (3.21) as a dimensionless new matrix scheme. They use a pure Coulomb potential with a cutoff at the Debye length, introduced by Iben & MacDonald (1985) to determine various $z_{st}, z''_{st}, z'''_{st}$ coefficients. Thoul's approach has allowed MESA to implement the scheme into a correct and suitable numerical calculation in its routine for an entirely closed system. Contributions from pressure, temperature, or concentrations from the left-hand side of Equation (3.21) will provide the construction of the diffusion velocities for each species, W_j on the right-hand side.

$$\frac{p}{K_0}(\alpha_i \frac{dlnp}{dr} + v_i \frac{dlnT}{dr} + \sum_{j=i}^{s} \gamma_{i,j} \frac{dlnC_j}{dr}) = \sum_{2S+2}^{j=1} \triangle_{i,j} W_j \quad . \tag{3.21}$$

with the boundary conditions,

$$W_j = \begin{cases} w_j & \text{for } j = 1....S \quad (3.22) \\ r_j & \text{for } j = S + 1...2S \quad (3.23) \\ K_0^{-1} n_e e E & \text{for } v \quad (3.24) \\ K_0^{-1} n_e m_p g & \text{for } j = 2S + 2\ . \quad (3.25) \end{cases}$$

where S is the total number of species in the gas and $C_j = n_j/n_e$ is the concentration of j species. The physics of the particular types of interactions within ideal gases is fully contained in the coefficients K_{st}, z_{st}, z'_{st}, and z''_{st}. Details of the full implementation of the matrix scheme into the MESA diffusion routine and their definitions of K_0, α_i, v_i, γ_{ij}, and ∇_{ij} can be found in Paxton et al. (2015); Thoul et al. (1993).

As a result, the mass fraction of species s due to the atomic diffusion is given by the Equation (3.26). The $\xi'_{\mathbf{s}}$ here is the derived function that depends on determined parameters in Equation (3.21) and their corresponding coefficients (Equations (3.22) to (3.25)).

$$\frac{\partial X_s}{\partial t} = -\frac{1}{\rho r^2}\left(\frac{\partial}{\partial r}[r^2 X_s T^{\frac{5}{2}} \xi'_s(r)]\right). \tag{3.26}$$

Hereby, we present the numerical implementation of the atomic diffusion, gravitational settling, convection, and convection-overshooting in the stellar chemical compositions. Then, to be able to solve the complex abundance equations together with other stellar structure equations, MESA organized so that every physics module (EOS, opacities, reaction rate, initial compositions, etc..) or the matrix operations to be independent of each other in the code. Therefore, it is easy to call in from an external module and compute them in the right order as intended. In MESA, a module named 'star' is the main module uses to call in other modules. We illustrate the computational process with flowchart 3.1 to give an overview of how the MESA star module (refer to $MESADIR_star) evolves a star over a course of time with a 1D approximate solution.

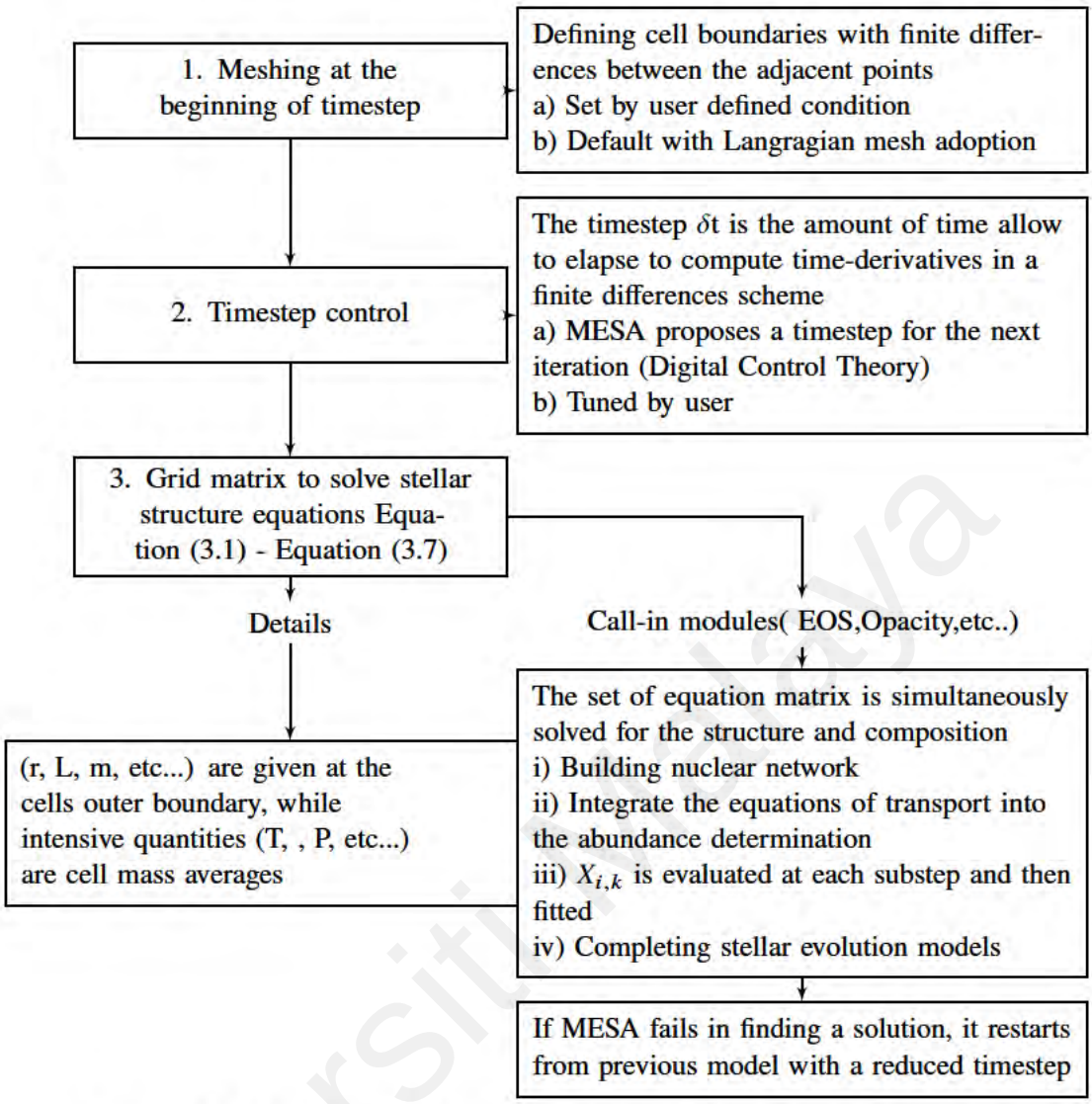

Figure 3.1: Flowchart of the the main module algorithm in MESA star.

3.2.3 Standard Solar Model Calibration

To confirm the quality of the MESA evolution module used in this research computation, any solar modeling made should be validated first and they should be consistent with the helioseismology. Hence a model must be calibrated to fit the observational constraints such as the present-day solar luminosity, solar radius, metallicity, and the flux of solar neutrinos. Other constraints widely used are the seismic surface helium solar abundance, radius of the convection zone and the sound speed profile. Generally, we will calibrate model by using a simplex search method to acquire a set of input parameters that represent the inferred solar properties. Here we adopt the initial metallicity mass fraction, $Z = 0.02$, whereas

the hydrogen mass fraction, X would follow according to the fraction rule $X = 1 - Y - Z$. Table 3.1 summarizes of other inputs adopted in the calibration.

The best calibrated model named 'fitted model' was obtained by adjusting two free parameters, which are initial helium, Y_{ini} and mixing length, $\alpha_{\rm mlt}$. The MESA code provides a built-in simplex optimizer routine called SIMPLEX SOLAR CALIBRATION to finely tune these 2 parameters, proposing the best matching model to fit helioseismology constraints. For each iteration in the calibration routine, a new set of parameters Y_{ini} and α are drawn for each process until the χ^2 value seizes to nearly zero. χ^2 analysis determines whether there is a significant difference between the fitted solar model generated and the solar observations. Table 3.2 shows our calibration results with their respective fractional percentage of errors.

Table 3.2: Result of the fitted solar model calibration at solar age of 4.57×10^9 year.

Model	Y	L(erg s^{-1})	$R\times10^{10}$(cm)	R_{cz}	$T_{\rm eff}$ (K)
Standart Solar Model	0.2485	3.839x10^{33}	6.957	$0.713R_\odot$	5778
Fitted Model	0.251	3.843 x 10^{33}	6.967	$0.713R_\odot$	5778
Fractional Error %	1.2	0.10	0.14	5x10^{-2}	5x10^{-3}

The results of the standard solar model, (SSM) in Table 3.2 were obtained from the observed frequencies of solar oscillations by Basu and Antia (1997). They are all in excellent agreement with our fitted model with good statistic χ^2 except for the surface helium abundance. Although there is a noticeable discrepancy for the helium, the percentage of fractional error is still within the acceptable margin. Figure 3.2 shows that the sound speed profile of the fitted model is also in a good agreement with the standard solar models by Bahcall et al.(2000, hereby BP2000) and Bahcall et al. (1998, hereby BP98).

Besides, even the solar interior structures of our model are identical to BP2000. The similarities of both structure models were presented in Figure 3.3 and Figure 3.4. Results on the total solar luminosities, solar radius, as well as the evolution of convection zones and nuclear power burning are shown in the remaining figures as a function of the star's age (Figures 3.5 - Figures 3.7). Note that the model presented is calculated from the PMS to the present-day by adopting a maximum of the time step, δt_{max} = 0.1 Myr with a total number of 50,000 step models. Overall, the results on the evolutionary tracks and the Hertzsprung-Russell, HR diagram in Figure 3.8 present trends that are matched with the proposed solar evolution in Kippenhahn et al. (1990); Taylor (2001). Therefore, it demonstrates that the MESA module is capable of stellar evolution calculations, particularly for the solar type-stars in this work.

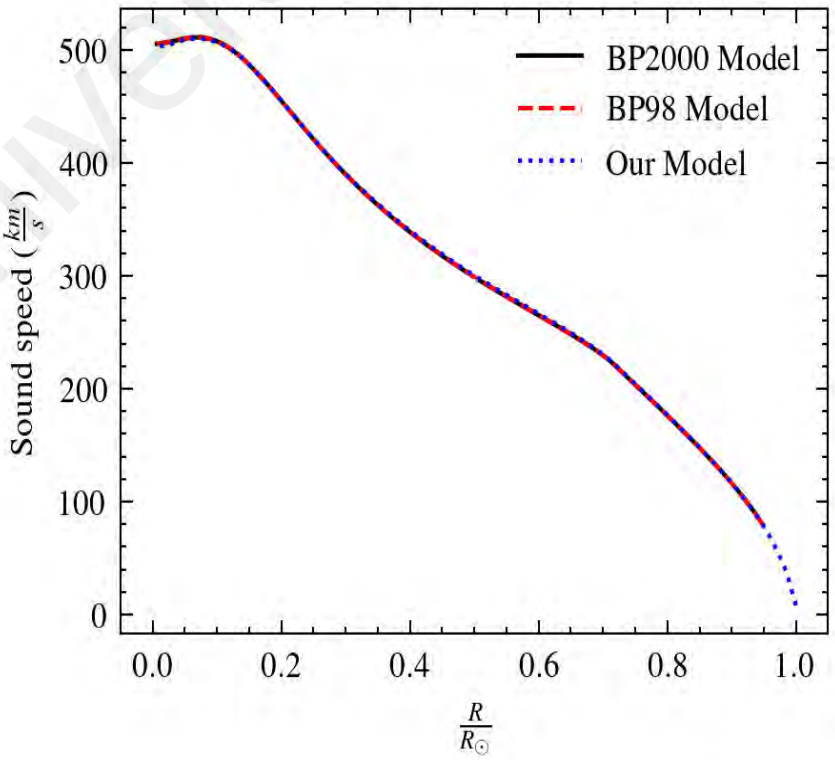

Figure 3.2: Sound speed profile of the solar interior.

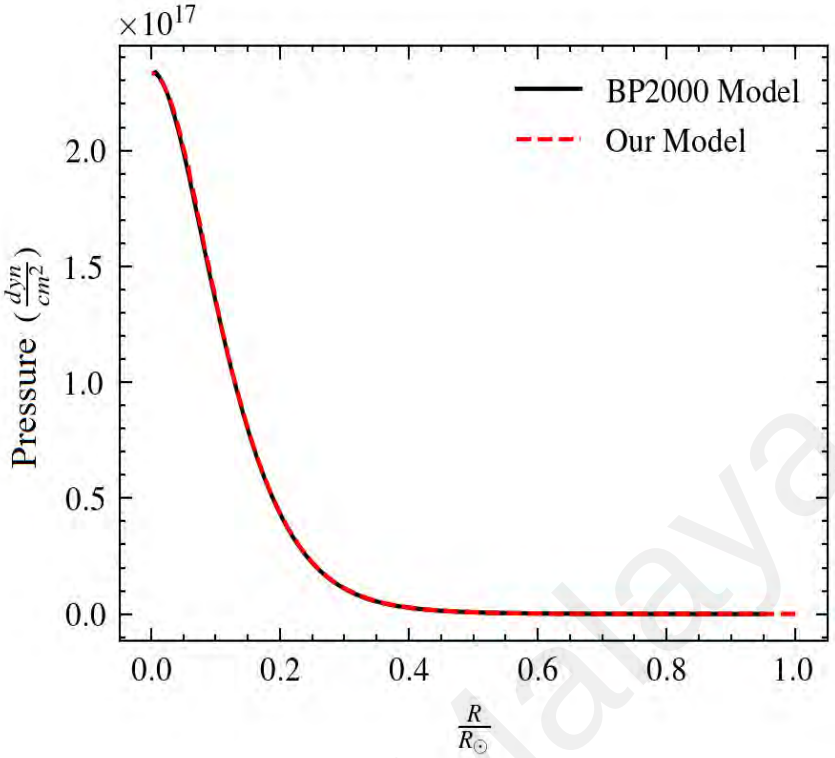

Figure 3.3: Pressure againts solar radius.

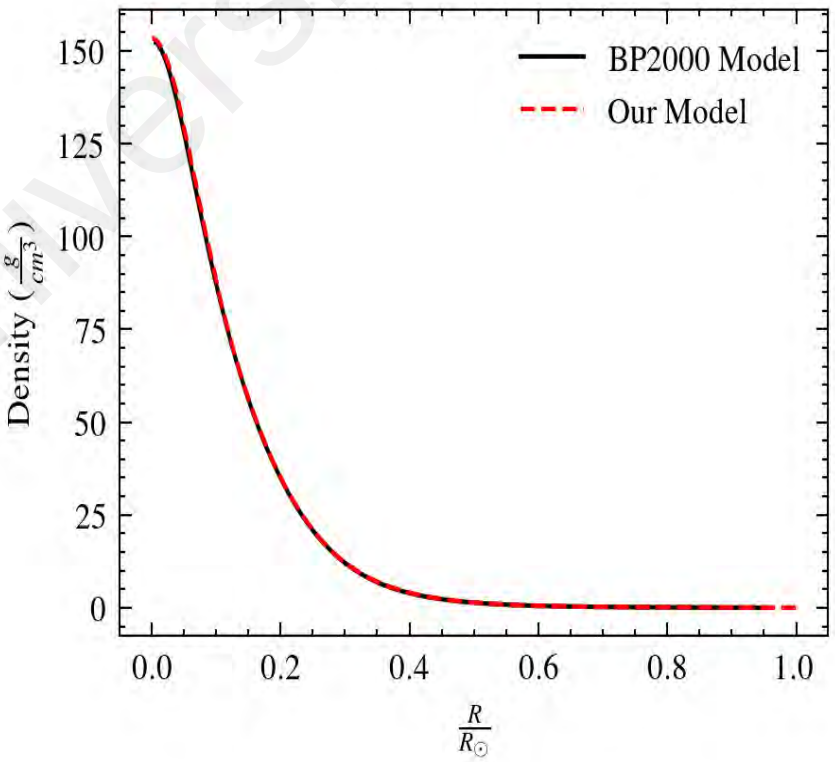

Figure 3.4: Density againts solar radius.

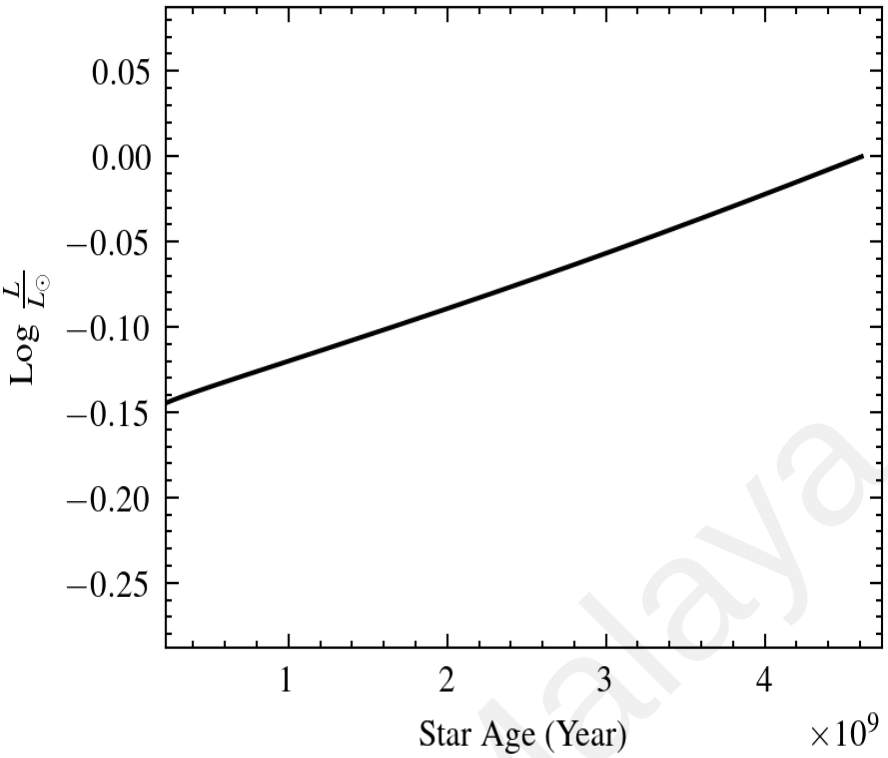

Figure 3.5: Evolution of solar luminosity from PMS to the present solar age, 4.57×10^9 year.

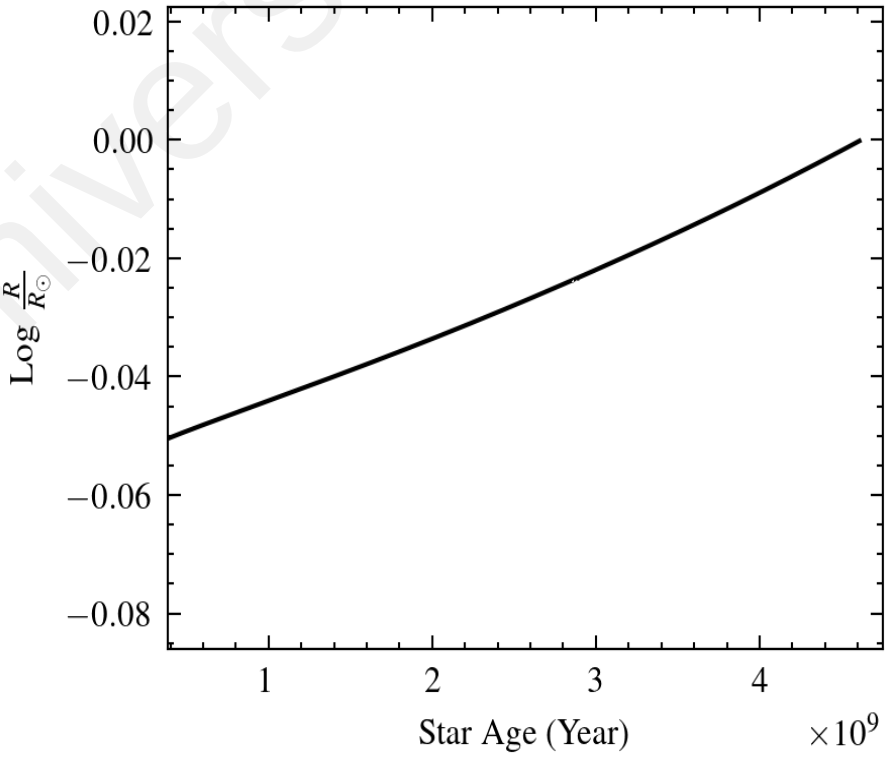

Figure 3.6: Evolution of solar radius from PMS to the present solar age.

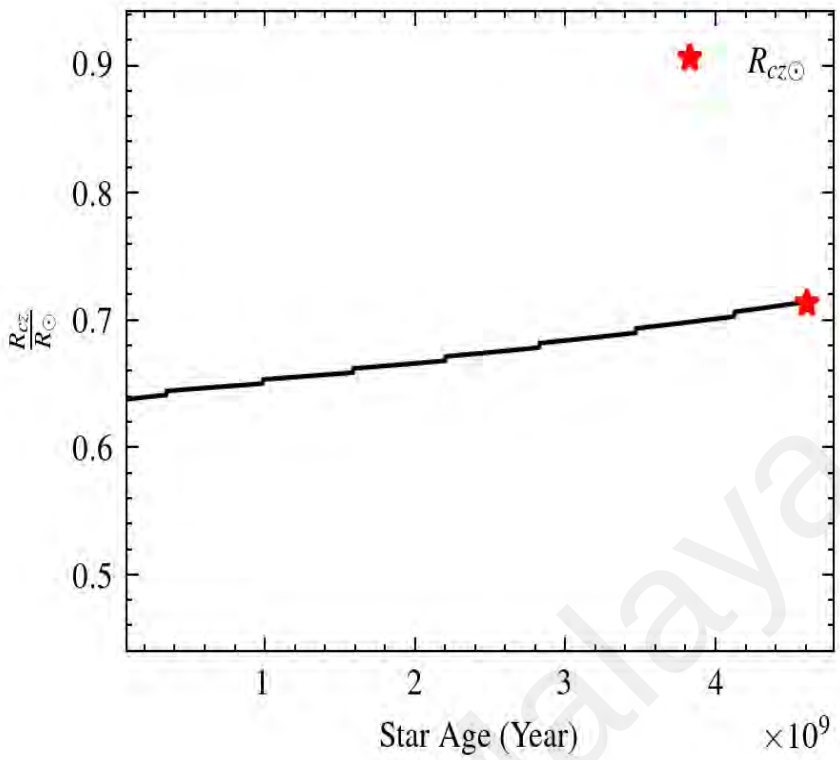

Figure 3.7: The fractional radius of the convection zone, R_{cz} in respect of solar radius against time. The evolution starts from PMS to the present solar age. The red star indicates the location of helioseismology, R_{cz} at $0.713R_\odot$.

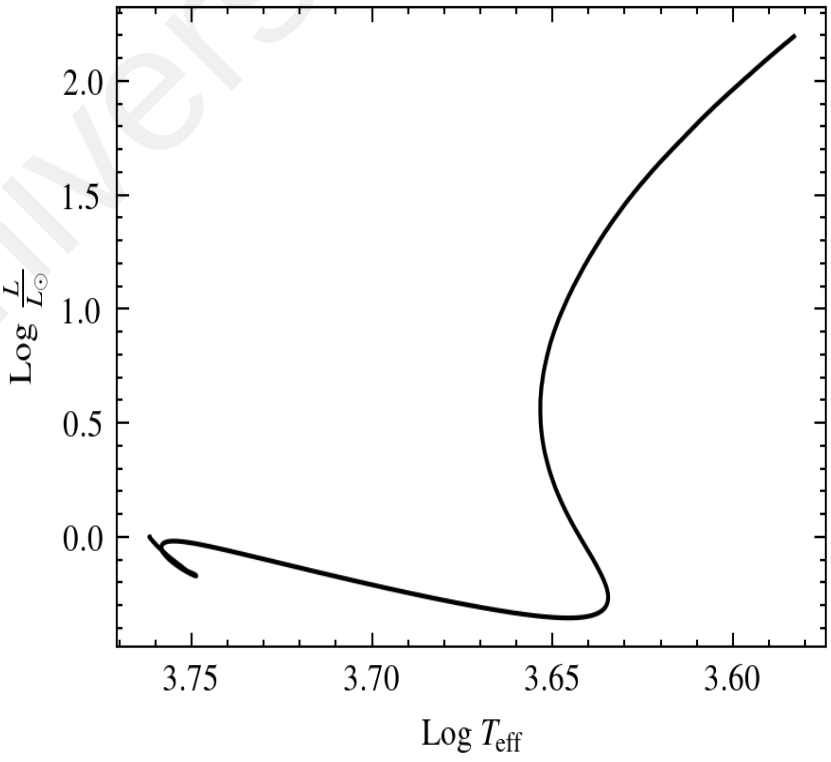

Figure 3.8: HR diagram for 1 $M_\odot$ from PMS until the present solar age.

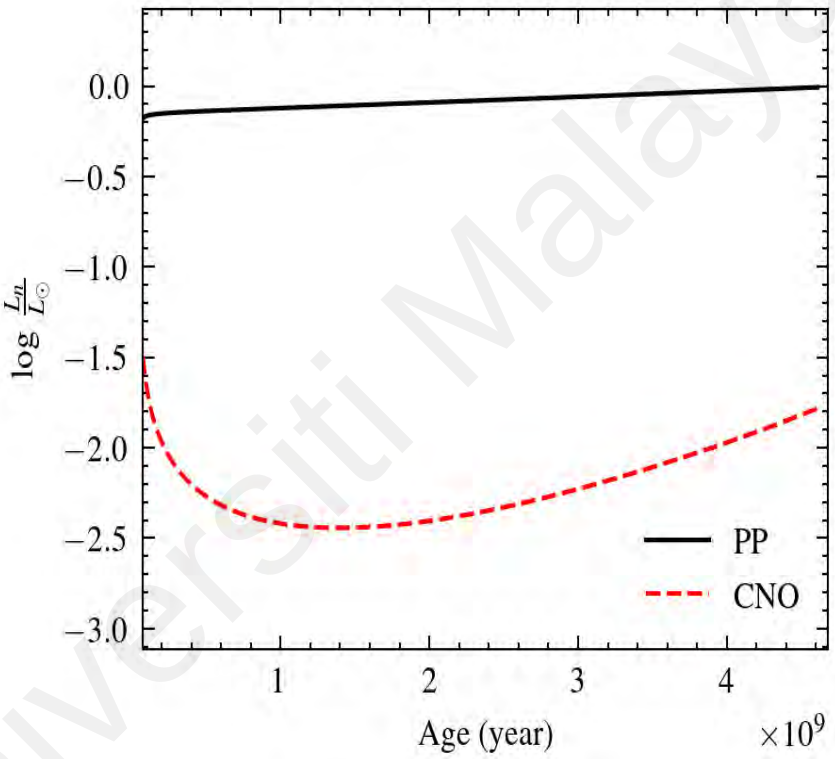

Figure 3.9: Evolution of radiant power emitted by nuclear burning, L_n(nuclear) by the PP and CNO with respect to solar luminosity, $L_\odot$ unit until the present age.

3.3 Determination of Solar Abundances

It is necessary for this work to compute chemical compositions that is consistent with the observations. Therefore, we compare the profile of our main solar abundances, ^{1}H and ^{4}He to the abundances derived from the standard solar model, BP2000 in the following Figure 3.10. Comparing between these two models demonstrates an excellent match for the hydrogen and helium abundances, whereas Figure 3.11 shows a similar trend for other smaller fraction compositions except for some discrepancy at 9% with ^{16}O. The possible reason for such ^{16}O difference may come from the fact that BP2000 was computed with the fusion cross sections by NACRE (Angulo et al. 1999) rather than the JINA database in this work. JINA (Cyburt et al., 2010) implements a much lower computation of ^{14}N(p, γ)^{15}O event rate for the low temperatures compared with the rate is given in NACRE, therefore reducing the burning of ^{14}N in our computed model.

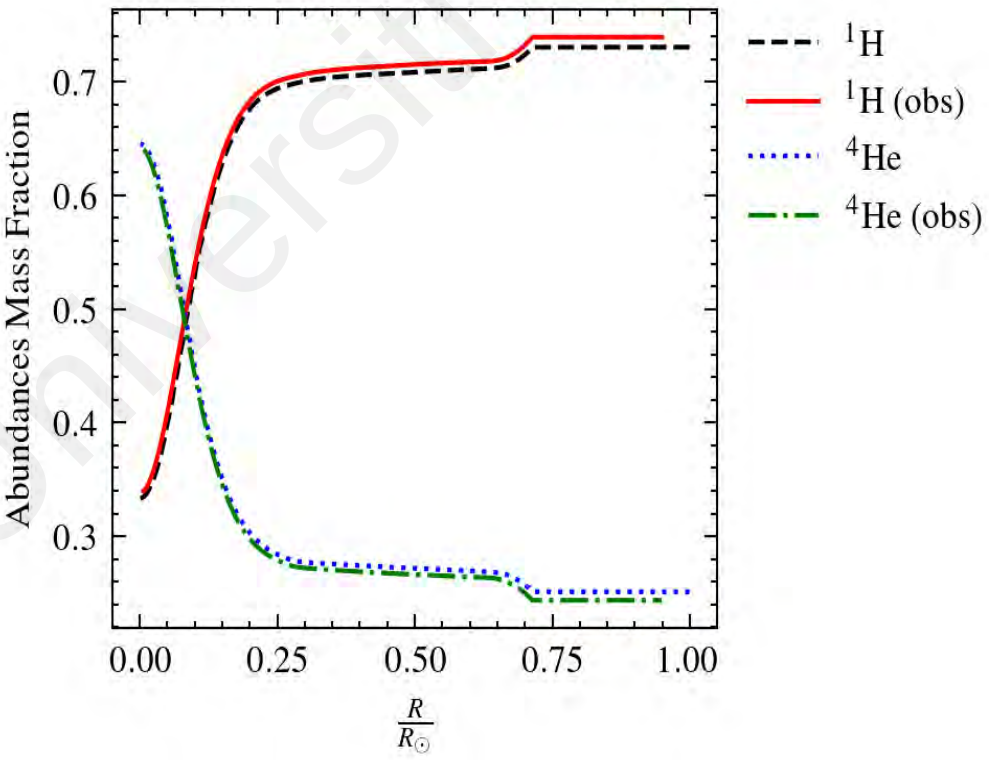

Figure 3.10: Profile of ^{1}H and ^{4}He abundances in terms of the mass fraction at the present age. The observed results (obs) are obtained from the standard solar model, BP2000.

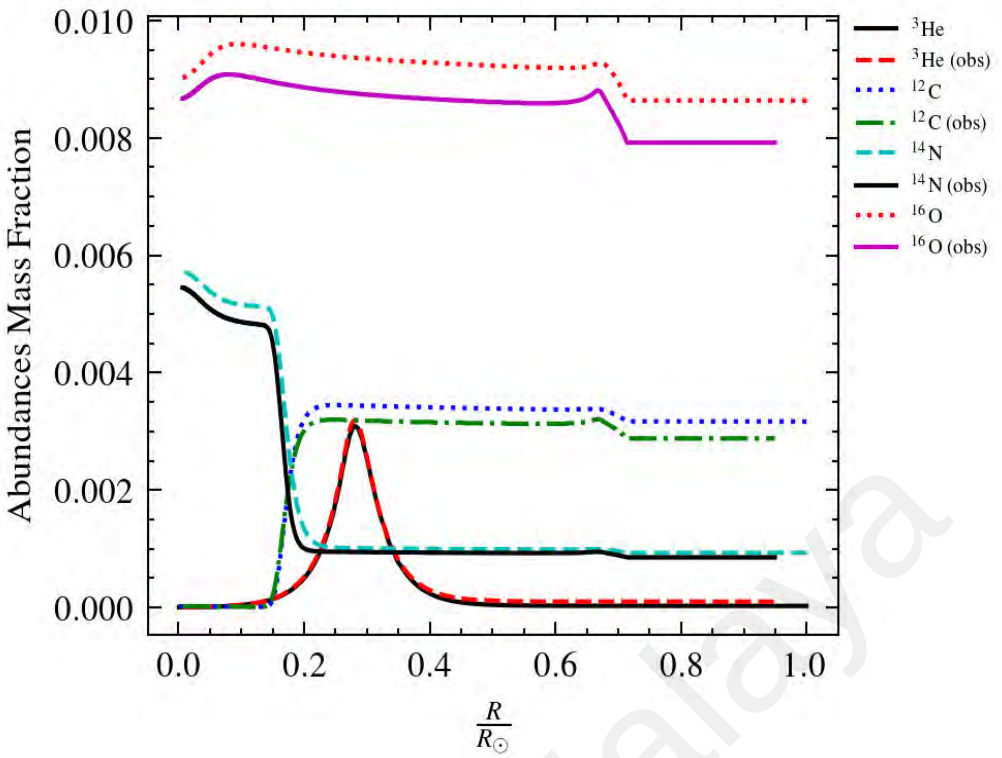

Figure 3.11: Other chemical abundances against solar radius in terms of the mass fraction at the present age.

Other than that, no dramatic difference was found in our calculated chemical compositions. We would want to emphasize that our work is not a systematic exploration of the sensitivity due to the different nuclear rate databases, hence general conclusions drawn from the previous solar calibration model, therefore remain valid. The MESA computation indeed has been able to reproduce similar surface solar abundances as inferred in the helioseismology. We hereby defined this fitted model as our standard solar reference used consistently in this thesis. We will then continue to investigate the importance of the transport mechanisms and how they may affect chemical compositions and interior solar structure in general.

3.4 The Effects of Solar Transport Mechanisms

Even though the theory of local convection mechanism has generally been recognized as a standard process working in stars modeling, however the determining of the exact depth of overshooting zone is still a controversial subject. The trouble is caused by the

undefined properties in the occurred turbulence convection. It is possible to apply an overshooting parameter, f up to $\approx$ 1 upper limit, however, the convective flows under adiabatic conditions move so fast that they will not be able to exchange heat efficiently with the surrounding when entering into the stable region (Herwig, 2000). In fact, Herwig et al. (1997); Paxton et al. (2010a); Schlattl and Weiss (1999) suggested an overshooting about $f = 0.016$, (which is equivalent to $\approx 0.2H_{\rm p}$ in the non-local theory) is sufficient enough to demonstrate a smooth extended temperature gradient below the solar convection zone with the influence of the helium and heavy metal diffusion. Therefore, we shall discuss the implication of adopting three different internal processes here which are distinguished by the fitted-overshooting, deep overshooting, and with the inclusion of diffusion mechanism in the modeling. Note that we will not tune each model to be solar-calibrated as we only want to get some hints about the chemical changes in the solar structure, and explanations for discrepancies between implementing different transport mechanisms. Besides, we had to carefully introduce the microscopic diffusion and gravitational mass settling in stellar evolution due to the problem arise in which in principle, the radiative levitation can be extremely efficient, following a a substantial mass loss. Therefore, the mass loss effect will be neglected in this study.

We first show the result of the temperature gradient against the solar fractional radius in Figure 3.12. In the absence of a diffusion mechanism, the model with overshooting of f = 0.014, produces a shallow sub-adiabatic region with a sharp transition of a temperature gradient to the radiative interior, which was to be expected. Meanwhile, when downflows strength was increased to the deeper region, $f = 0.05$, the temperature gradient has been smoothed out at the discontinuity and somehow destroys the adiabatic-radiative transition, including the convection bottom radius. Therefore, we interpret such deep overshoot mixing as impossible to be implemented in solar-type stars. It appears that the model

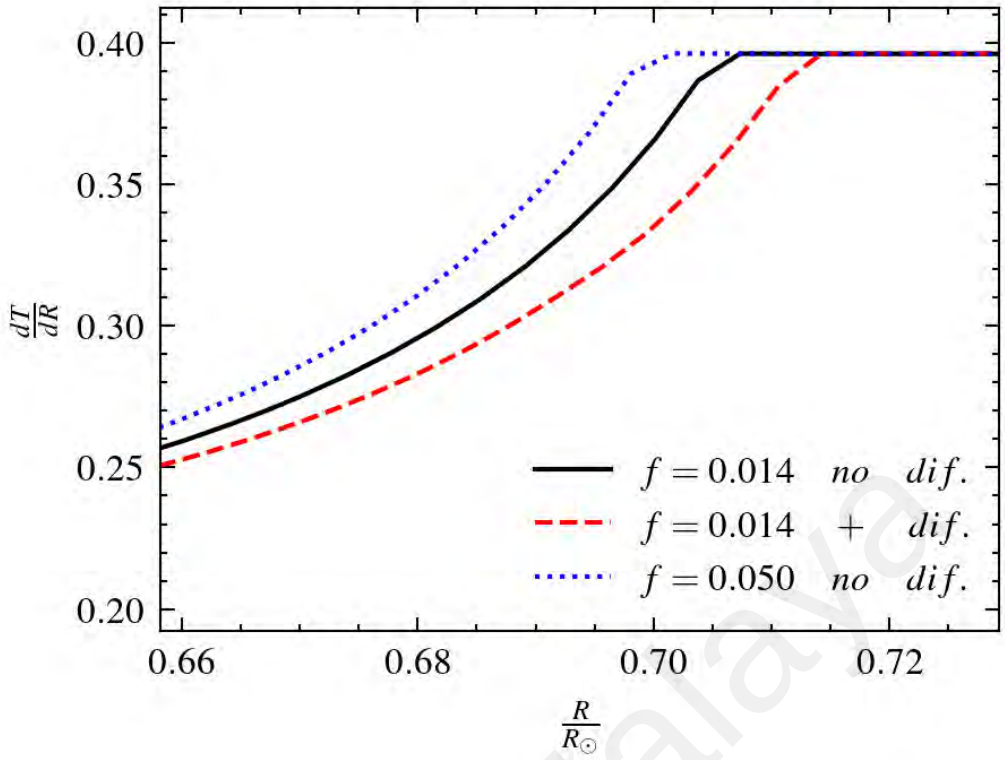

Figure 3.12: Temperature gradient against fractional radius near the mixing region. The solid line (black) adopting overshooting value as stated with no diffusion. The dashed line (red) is adopting a similar overshoot value but with diffusion (dif). The dotted line implies the deep overshooting without diffusion. Every model is adopting a local-mixing length theory with α_{mlt}=1.92.

with diffusion and some moderate overshoot value f = 0.014 may best preserve the super-adiabatic convective region without jeopardizing the radius of convection zone in the mixing. We then compute the convection velocity, v_d and as expected, we had a lower v_d when diffusion is included despite both models adopting the same parameter f = 0.014. The reason is, inclusion of diffusion model has however reduced the infer overshooting effect due to the increase in metal abundances right below the convective radius which follows a higher opacity value and decreases the convection efficiency.

However, the change in the abundance of each species is generally calculated based on the total summation of the v_d together with the atomic diffusion velocity, w_j. The diffusion velocity, w_j in Figure 3.13, shows that lighter element in the surface like ^{1}H has a positive diffusion value, proposing the outward motion.

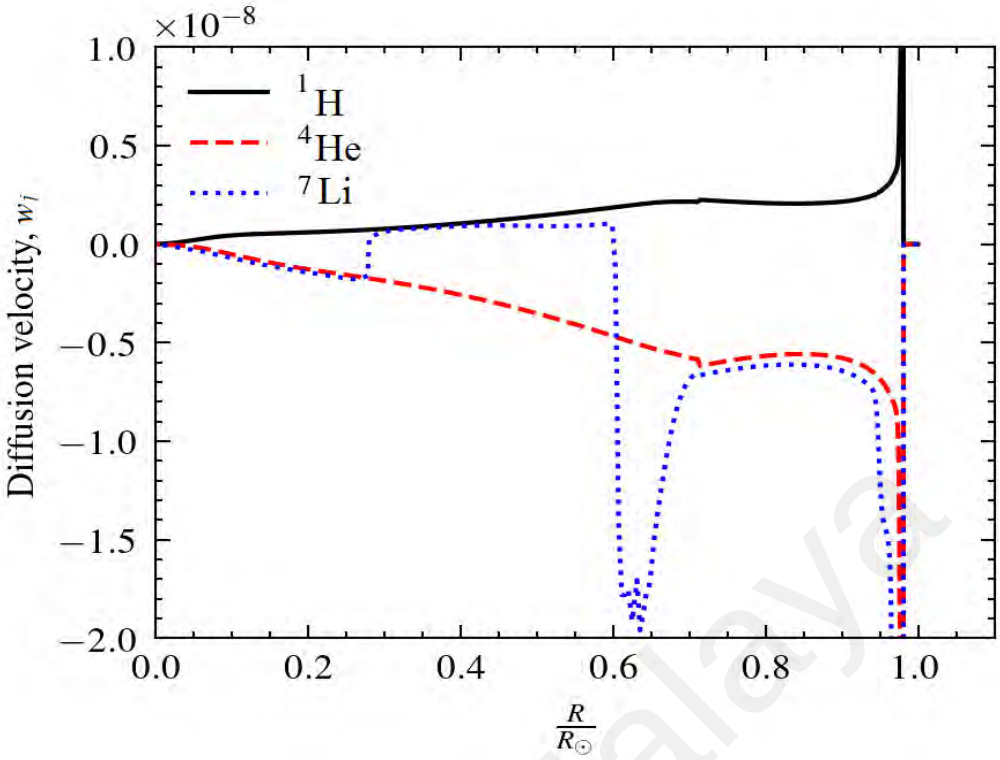

Figure 3.13: Profile of diffusion velocity in the solar interior for diffusion model. The diffusion velocity is in the unit of cm/s^2.

In contrast, some heavier elements such as ^{4}He and ^{7}Li with a negative velocity, will fall into the star's interior, leading to a lower value in the surface. The local increase in opacity must be considered when computing stellar internal structure and oscillation frequencies. Besides, Bahcall et al. (1995) had explained that the effect of the pressure gradient always dominates the diffusion velocities. Hence, we had noticed that if diffusion is neglected entirely, our calculated surface abundance of helium is Y_s= 0.278 (in mass fraction), which disagrees with the observed value by 12%. The model that includes both metal and helium diffusion has shown the best match with literature, which agrees with the observed value determined from p-mode oscillation data of R_{cz} = (0.713 ± 0.003). and determination of helium surface abundance (Basu & Antia, 1997).

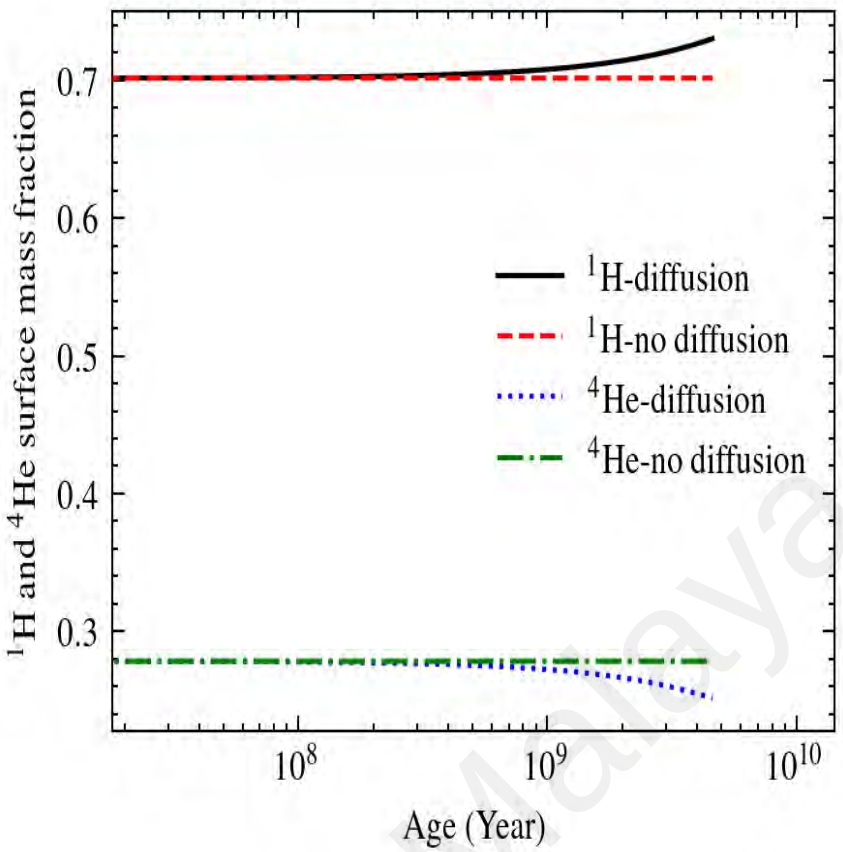

Figure 3.14: Evolution of ^{1}H and ^{4}He abundances from PMS to present age.

Figure 3.14 presents that the inclusion of diffusion had caused the surface abundance of hydrogen to increase higher in time and the surface abundance of helium to decrease lower in time compared to the convection-shooting model alone. Therefore we show the gravitational field in the solar interior at the present solar age for diffusion and non-diffusion models in Figure 3.15. There is gravitational settling in the solar interior, which follows a higher field towards the solar center and causes heavy elements to propagate inward despite the radiative force in the opposite direction. We then include a discussion on the internal solar structure in Figure 3.16 to show the tendency of ^{4}He to be pulled in gravitationally following a decrease in the surface whereas, lighter abundance, ^{1}H is transferred in the reverse direction. The result clearly suggests that diffusion can be an effective mechanism to transport the lithium abundance and lowering its surface value efficiently .

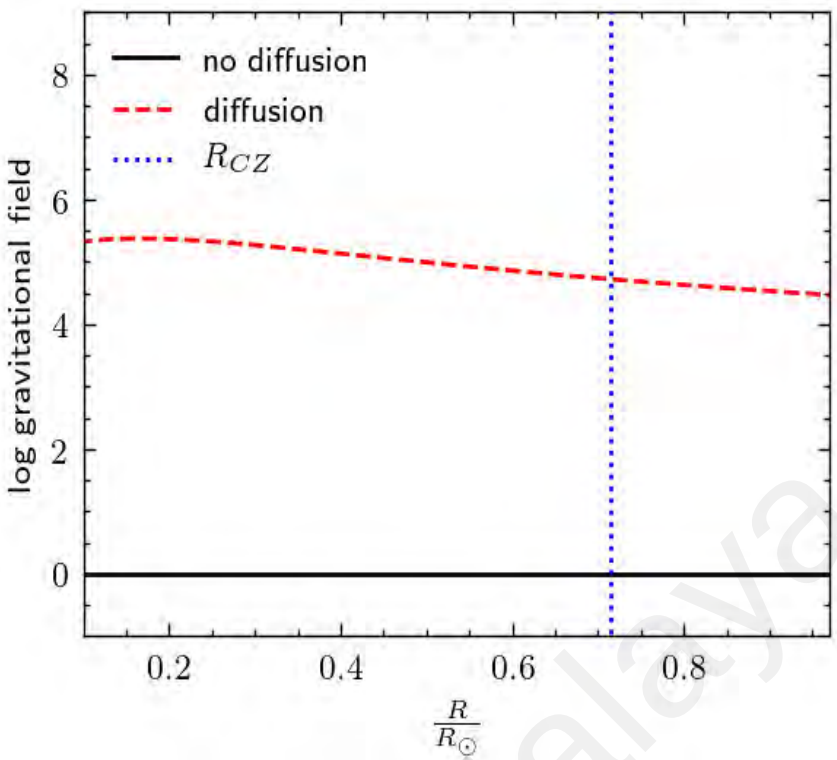

Figure 3.15: The log value of the gravitational field with respect to solar radius. The model with atomic diffusion can transport heavier elements effectively.

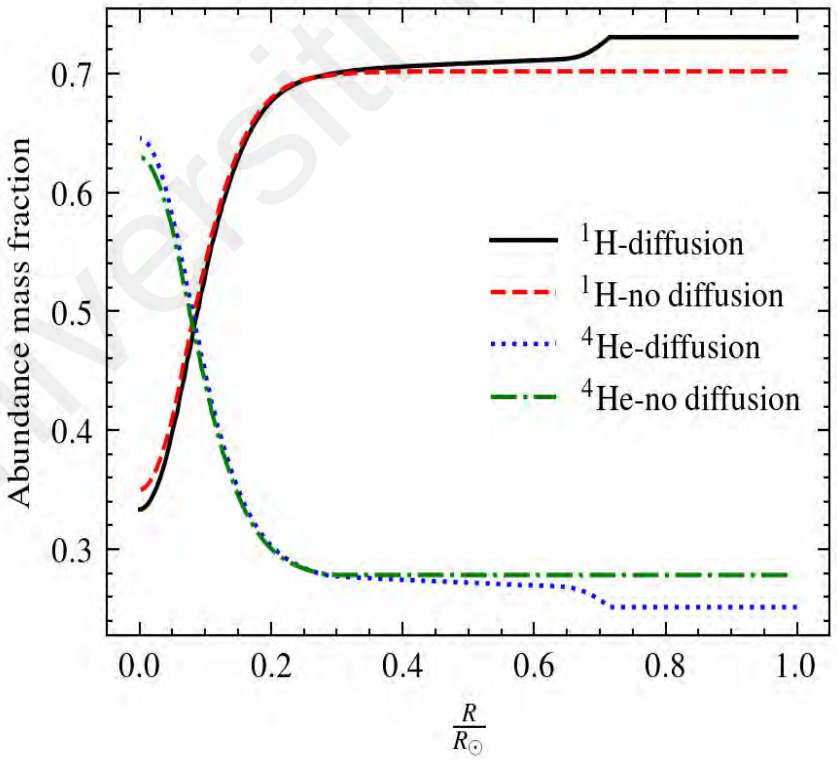

Figure 3.16: Profile of ^{1}H and ^{4}He abundances against solar radius at solar's present age.

3.5 The missing ^{7}Li abundance

At this point of research, we have concluded that the convection-overshooting model with the inclusion of diffusion treatment has consistently given the best match of the solar-type properties. Then, we continue to evaluate whether the mechanisms can answer the major lithium depletion on the solar surface. Figure 3.17 presents the profile of lithium abundance in the solar structure. We had discussed in the literature where lithium will undergo a beta decay if exposed to an extreme temperature in the radiative region. Hence, a sharp gradient of lithium burns can be examined at the mixing zone, which is in between the convective and the radiative zone, while leaving the stable lithium dwells on the base of convection radius and above. As expected, the ^{7}Li abundance of the observed photospheric in AGS98 is indeed 2 times lower compared to our predicted value which is shown in the summary Table 3.3. Furthermore, we present the evolution track of ^{7}Li abundance against time until the present age in Figure 3.18. It was verified that the model with diffusion or no diffusion has failed to explain the missing lithium. Besides, the rapid depletion had occurred mainly at the pre main-sequence years, $\approx 10^7$ years with the temperature at 10^6 K, right before the protosolar reaches the fusion temperature (14×10^6 K). There is no significant change in the lithium content between the Zero Age Main Sequence and the present solar age, which can be concluded.

Overall, we draw a conclusion that even though the diffusion transport mechanism has brought a higher lithium diffusion mixing, it is shown that the abundance was just scarcely modified by the standard mixing processes adopted here, confirming the failed attempts made in the past to solve the lithium problem. Therefore, we continue to investigate other proposed solutions by looking beyond the standard solar model, such as the implementation of solar rotation and the rotation-induced magnetic field to explain the missing ^{7}Li.

Table 3.3: Comparison of surface lithium abundances of the calibrated model and the Grevesse and Sauval (1998). The X, Y and Z are the inputs adopted in the model in the unit of mass fraction. The ^{7}Li abundance is in the unit of dex.

Z	Y	X	THIS WORK (^{7}Li)	GS98 (^{7}Li)
0.02	0.278	0.702	3.103	1.07

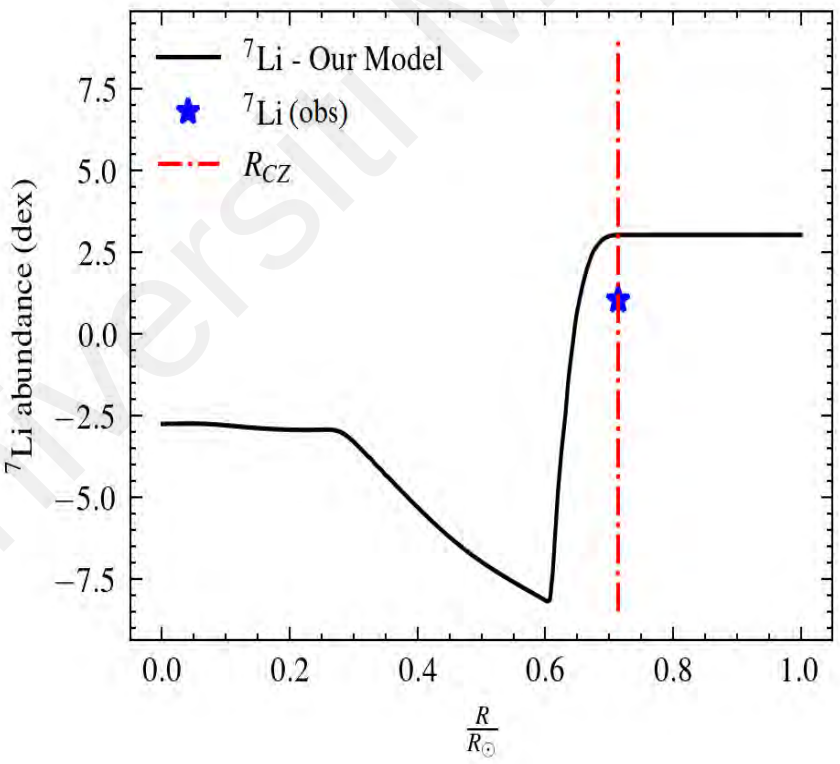

Figure 3.17: Profile of lithium abundance against radius at solar's present age. The star is the observed value inferred by GS98, whereas the vertical blue line is the convection radius at R_{CZ}=0.713$R_\odot$.

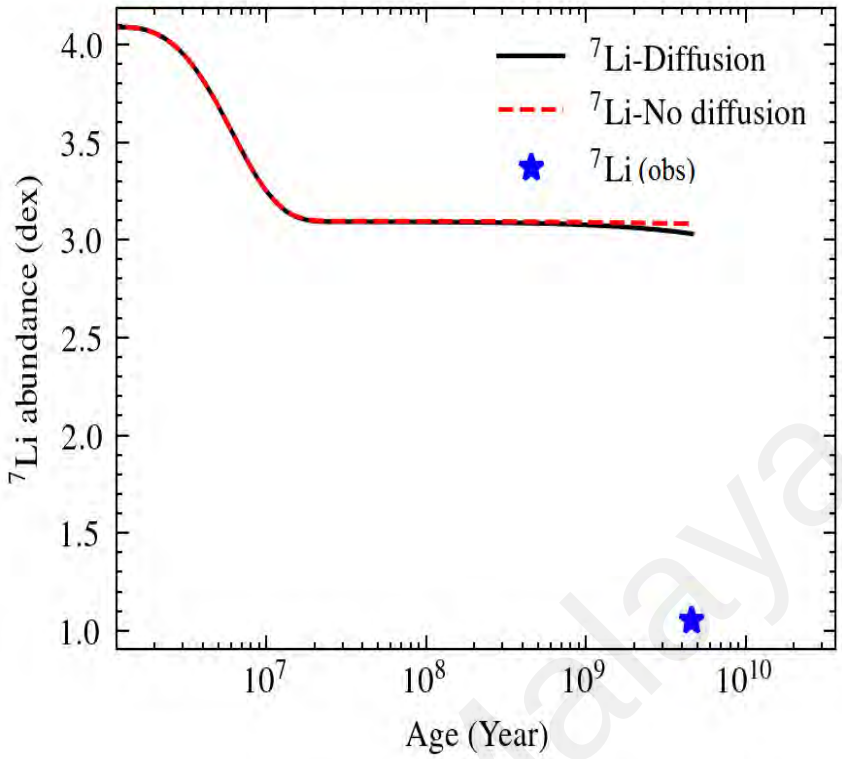

Figure 3.18: Evolution of ^{7}Li abundance from PMS to present age.

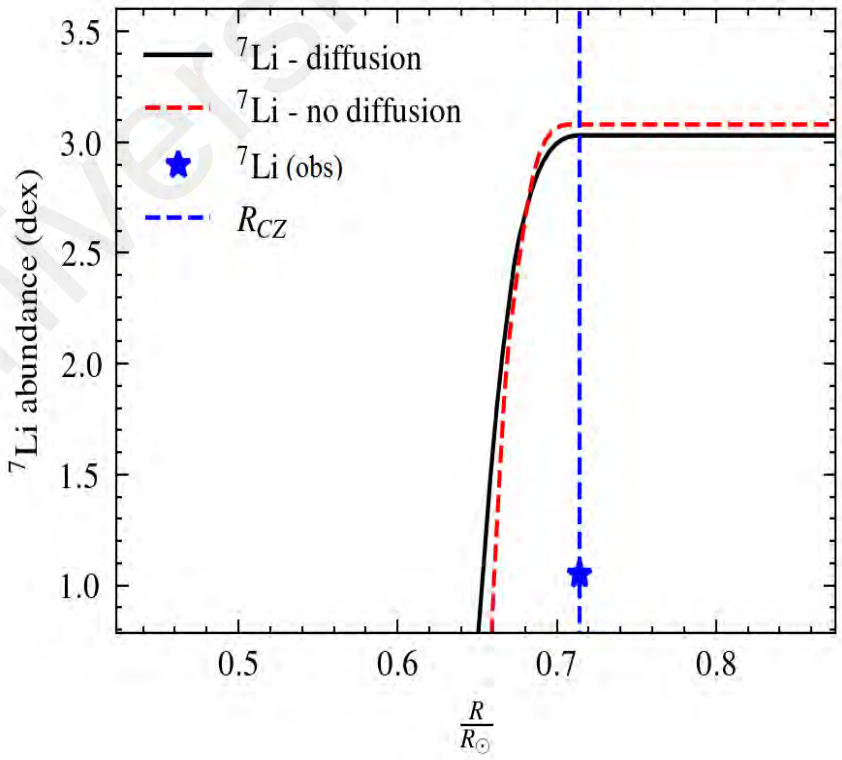

Figure 3.19: Comparison for ^{7}Li solar abundance against fractional radius at present age with and without diffusion treatments.

3.6 Non-Standard Solar Model

In this subsection, we will then study the effect of solar rotation on the chemical abundances to account for the missing ingredient to enhance the mixing process in the solar interior. MESA computes the rotation module by treating the mass shells correspond to chemically homogeneous cylindrical fluid parcels (so-called isobars) instead of spherical shells. Then solve the stellar structure equations in one dimension with constant angular velocity, ω_i to change acceleration and the radiative temperature gradient. The changes can cause strong an-isotropic turbulence acting in the direction of the isobar. While in radiative regions, such turbulence is caused by differential rotation and effectively removes gradients along isobars while enforcing shellular rotation (Meynet & Maeder, 1997; Zahn, 1992). Furthermore, centrifugal forces act on material in rotating stars can disrupt the initial assumption of a star's spherical symmetry. But for slow to moderate rotation, these deformations can remain as rotationally symmetric with some modifications to the equations of constant pressure, constant density, and constant temperature (Langer et al., 1999; Tassoul & Tassoul, 1984)

After that, the chemical mixing due to rotational instability is implemented via diffusion approximation technique (Paxton, 2013; Endal & Sofia, 1978; Pinsonault et al., 1989; Heger et al., 2000). Methodically, the final turbulent viscosity, v is calculated based on the total summation of diffusion coefficients from both convection and rotational-induced mixing. We present diffusion coefficient, D_{mix} for rotational which have accounted for five different causes of instability. They are Dynamical Shear Instability (DSI), Eddington-Sweet Circulation Instability (ESC), the Goldreich-Schubert-Fricke (GSF), Solberg-Hoil Instability (SHI), and Secular Shear Instability (SSI). A more detailed discussion on the physics derivation on each mixing coefficients, D can be referred to Heger et al. (2000). The diffusion coefficients used in this study are susceptible to some uncertainty because

they are based on order-of-magnitude estimates by computation timescales.

$$v = D_{convection} + D_{DSI} + D_{SHI} + D_{SSI} + D_{ECS} + D_{GSF}. \tag{3.27}$$

Finally, the computation will include the angular momentum and atomic diffusion equations, which will be solved for each time step. Adopting rotation in the model also implies magnetic field generation. The magnetic fields might transport angular momentum by torques or cause instabilities by magnetic buoyancy resulting from the winding up of magnetic field lines by differential rotation. Besides, Spruit (2002) has reported that the measured rotational gradient in the tachocline of the slowly rotating Sun is large enough for dynamo action to set in but only valid within the presence of microscopic magnetic and thermal diffusion in the analysis. Hence, MESA executes the magnetic field effect as prescribed by Tayler-Spruit-Dynamo theory (Spruit, 2002) which will modify the angular momentum transport, which leads to greater chemical mixing efficiency. Therefore, we construct two comparison models which include rotation without the magnetic field and another with the presence of the magnetic field. Here solar evolutionary sequences adopt a helioseismic rotational velocity of the solar surface, 2 km/s, and increase differential rotational speed as spherical shells move towards the solar core. The result in Figure 3.20 shows no variation in general to the luminosity nor the solar structure between the comparison models. In fact, the rotation model without the induced magnetic field has a similar radius of the convection zone, $R_{cz} = 0.713 R_{\odot}$, with the standard solar model SSM earlier. Whereas the model with the magnetic field inclusion increased R_{cz} slightly by 0.05% compared to the rotation-only model. Figure 3.21 and Figure 3.22 show the evolution of lithium abundance and the lithium profile in the solar interior respectively.

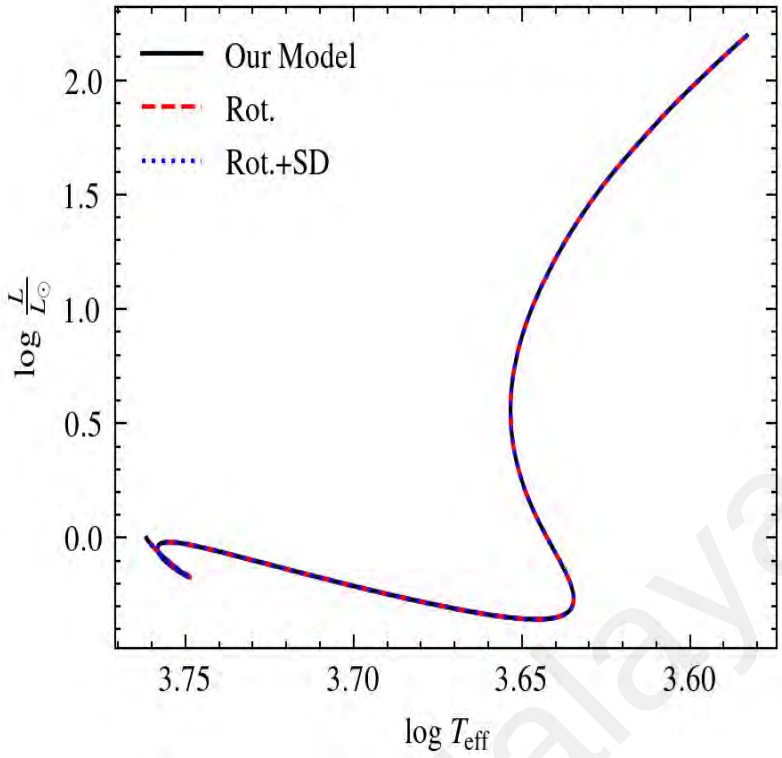

Figure 3.20: Log L against log R for different solar models comparison from the age of PMS until the present-day. The fitted model is from the SSM calibrated model, the 'Rot.' defined as the rotational-only model, and 'Rot.+SD' is the rotational model with the induced magnetic Spruit-Dynamo.

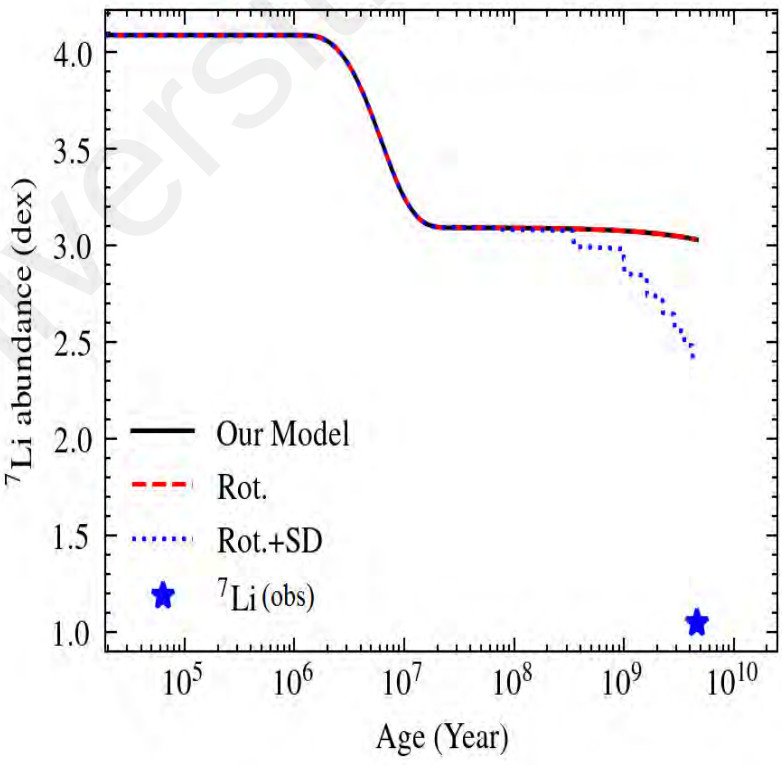

Figure 3.21: Evolution of ^{7}Li abundance from PMS to present-day. The blue star holds the same definition as previously.

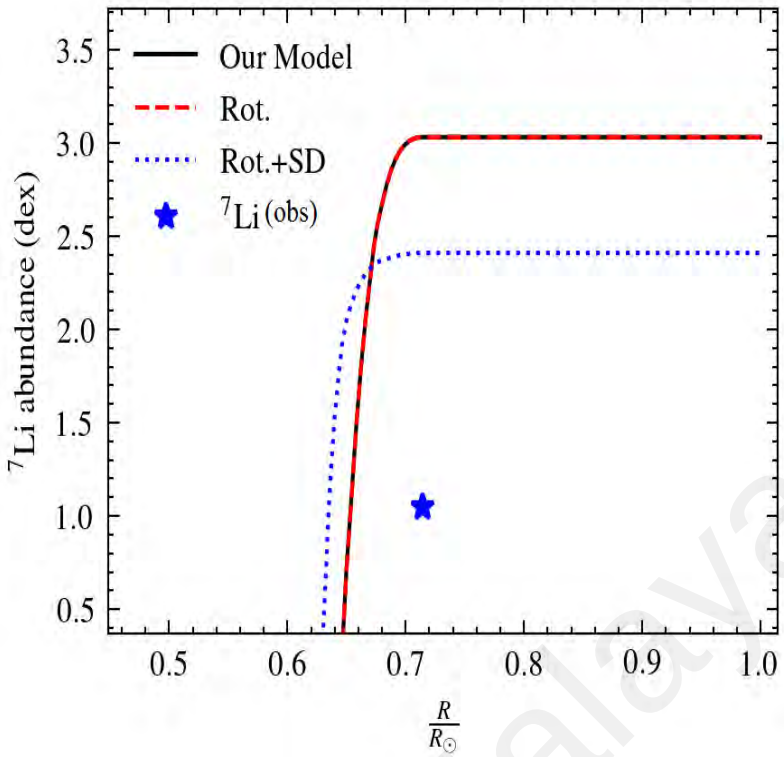

Figure 3.22: Profile of ^{7}Li abundance in solar structure. Symbols as in Figure 3.18.

Surprisingly, we found some interesting lithium depletion although the comparison models have about similar solar properties. This can be explained by looking at Figure 3.23 where the diffusion can occur inside the radiative layers for the rotating models. We observed that the rotational-only model has a diffusion discontinuity and odd abrupt transition at the mixing region, which might explain the undisturbed solar abundances comparison. On the other hand, lithium depletion was enhanced by 0.94 dex at the MS when we had adopted a rotation with the Tayler-Spruit dynamo mechanism. This result due to magnetic stress angular momentum transport is highly anisotropic and far more effective at smoothing out horizontal variations in rotation. Therefore the surface rotational of stars can carry the abundances and cause mass overshooting within the star (Endal & Sofia, 1978; Pinsonneault et al.,1989). Even though rotational with the induced magnetic field had offered such a promising solution, the approach has also failed to reproduce the desired result. We will investigate this further in chapter 4 to cater to the possibility of increasing mixing by exploiting higher solar rotation rates.

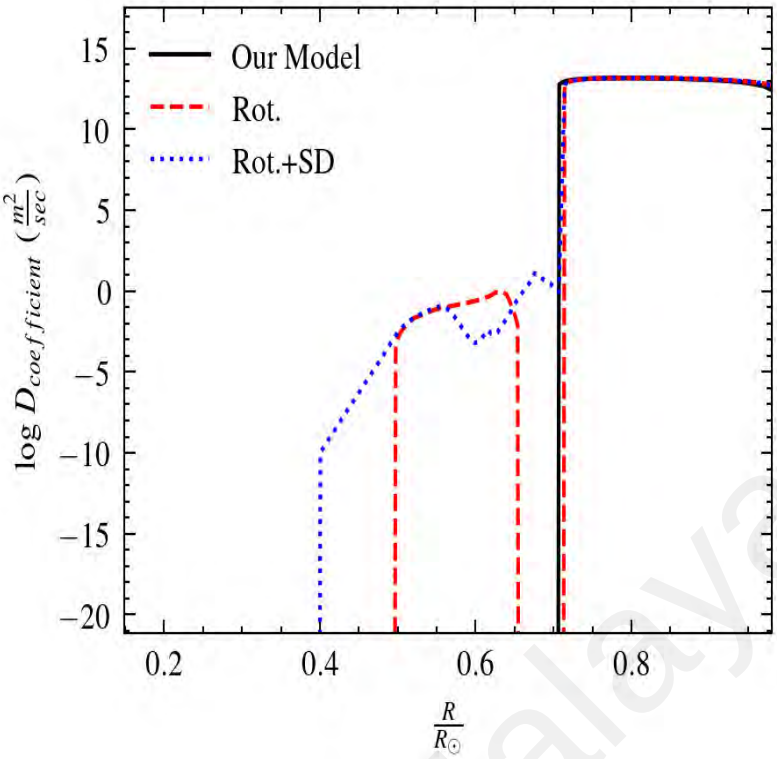

Figure 3.23: Profile of diffusion coefficient in the solar interior at the present age for rotational mixing models. Symbol as in figure and $D_{coefficient}$ mixing is in eulerian.

3.7 The evolution ^{7}Li Abundance in Solar-type Stars

The observations of surface lithium abundance in stars at old age demonstrate a similar conclusion in literature. The depletion of ^{7}Li become ineffectively and plateau after 1 Gy with no correlation to their masses (Spite & Spite, 1981). Therefore, here we construct solar-type models with 0.9 $M_\odot$ - 1.2 $M_\odot$ from PMS until the end of helium burning while adopting all transport mechanisms discussed previously. The lithium abundance at the different stages of evolution are investigated. We first present the HR diagram in Figure 3.24 to obtain the relationship between mass and effective temperature to search for *Boesgaard Lithium Gap* problem mentioned in the Chapter 2. The lowest mass, 0.9 $M_\odot$ has smallest effective temperature correspond to 5300 K whereas highest mass, 1.2 $M_\odot$ incorporate an effective temperature of 5900 K at the age of 5 GYr.

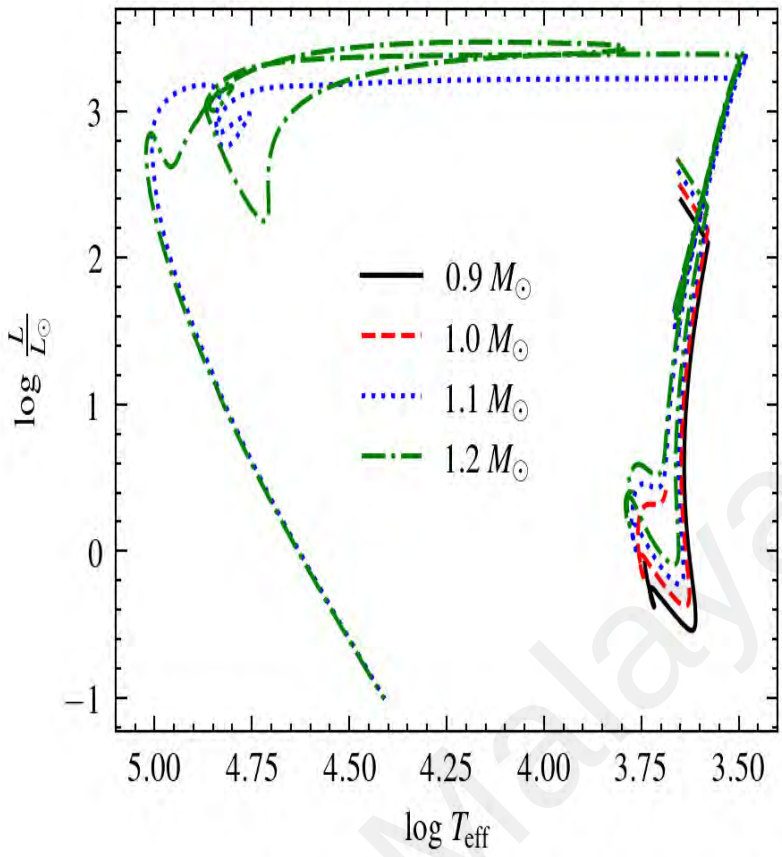

Figure 3.24: HR diagram for 0.9 $M_\odot$ - 1.2 $M_\odot$ from PMS to end of the helium burning.

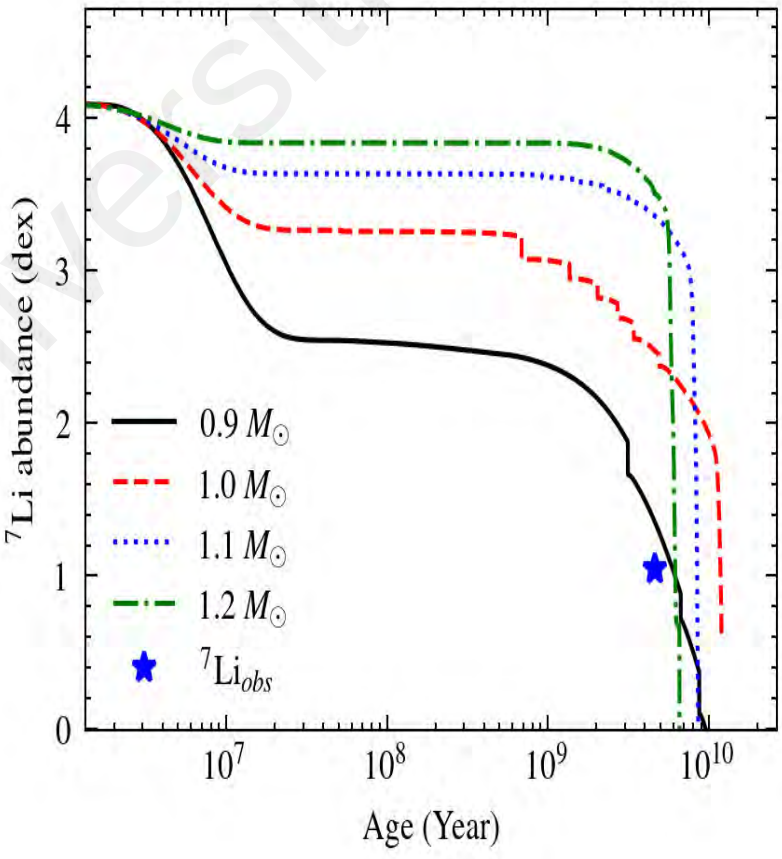

Figure 3.25: Evolution of ^{7}Li abundance for 0.9 $M_\odot$ - 1.2 $M_\odot$ from PMS to end of the helium burning.

As expected, lithium burning is greatly depleted on the PMS, especially for the lower mass stars as shown in Figure 3.25. The reason of this might be because the burning of the pristine lithium proceeds faster than the restoring effect of the new lithium formation by the nuclear reaction. Then, the abundance continues to slowly deplete from ZAMS towards the end of hydrogen burning by the impact of convection, diffusion, rotation, and induced magnetic field. At this stage, the mass model presents a similar pattern with observations by Ramirez et al. (2012). Lower mass stars impose higher lithium depletion than higher mass stars. It has been suggested that lower-mass stars incorporate a higher interior rotational rate, therefore lowering their effective temperature and deepening their convective envelope, CZ. Figure 3.26 shows the evolution of fraction convective bottom radius for masses between 0.9 $M_{\odot}$ - 1.2 $M_{\odot}$ at 1 Gyr, 5 Gyr and 8 Gyr on the main sequence. There is a strong dependency between stellar mass and the location of CZ, where higher masses stars have thin and shallow convection zones, whereas low mass stars are nearly fully convective. Besides, a mass star greater than 1.1 $M_{\odot}$ has a convective zone that is underdeveloped at very young ages, 1 Gyr, and has quickly vanished at 8 Gyr due to its shorter lifetime. In a later age scenario, we observed lithium Spite Plateau and its falling branch for 1.1 $M_{\odot}$ and 1.2 $M_{\odot}$ while the lithium abundance on the other two lower masses was exponentially decayed before they can even reach the end of helium flash. Another important to notice, the *Boesgard Lithium Gap* was not found in our produced models as we managed only to impose an inverse lithium-temperature proportionality in which, higher $T_{\rm eff}$ in higher mass star has smaller lithium burning at any evolution age. Hence, additional studies are needed to understand how lithium abundance is oddly varied at different ranges of effective temperature mentioned by A. M. Boesgaard et al. (2005). In summary, we had replicated most solutions in the past to answer our lithium problem. No methods attempted so far successfully managed to explain the lower lithium content in the

current solar abundance. Hence new approaches and perspectives are therefore offered in Chapter 4 to account for the missing lithium.

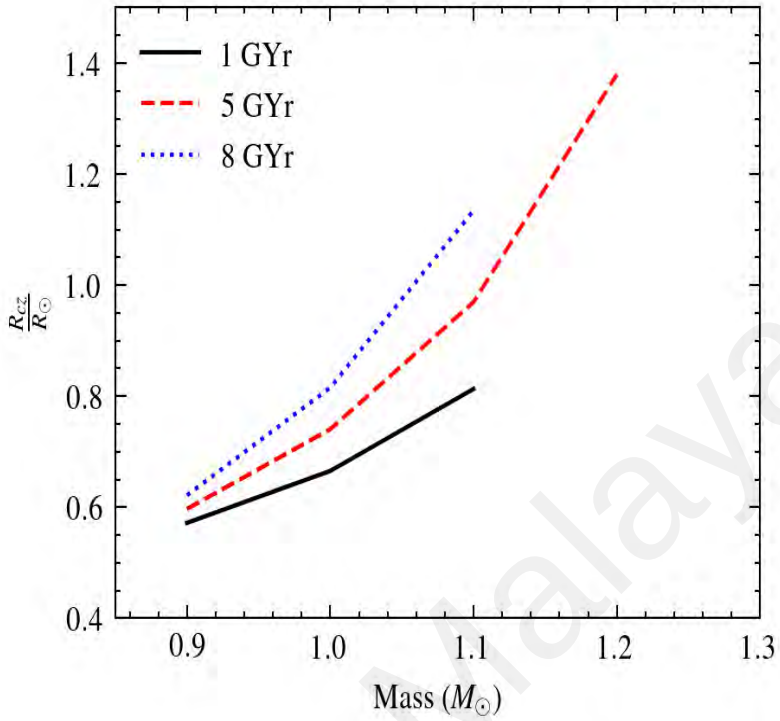

Figure 3.26: Location of the convection zone, normalized by the solar radius as a function of mass.

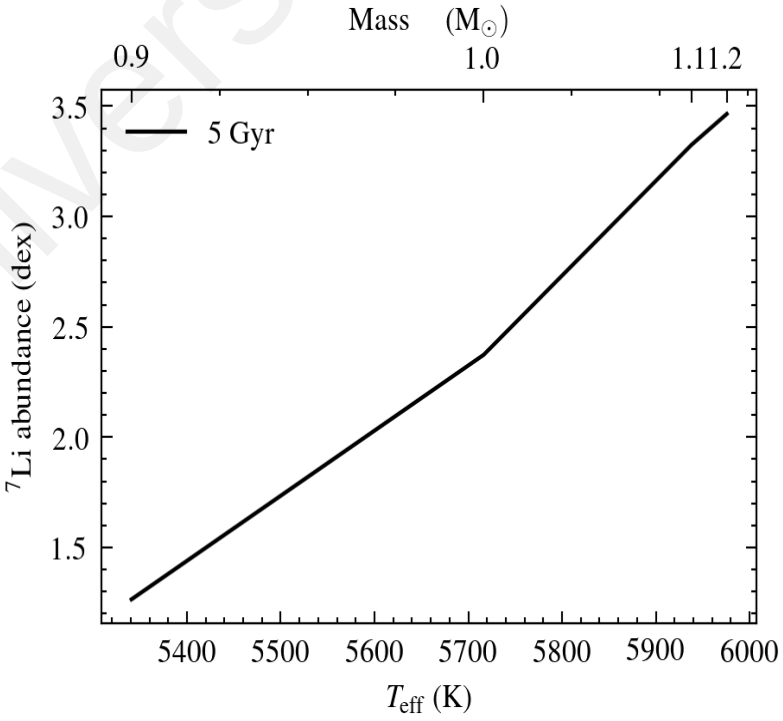

Figure 3.27: Lithium surface content against the effective temperature. The variation of temperatures are based on their repective solar mass at 5 GYr.

CHAPTER 4: RESULT OF THE PROPOSED SOLUTIONS

4.1 Effect of Enhanced Convection Mechanism

Many tests performed by several different groups conclude that the more significant convective eddy sizes make convection more efficient and a star much hotter (Basu & Antia, 1997; Christensen-Dalsgaard et al., 1993; Demarque & Robinson, 2003; Yi et al., 1997). Therefore, we plan to study the correlation between the enhanced convection parameter $\alpha_{\rm mlt}$ with solar metallicity, particularly looking at our ^{7}Li value. However, care to be taken following a suggestion from Joyce and Chaboyer (2018), proposing the implementation of the α value greater than 2.5 in solar-type stars will cause a severe adjustment needed to conserve the total mass and the observed effective temperature. Hence in this work, we simulate a model with $\alpha_{\rm mlt}$ = 2.4 to mimic the extent limit of the possible eddy stretch found in the solar-type stars in the Keppler's (Bonaca et al., 2012). We treated the $\alpha_{\rm mlt}$ parameter as constant in the local MLT through the stellar life, although recent evidence suggests that the $\alpha_{\rm mlt}$ parameter could be changed adjustably for stars of different evolutionary stages (Song et al., 2020). The convective-enhanced model is then compared with the standard solar model calibration adopting $\alpha_{\rm mlt}$ =1.92 determined in Chapter 3.2. Other physics inputs are applied similarly here to both models. Figure 4.1 shows the comparison of the convection velocity against solar radius for both models at $\tau\odot$. It turns out, higher $\alpha_{\rm mlt}$ forms a deeper base of the convection with an equal size of the convective envelope, therefore, proposing a smaller total radius of the convective-enhanced model by 5%. The figure also shows that the convection velocity in the convective region is slightly higher with the increased $\alpha_{\rm mlt}$ parameter.

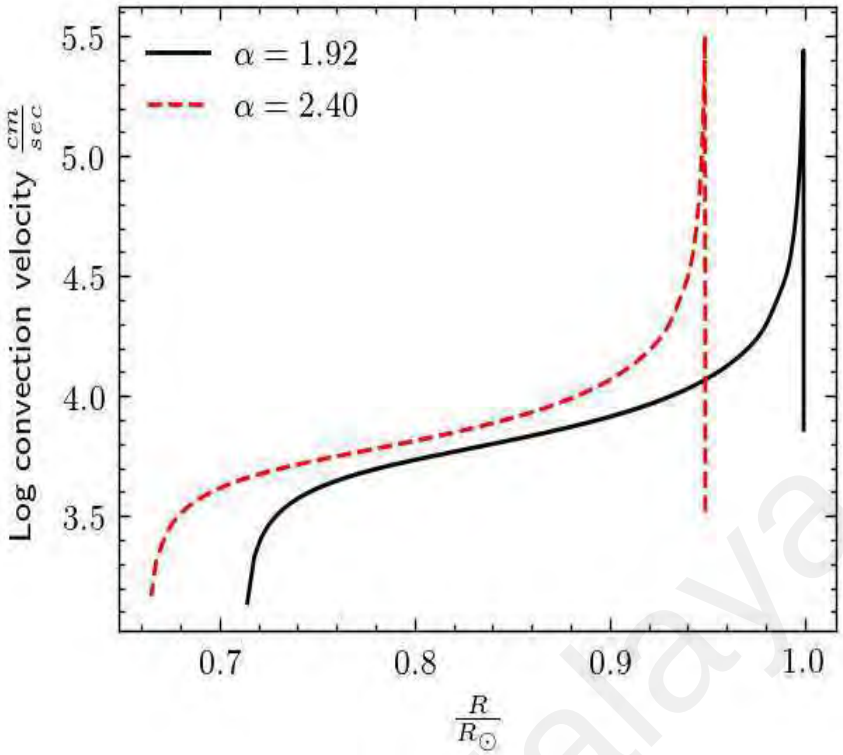

Figure 4.1: Convection velocity of elements against solar radius. A higher α_{mlt} value will decrease the solar radius.

The result is consistent with Christensen-Dalsgaard et al. (1993), in which stellar radius is very sensitive to the mixing length variation but not the depth of the convection envelope itself. To understand the mechanism, we describe in Figure 4.2 where the enhanced convection mixing length has widened the distance over which gas bubbles rise before dissipating and falling towards the interior. The impact will cause a small entropy jump between the bottom mixing length to the adiabatic convection radius. This can significantly modify the temperature gradient at the point in which the adiabatic crosses the radiative stratification of the interior. Nevertheless, the amount of falling mass elements must be equal to the amount raised to conserve the mass in each shell, causing a higher gravitational field that follows the reduction of the solar radius. However, we had concluded that the model is unrealistic as the effective temperature rises to 5899 K at the present solar age. Perhaps with some age calibrations, we could correctly reduce the model towards the solar properties.

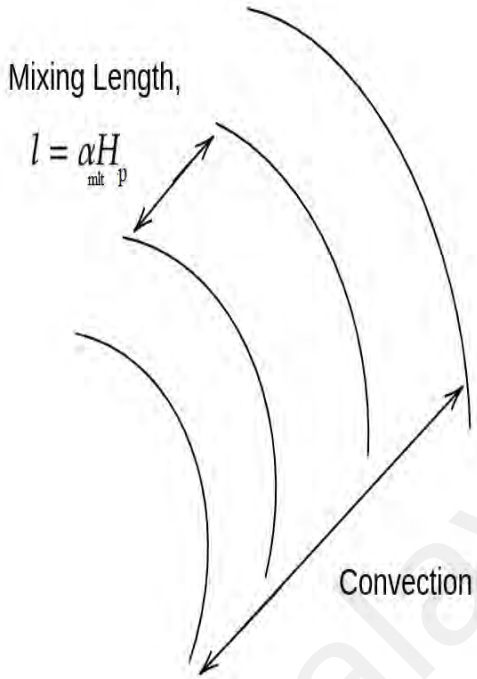

Figure 4.2: The characteristic of convective mixing region with respect to $\alpha_{\rm mlt}$ parameter. The mixing length l indicates where the up flows and down flows of the convective elements accommodate before they are dissipated. Mixing length, l depends on the free parameter $\alpha_{\rm mlt}$ and the pressure scale height, $H_{\rm p}$.

The metallicity appears to be relatively dependent on the parameter $\alpha_{\rm mlt}$. It is most possibly influenced by the temperature sensitivity of the hydrogen ions density near the surface and, as a result, higher $\alpha_{\rm mlt}$ contribute to the strong optical opacity and more excellent contrast between upflows and downflows. Therefore, convective elements on the surface, such as lithium, can penetrate downward efficiently to the deeper range of depths in where the downflows will be cooled (Bonaca et al., 2012). The result present in Figure 4.3 proves that higher $\alpha_{\rm mlt}$ indeed enhance the lithium depletion but only by one dex. Hence, it is insufficient to explain the low photospheric lithium abundance observation despite the maximum of the $\alpha_{\rm mlt}$ constraint that we had implemented.

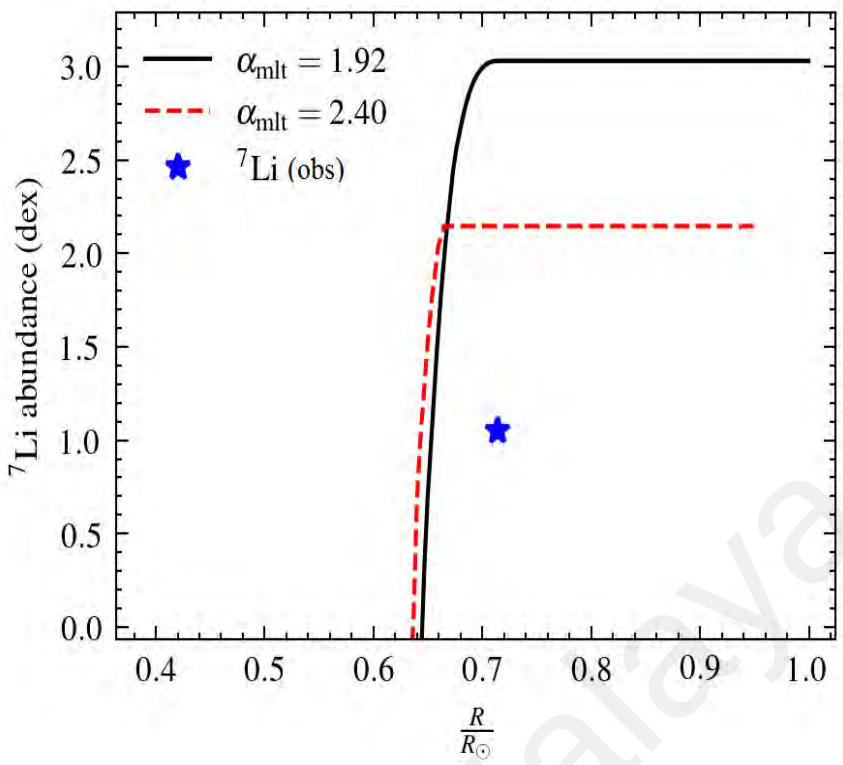

Figure 4.3: Graph of ^{7}Li abundance against solar radius at the solar-present day.

4.2 Higher Gravitational Settling in The Atomic Diffusion

The atomic diffusion module in MESA can be controlled by the relative importance of gravitational settling "factor" that specify the strength in the sedimentation of the surface elements. The "factor," which governs the settling of helium and heavy metals, can be used to arbitrarily enhance or inhibit higher diffusion mixing from the convective region towards the interior. Even though the gravitational settling appears to be very small, many have argued on the amount of settling allowed in the atomic diffusion (Iben Jr & MacDonald, 1985; Proffitt & Michaud, 1991; VandenBerg et al., 2002). Therefore, we embark on the quest to exam the impact of adopting a higher gravitational sinking to the lithium depletion. For this work, we increased the sedimentation factor by three times the calculated value from the calibrated solar model in Chapter 3.2. We have included a model without any gravitational settling as our control model.

Figure 4.4 shows how the different settling strengths change the amount of mass affected by the gravitational field. The increase in the sinking causes more cover on the solar surface radii compared to regular implementation. Varying the sinking will follow some changes in the solar abundances, opacity, and pressure gradient. Based on the computation, only 0.3% of deviation was found when the higher gravitational settling model is compared with the helioseismic luminosity and the effective temperature. However, the convection zone of the settling-enhanced model is shallower by 2% than the standard solar model. Despite having a change in the convection zone's radius, we determine that the lithium abundance in Figure 4.5 only presents a small lithium abundance drop with the increase of the gravitational strength. The extra settling proposed in the model has failed to justify the result of photospheric lithium abundance, ^{7}Li =1.05 dex. Besides, any further increment of sedimentation of more than a factor of three has worsened the solar radius. One of the possible explanations for such brief depletion behavior is that the imposed inward gravitational acceleration has been countered with radiative acceleration at the increased settling strength. At this point, we highly believed that the primary mixing of the lithium abundance perhaps is not due to some radial diffusion transports but mostly in favor of a wave turbulence interaction.

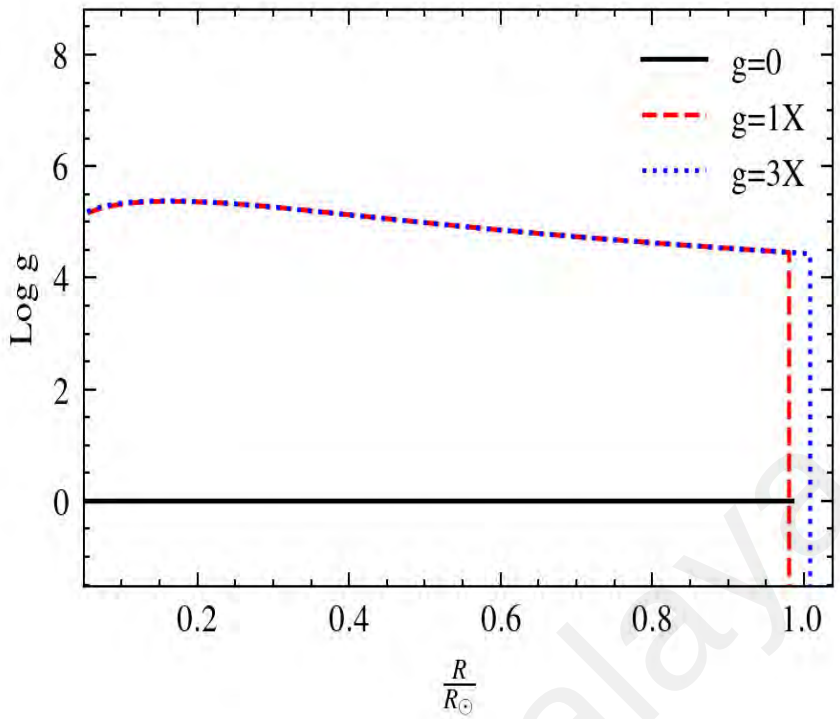

Figure 4.4: Log gravitational field for elements diffusion against solar radius at the present-solar age. The symbol used g = 0, g = 1X, g = 3X are defined as the model with no inclusion of gravitational settling, normal strength, and a factor of three times greater of the settling strength, respectively.

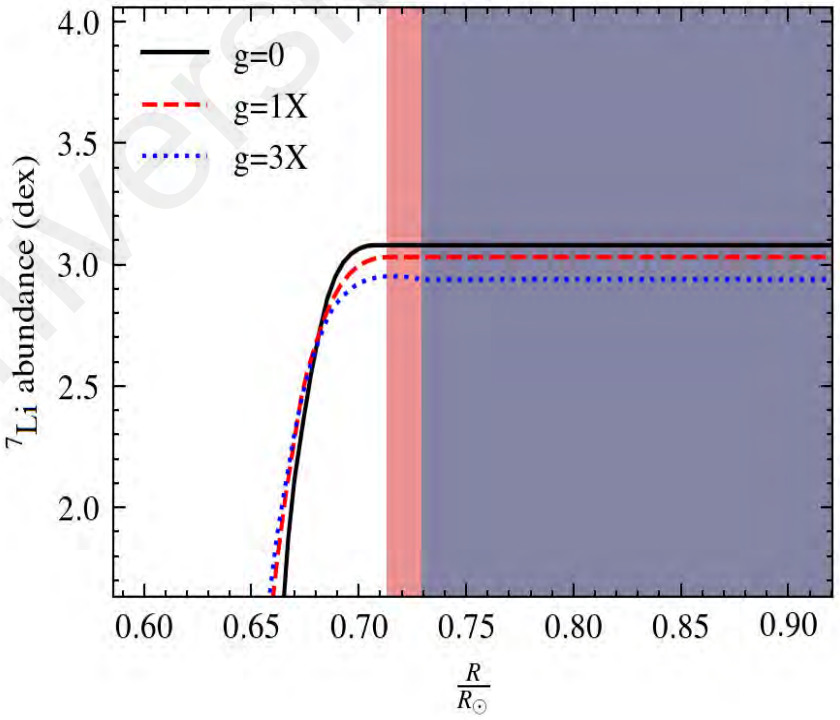

Figure 4.5: ^{7}Li abundance against solar radius at the present-solar age. The red-colored region is the convective envelope of the normal strength, which overlaps with the enhanced-settling model in the blue-colored region. The R_{cz} for the control, normal, and enhanced models are $0.729R_\odot$, $0.713R_\odot$, $0.707R_\odot$, respectively.

4.3 Higher Rate of Rotational-Induced Mixing

It is theoretically assumed that stars are fully convective on the Hayashi line to enforce uniform initial rotation profile. Then, for solar-like stars moving to the MS, the evolution of rotational rate will follow some slight change. However, we postulate that the lithium depletion problem may arise due to the wrong implementation of the spin-down rate in the evolution of the solar rotation. Assuming that the initial internal rotation velocity is not as slow as expected, one can argue the accuracy of the rotational mixing adopted so far in most evolution solar models. Covey et al. (2016) have identified that some solar-mass members in Pleiades reported having an initial mean velocity of about v = 40 km/s on the early main sequence years. Similarly, it is presumed that the rotation of the Sun could be kicked off at higher angular velocity before it gets spin down to the present slower rate. Besides, the improved angular momentum evolution models recently predict that low-mass stars can be locked to their circumstellar disk over a longer duration than massive stars (Bouvier, 2008; Gallet & Bouvier, 2015), forming a faster rotating radiative core. Furthermore, solar-type stars which categorized as slow-rotator have a better extension in the core-envelope coupling timescales which follows a higher degree of differential rotation between the radiative core and the convective envelope (Bonanno et al., 2007; Küker et al., 2011). Differential rotation is defined as when different parts of rotating fluid layers move with different angular velocities at different depths due to the fluid interaction with the Coriolis forces (Brown & Morrow, 1987; Howe, 2009). Therefore, the raised in the rotational induced dynamical and secular instability may result in the greater promotion of the chemical transport towards the solar interior.

Besides our postulation of an existing higher rotational kick-off, solar-type stars are also expected to have an internal temporal differential rotation cycle as suggested by Howe et al. (2000) and Antia et al. (2008), perhaps causing incorrect angular velocities adopted

in the rotational computation. This is based on the 107 years of data of temporal variations of the solar rotations from the year 1874 to 1981, determined by Sunspot groups Brajša et al. (2006). They found that Sun has a secular deceleration cycle at the equatorial rotation velocity on the solar surface. The determination of secular solar deceleration has been consistent with Balthasar et al. (1986) and Javaraiah et al. (2005) using other observation methods. Although one can argue that the internal solar rotation profile is independent of the profile on the surface rotation, we firmly believe that both profiles can not be intimate too far from the processes that drive the activity cycle. In fact, there are issues with the present angular momentum transport and many more uncertainties of modern stellar physics, which have caused the rotation mechanism to be challenged. As we know, these are few reasons why rotation-induced mixing has not to be included in the standard solar model to this date.

Likewise, the one-dimensional computation made in MESA is obviously too simple and does not present the complexity, particularly the free parameters related to the inclusion of possible higher rotational kick-off and the temporal variation in the rotational cycle. So, we can only offer a solution by involving a combination of several different velocities in the evolution. We remodel our solar evolution with much higher initial angular velocity but still under a slow-rotator constraint, $\frac{\Omega_{sur}}{\Omega_{crit}} < 0.1$. We emphasize that in this work, we cannot project the temporal variation as discussed but only present possible postulation of how the higher initial rotation can cause extreme lithium burns, especially on the first 100 million years after ZAMS. In general, we first evolved a one solar mass star with the observed angular velocity, $\frac{\Omega_{sur}}{\Omega_{crit}} = 0.004$ (equivalent to $v = 2$ km/s) and then compared it with higher rotation models, $\frac{\Omega_{sur}}{\Omega_{crit}} = 0.01$, $\frac{\Omega_{sur}}{\Omega_{crit}} = 0.1$, and including previous induced magnetic field dynamo model (in Chapter 3.6). We consistently applied other input physics from the solar model calibration and summarized the adopted rotational controls with their

respective model names in Table 4.1.

Table 4.1: Summary of rotational models adopted in the studies.

Model	Initial Rotation	Label
Standard solar model	$\frac{\Omega_{sur}}{\Omega_{crit}} = 0.000$	SSM
Non standard model with standard rotational velocity (2 km/s)	$\frac{\Omega_{sur}}{\Omega_{crit}} = 0.004$	NSSM
Non standard model with fast rotational velocity (4.6 km/s)	$\frac{\Omega_{sur}}{\Omega_{crit}} = 0.010$	NSSMhigh
Non standard model with high rotational velocity (46 km/s)	$\frac{\Omega_{sur}}{\Omega_{crit}} = 0.100$	NSSMxtrm
Non standard solar model with Spruitz-Tayler Dynamo (2 km/s)	$\frac{\Omega_{sur}}{\Omega_{crit}} = 0.004$	NSSMsd

Figure 4.6 and Figure 4.7 show that the variation of the rotational rates is still slow enough to have any negligible effects on the observed solar structure and convection radius. Even with the extreme rotation, the NSSMxtrm model inferred small deviations of R_{cz}, solar radius, and luminosity properties by 2%, 3%, and 3.7%, respectively. Therefore, it is highly possible to implement the NSSMxtrm behavior model, which adopts a kick-off velocity of 46km/s for solar-type stars to induce higher turbulence mixing. However, the current rotational-mixing theory does not cover the possible rapid velocity spin down from 46km/s to the helioseismic velocity of 2km/s. Perhaps, the rapid loss of solar rotation due to some gradual loss of angular momentum over the MS life and some magnetic coupling to the solar wind of a star (Charbonneau & MacGregor, 1993; Mestel & Weiss, 1987; M. J. Thompson et al., 2003). Nevertheless, our interest here is to determine whether higher rotational kick-off can enhance lithium depletion during its early years.

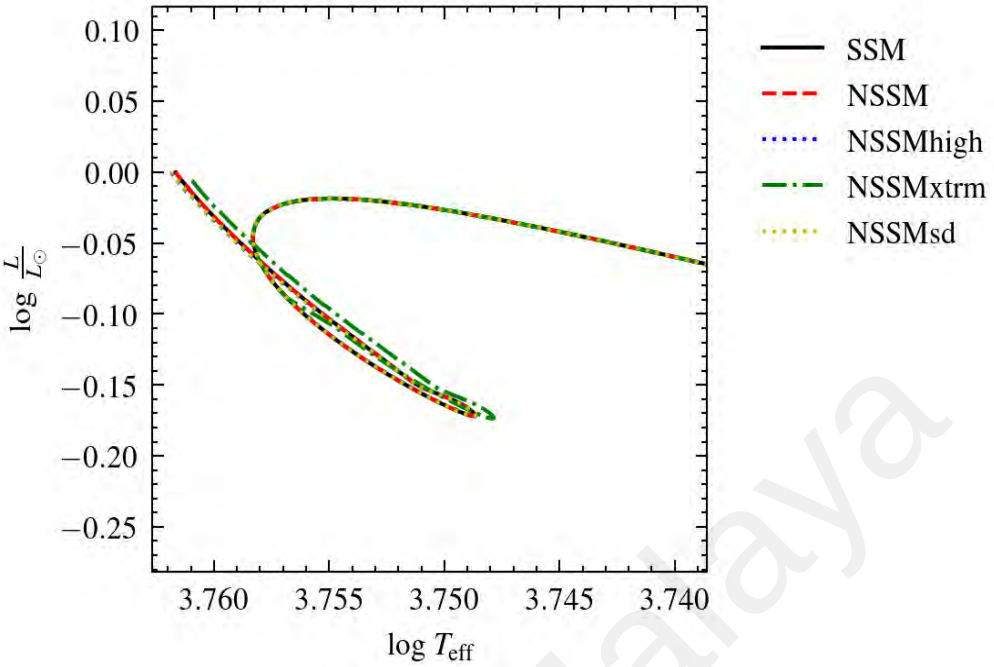

Figure 4.6: HR diagram of the difference rotational models.

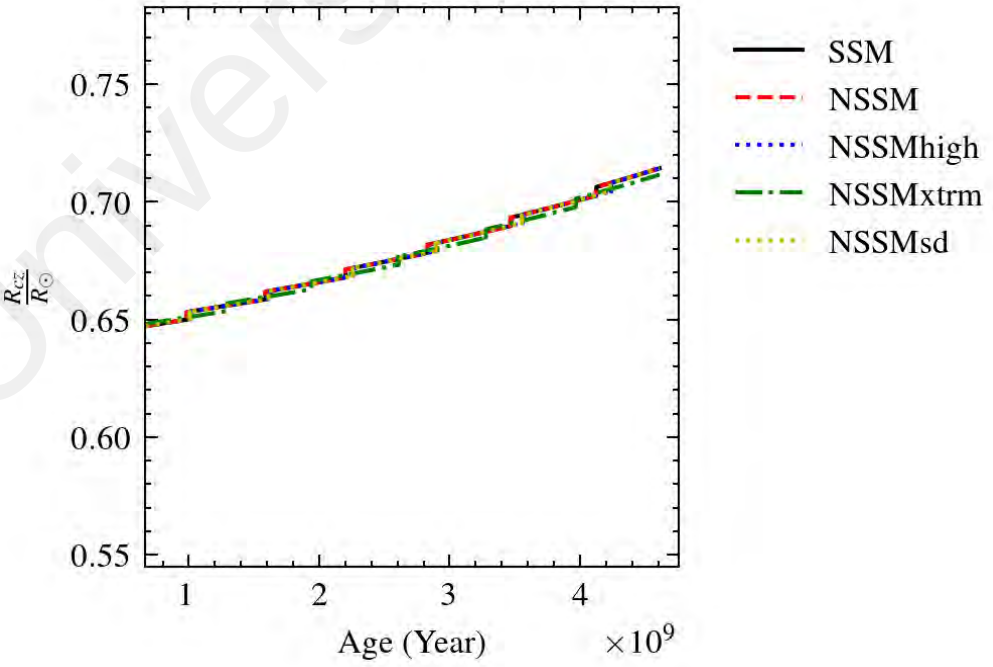

Figure 4.7: Evolution of convection zone's radius vs. solar age due to the rotational effects.

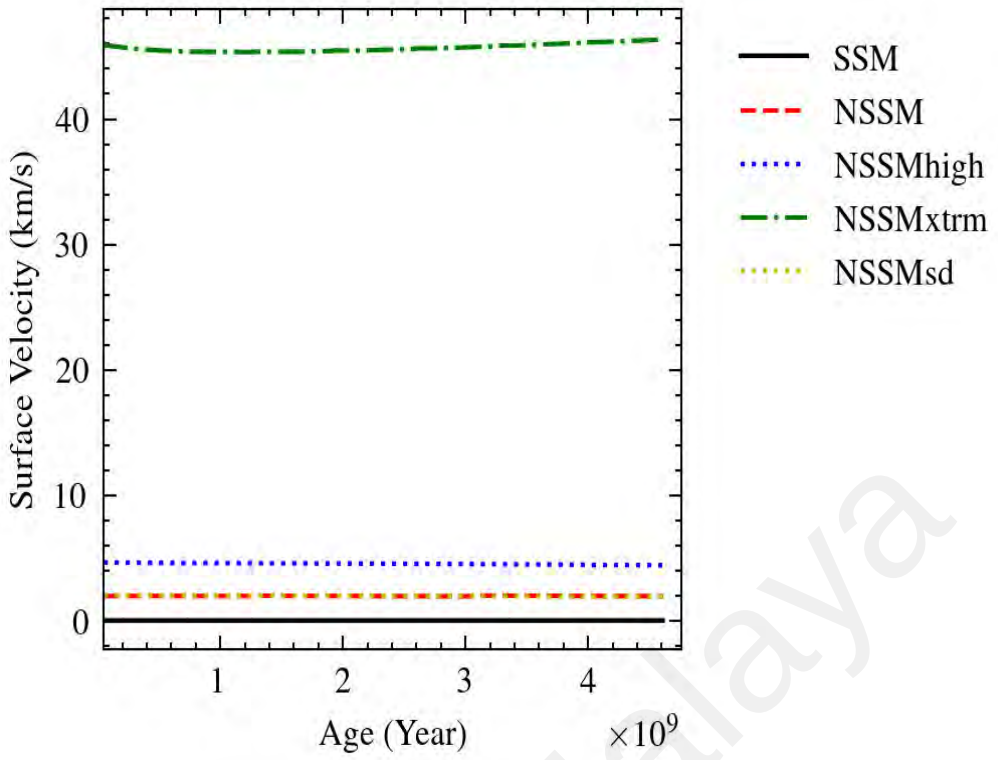

Figure 4.8: Evolution of surface velocity.

Figure 4.8 shows the evolution of solar surface rotation for the comparison models in which we had rotation included in the MESA control after the protostars reach the Zero Age. The rotator models, NSSM and NSSMhigh, follow a slower rotation with time and surprisingly the NSSMxtrm model somehow presents an increase in the rotation after 2 GYr. The NSSMxtrm model appears to rotate faster due to the conservation of angular momentum in which cause by a small contraction of its radius with the inferred lower temperature. We also are not able to present cyclic variation in the evolution of solar rotation based on the current rotational-mixing theory. Figure 4.9 shows that the rotation period at the base of the convection zone for the NSSM model is consistent with helioseismology which is around P = 25 days (M. Thompson et al., 1996) whereas the radiative core would rotate with a much shorter period (Fossat et al., 2017). Hence, the internal rotation profile observed in the NSSM has a higher degree of differential rotation compared to the fast rotating star, NSSMxtrm.

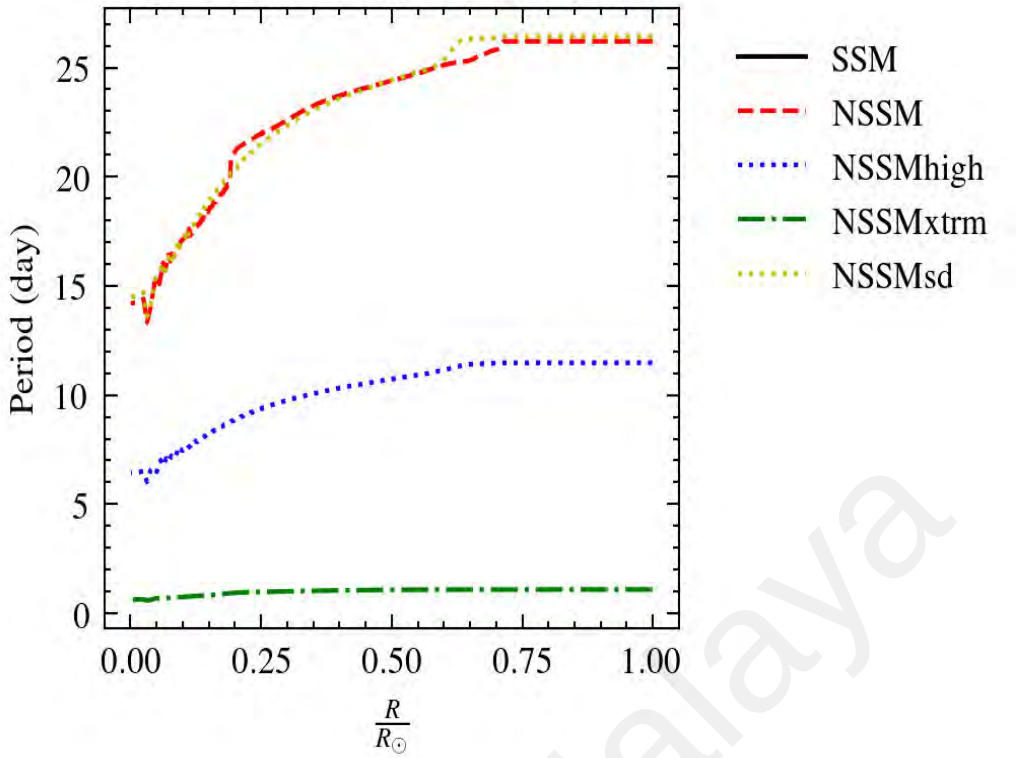

Figure 4.9: Rotation period against solar radius for different rotational models.

We then relate the profile of lithium abundance in Figure 4.10 to show that despite the small differential rotation in the NSSMxtrm model, it can reproduce the observed surface lithium at the present solar age. It is determined that lithium depletion is not dependent on the different degrees of differential rotation as previously suggested but on the existence of the tachocline instability mixing. The tachocline is where the layer of transition occurs in between the radiative and convective rotations. It is also where the magnetic-induced dynamo is expected to be generated. Besides, NSSMxtrm model determined to has a lower depth of R_{cz} which can only means a lower tachocline as well. Therefore, lithium on the base of convection zone can easily reach burning temperatures and depletes even in the absence of the magnetic field-dynamo.

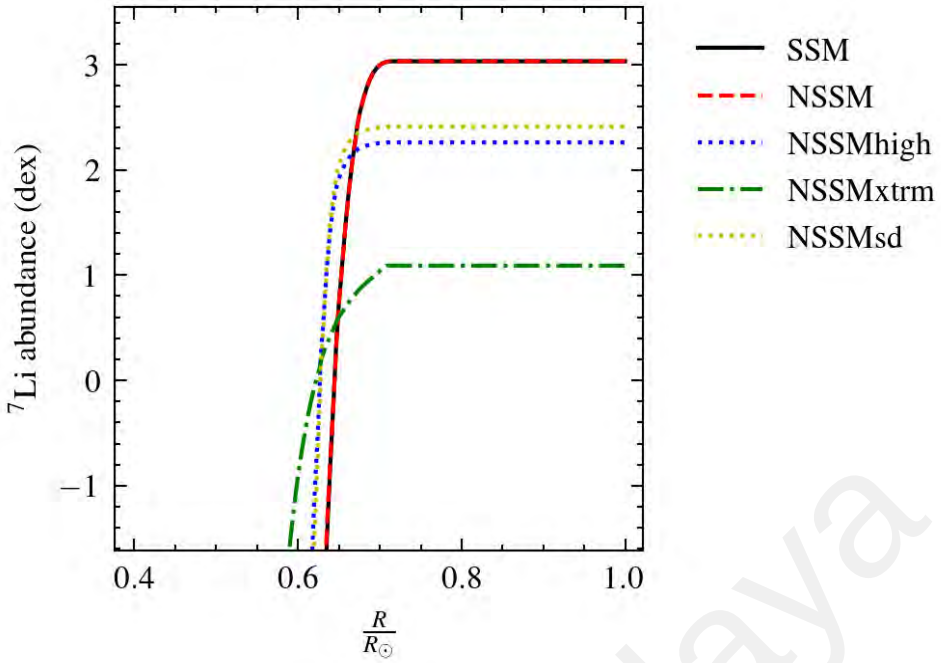

Figure 4.10: Lithium abundance against solar radius at the solar present-day due to rotational effect.

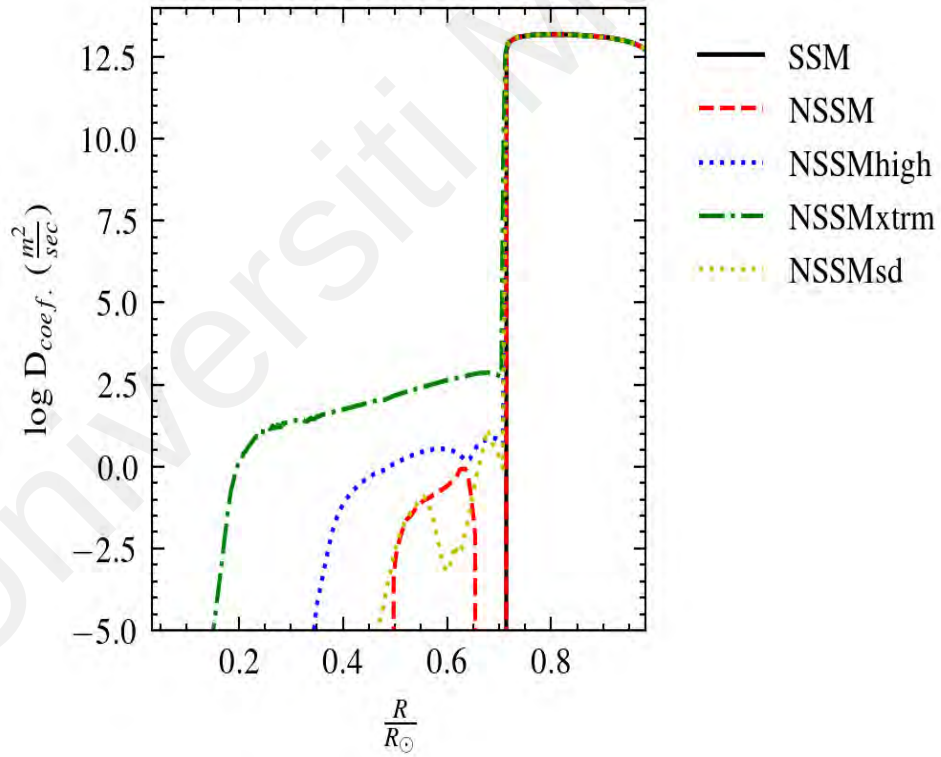

Figure 4.11: Log diffusion coefficients for transportation of elements with respect to solar radius in Eulerian.

The high rotational-induced mixing has significant consequences to the efficiency of element transport. We observed an enhancement of surface abundances variation on the MS based on the determined diffusion coefficient in Figure 4.11. Therefore, higher lithium

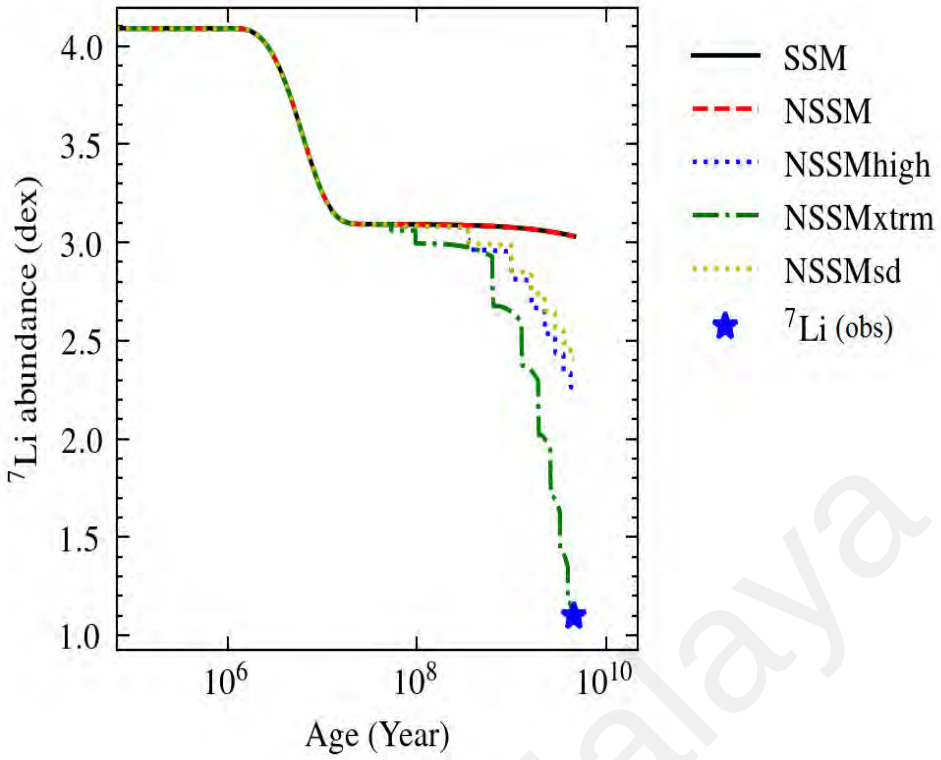

Figure 4.12: Evolution of lithium abundance for difference rotational models.

depletion is to be expected by the same diffusion variation. We then present Figure 4.12 to show the evolution of surface lithium abundance for the variation of difference rotational rate. We declare that NSSMxtrm, which adopts the highest solar rotation, can reproduce the observed lithium abundance at the selected evolutionary stage > 2 GYr. Our result with the extreme rotation rate model coincides with many other groups which support that the major lithium depletion should occur at the MS rather than PMS (Charbonnel & Balachandran, 2000; Ramirez et al., 2012). However, if we assume that surface rotational velocity had to be spun-down at an exponential rate to reach the observed rotation, then the surface lithium burning found during the MS after 2 Gyr would challenge our result. Therefore, the confirmation of the lithium result has to be postponed until we manage to solve the issue with the peculiarity of the rotational and angular transport mechanism in the stellar evolution. We conclude that higher rotational kick-off of solar-type stars does not enhance the lithium burn at PMS or early years but rather at the MS, which we consider implausible with the current angular momentum theory.

4.4 Lithium Abundance with Different Chemical Compositions

Our attempts to solve the lithium problem with the enhanced internal mixing processes available in solar-like stars have finally reached a point. We analyze that the different amount of the lithium burning is closely related to certain physical and chemical properties such as the size of the convective envelope, the opacity, and the effective temperature particularly at the base of convection zone. Therefore we suggest testing this theory by adopting several different chemical mixtures, which follow the opacity change in the radiative and convective regions. Focusing on two different evolution stages, which are PMS to ZAMS, and ZAMS to the present-day, we computed the evolution of lithium abundance by using three selected chemical compositions of our choice with their corresponding initial mass fractions as given in Table 4.2 (Asplund et al., 2009; Grevesse & Sauval, 1998). To treat the internal transport mechanism, we had included diffusion and convection as the main mixing processes. The rotation is not included here due to its uncertainties, and besides it is known that the rotational turbulence will rub out the atomic diffusion efficiency below the base of the convection zone. We clarify that we do not intend to calibrate models to fit the helioseismic but simply to investigate the opacity and metallicity effects on the lithium evolution. Therefore, we adopt a standard convection parameter $\alpha_{\rm mlt}$ =1.72 and overshooting, f= 0.016 throughout the evolutionary computation. Based on the proto-solar abundances in Table 4.2, the GN93 model contains the highest metallicity, followed by GS98 and As09 models. However, As09 model has initially held more helium content, which can induce higher nuclear burning than the other two models.

Table 4.2: Proto-solar abundances.

Chemical Mixture	Z_{init}	Y_{init}	X_{init}	$(Z/X)_{init}$	Model
Asplund et al. (2009)	0.0142	0.2703	0.7154	0.0199	As09
Grevesse & Sauval (1998)	0.0180	0.2701	0.7120	0.0253	GS98
Grevesse & Noels (1993)	0.0190	0.2697	0.7112	0.0268	GN93

Table 4.3: The abundances of elemental species contributed to the solar opacity. The abundance are taken from the solar chemical compositions suggested by several authors with the unit of dex.

Element	GN93	GS98	As09
Fe	7.50	7.50	7.45
Ne	8.08	8.08	7.93
Si	7.55	7.56	7.51
O	8.87	8.83	8.69

The variation of opacity calculation in the mixtures is based on the density of each element in the compositions. Species in the sequence order, Fe, Ne, Si, 0, are essential elements contributing to opacity (Swenson et al.,1994a; Piau & Turck-Chi'eze., 2002). Hence, the related species are compared in Table 4.3 to show that the GS98 model has the densest mixture, followed by the GN93 model, whereas, As09 presents a significant lowest density due to the iron difference. We present the result of lithium evolution from the PMS until the Zero Age in Figure 4.13 and for the latter evolution stage in Figure 4.15.

Interestingly, the lithium had major burnt with the GS98 model during the end of the PMS despite having similar initial lithium abundance with the GN93. Initially, we predicted that the difference in the lithium depletion might relate to the early formation of the convection zone. It turns out, GS98 and GN93 models evolved about an equal depth of convection bottom's radius at Zero Age, but yet, producing 0.6 dex indifference of lithium depletion at ZAMS. However, smaller lithium depletion by the As09 model is strongly related to the formation of its thin convective envelope, as shown in comparison Figure 4.14.

Table 4.4: The summary of the lithium depletion by different solar mixtures from ZAMS to $\tau_{\odot}$.

MODEL	GN93	GS98	As09
Initial Li (CI Chondrite)	3.31	3.31	3.45
This work	2.15	1.90	2.80
% difference	35%	43%	19%

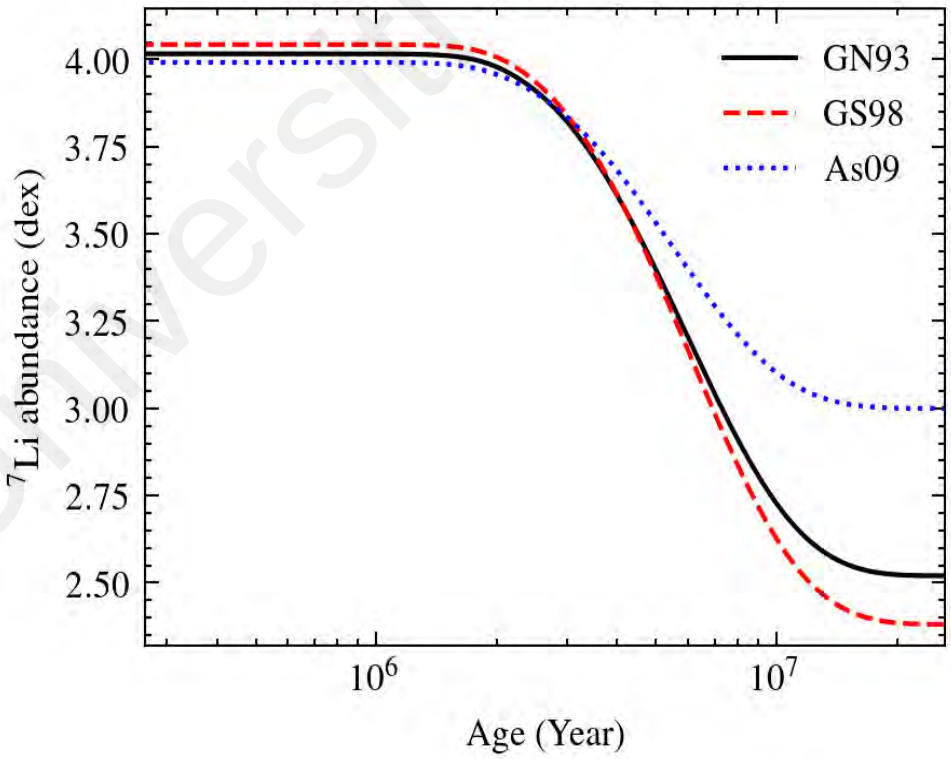

Figure 4.13: Evolution of lithium abundance on the PMS for different mixtures.

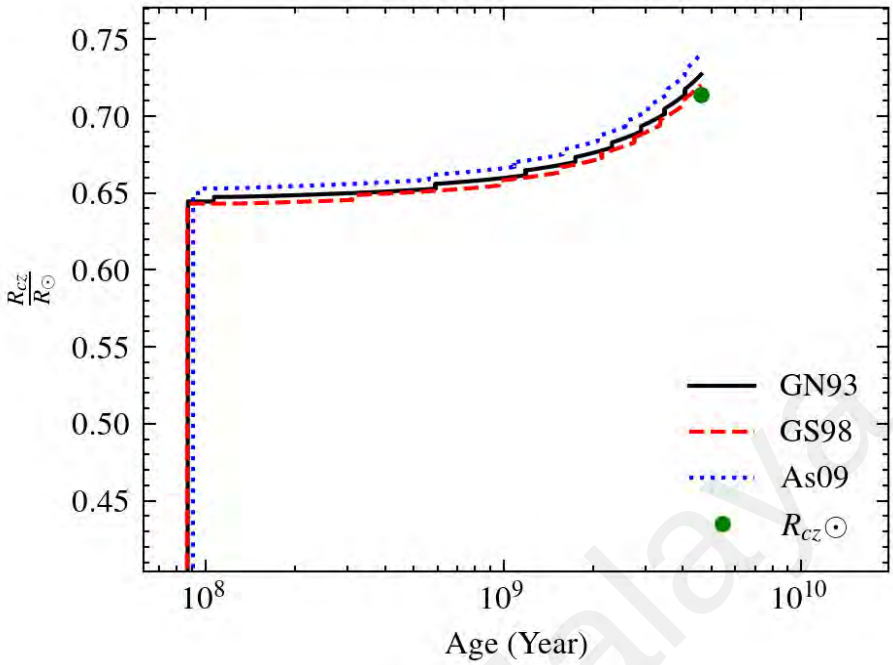

Figure 4.14: Convective bottom's radius as the function of age.

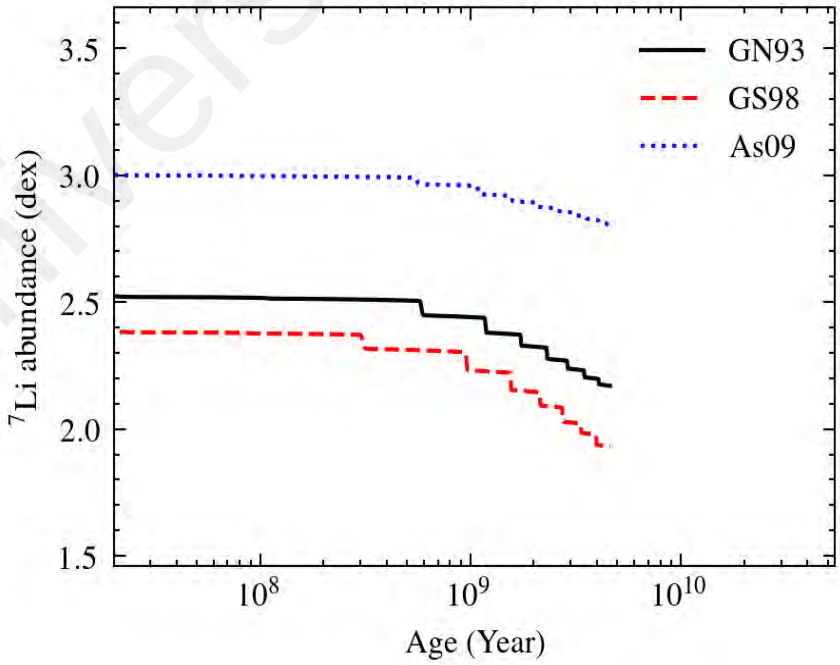

Figure 4.15: Evolution of lithium abundance on the MS until present-solar age for difference mixtures.

We have found a similar trend in the lithium evolution moving towards the solar present-day. It is determined that GS98 model depletes lithium about 0.4 dex, followed by the second higher, GN93 model with 0.35 dex and dropped at only 0.2 dex with the AS09 model. Here, the convective layer for GS98 is slightly broader and deeper, which yields to more extensive dispersion of lithium abundance. It is crucial to note that greater nuclear energy generated with AS09 model, which is shown in Figure 4.16, does not reproduce any enhanced lithium depletion. It is postulated that lithium abundance surviving at the top layer of the convective envelope is not affected by the increased nuclear energy by the radiative temperature but rather in the temperature near the surface. To understand the physical properties that may relate to the present-day lithium difference, we present the opacity and temperature gradient profiles of the models in Figure 4.17 and Figure 4.18, respectively. It follows that opacity has only started to vary at $0.6R\odot$ and above significantly. This must be due to the interaction of ions and electrons that begin to dominate over the outward radiative photons with the decreased temperature.

The GS98 profile model shows the most opaqueness near the surface. Whereas, As09 model exhibits the lowest opacity near the base of the convection zone, which consequently causes a smaller temperature jump in the adiabatic region. We present Figure 4.18 to explain how that mixture with a larger opacity value must have a steeper temperature gradient to carry the same heat flow. Following the diffusion Equation (3.8), a higher temperature gradient can effectively enhance surface elements' transport, leading to lithium depletion. Therefore we firmly believe that the lithium depletion problem is easily susceptible to chemical compositions, suggesting any slight change in the observed solar mixture could produce a different outcome for the surface lithium abundance.

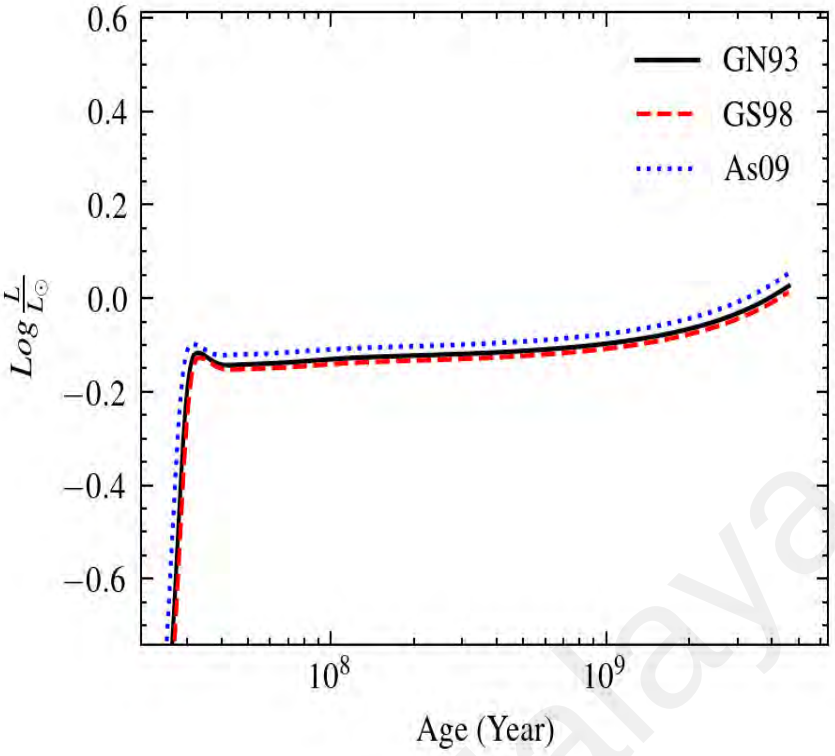

Figure 4.16: Evolution of nuclear power burning in the unit of solar luminosity.

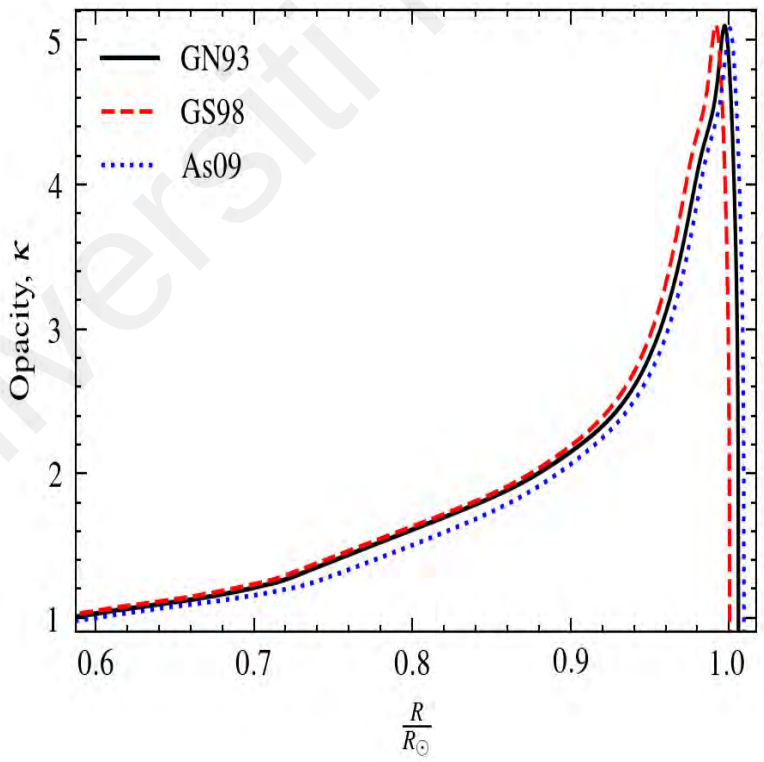

Figure 4.17: Profile of the opacity with respect to the solar radius at the present solar age.

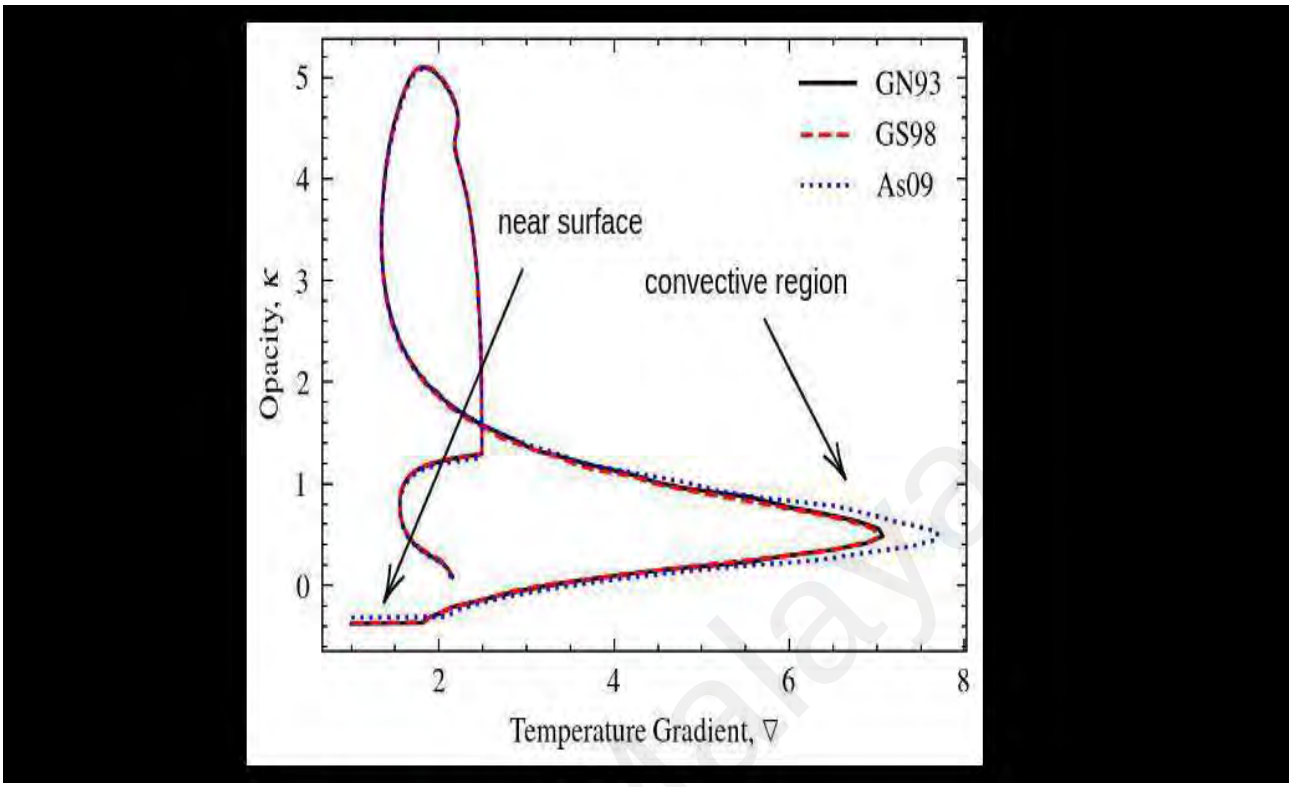

Figure 4.18: Profile of the opacity, as a function of temperature gradient at the present solar age.

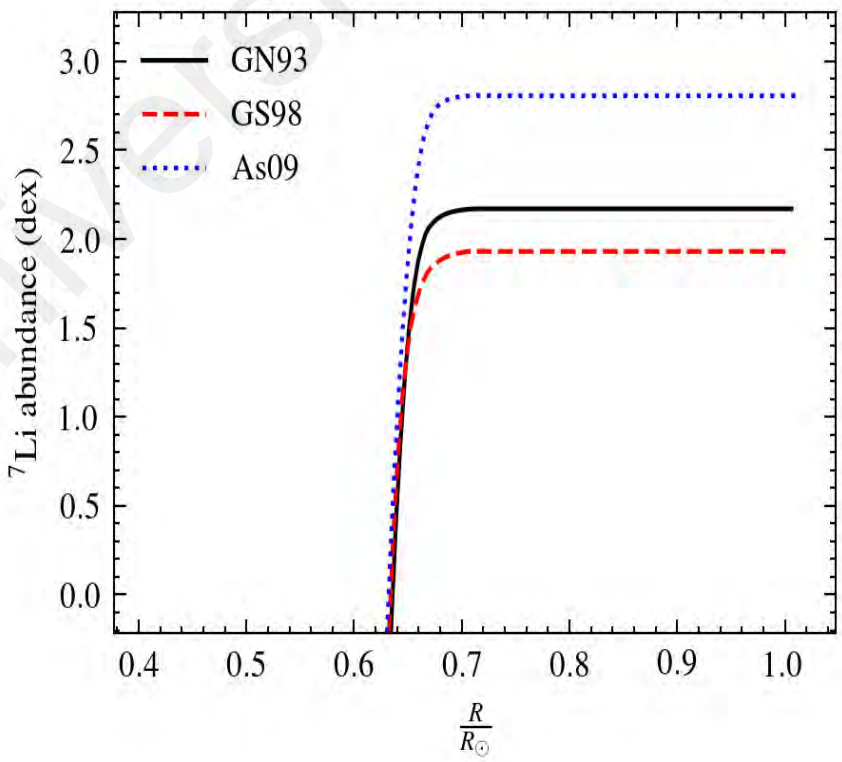

Figure 4.19: Profile of lithium abundance with different composition mixtures and metallicity at the present solar age.

4.5 Lithium Abundance with Photospheric Determination

We report that we have also found the common discrepancy regarding the radius of the convection zone, R_{cz} when adopting the As09 mixture, which was mentioned in Chapter 2. However, Grevesse et al. (2013) claimed that the As09 mixture is the most refined and comprehensive solar chemical composition today. Thus, this suggested that there is still a missing piece with current atomic physics calculations in the OP or OPAL opacities to model the observed R_{cz} correctly. Despite the complex solution that it may offered, another simple explanation may lie within the method used in the determination of the As09 solar chemical compositions. We have so far take into account that pristine lithium abundance and some other heavier elements are mostly taken from the *CI Chondrite* measurement. Hence, if we assumed that the initial solar abundances are entirely based on the photospheric observation, we can recomputed our lithium abundance with a much lower initial value. We clarify that lithium abundance variation due to different observation methods has a negligible effect on the overall opacity. This is since attributed important species in the mixture in Table 4.3 present no mass difference with both observation techniques. The result shown in Figure 4.20 is the evolution of surface lithium abundance with respect to the star's age. We find that lithium abundance is still over predicted despite the lower initial implementation of photospheric abundance.

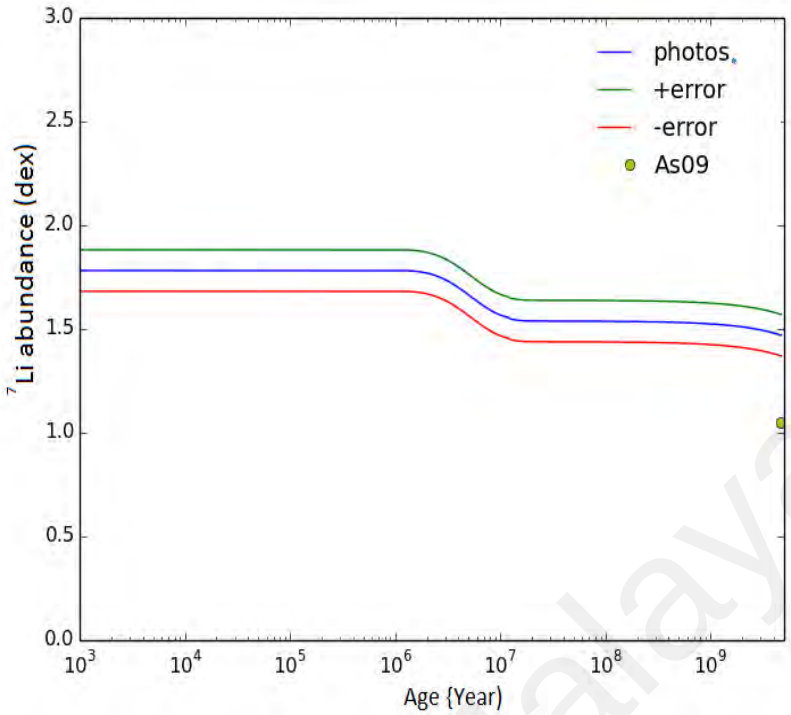

Figure 4.20: Evolution of lithium abundance with the photospheric mixtures by the Asplund et al. (2009).

4.6 Predetermine The Initial Lithium abundance

CI Carbonaceous Chondrites are a class of meteorites that is assumed to likely represent the fragments from the early solar system. The fragments were formed right after the nebula accreditation and survive on the asteroid belt, far from any further nuclear process until some of them fall on earth. Therefore, the specific *CI Chondrites* are believed to provide critical insights about solar cosmochemical when carefully analyzed in the laboratories. However, recent evidence shows that they have undergone considerable processing on earth due to the bombarded logistics and between the time frame of the first formation and the next 4.5 billion years (Palguta et al., 2010). To complicate the issue, it is possible that some of the asteroids detected were not originated from the closed solar system, but ejected from the nearest birth of stars a very long time ago (Meech et al., 2017). This could indicate that the meteorite fragments of the asteroid can come from the interstellar system and consequently do not reflect the pristine lithium abundance implemented in our

solar modeling. Although this is a remote possibility, it opens the opportunity for us to predetermine the initial lithium mass fraction that matches the present photospheric low lithium. For this study, we adopt As09 mixture and corresponding mass fraction from Table 4.2 to find the best fit of initial lithium abundance as the solar constraint. Then, various solar models are constructed by varying the initial lithium abundance where the other input physics remain unchanged. Finally, we have predetermined the initial lithium abundance to be 1.42 dex, which is 44% lower than the inferred by the lithium meteorites.

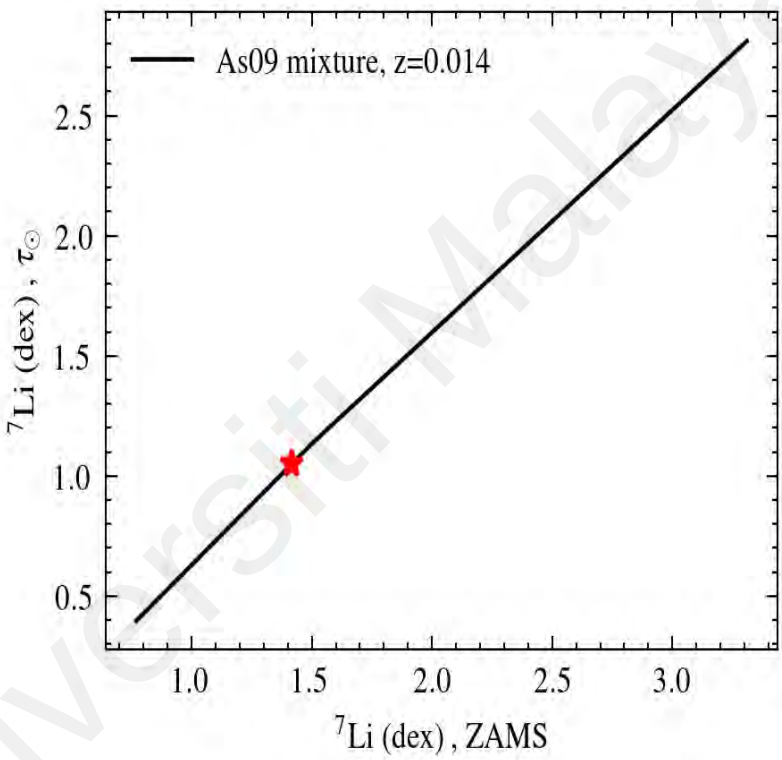

Figure 4.21: Variation of the initial lithium abundance at ZAMS to manually fit the observed photopheric lithium. The initial lithium abundance is determined to be 1.42 dex by extrapolation.

CHAPTER 5: CONCLUSION

As lithium is a very fragile element, it is assumed to be easily burnt by the internal mixing processes. Therefore, we reproduced every proposed solution in the past such as implementing mechanisms of convection, atomic diffusion, and rotation. As we have discussed, none of the descriptions of all major element transport mechanisms in modern stellar evolution calculations are able to answer the lithium depletion problem. Nevertheless, it appears that the low lithium abundance has to be dependent on some mixing processes near the bottom of the convective envelope. We then suggested enhancing the convection mixing length by varying the $\alpha_{\rm mlt}$ parameter. The efficiency of the mixing has caused an extra 1 dex lithium depletion, whereas the inquired lithium problem presents a missing of 2 dex as inferred by the observation. The result implies to consider other internal mixing process. We suggest that the gravitational field energy should be increased to cover more surface abundance to enhance diffusive processes. However, the sedimentation strength of 3 times higher has only yielded 0.1 dex of decrements with some consequences on the solar radii and the convection bottom's radius. It is unlikely that atomic diffusion and the extra gravitational settling would affect the surface lithium abundance. It is clear that the description of complex physical processes such as greater rotation-induced mixing are needed. Hence, we demonstrate our result with the variation of initial rotation rates to the evolution of lithium. We presented that we are able to reproduce the observed lithium abundance when adopting an initial rotational kicked off about 46 km/s. Besides, it is determined that the solar lithium destruction should be mainly attributed to the mixing at the MS rather than the PMS evolution stage. However, the approach utilized suffers from the limitation of the present observed solar rotation. This result also highlights that little is known about the angular transport mechanism in the solar interior, which might cause the rotational spin-down to present a slower rate. Therefore we can not

confirm the lithium result with the current rotational momentum theory. Overall, the investigation of the lithium depletion problem with the enhanced transport mechanisms has finally arrived at certain uncertainties. However, we now understand that lithium depletion is too delicate to slight changes in opacity and metallicity, which can not be ignored. We have shown that different compositions mixtures As09,GS98, and GN93 produced a wide lithium dispersion. The mixture with higher opacity can efficiently enhance the diffusion of the abundances on the adiabatic region. However no available solar mixtures today have significant iron abundance to present the necessary opacity to induce such lithium destruction. In conclusion, our efforts with astrophysical solutions to understand the behavior of lithium and the depletion problem in solar-like stars remain unsolved. Therefore, our plan in future work, would be to include a nuclear physics solution to this problem. The solar neutrinos can be used to probe the possibility of a solution to the ^{7}Be and ^{7}Li production rate. An improvement to certain cross-sections that may be affected by the extreme temperature should be determined. Finally, if the lithium problem arises due to difficulties in extracting the correct abundance origin, then we have predetermined the initial lithium to be ^{7}Li = 1.42 dex to present the observed lithium today.

REFERENCES

Antia, H., Basu, S., & Chitre, S. (2008). Solar rotation rate and its gradients during cycle 23. *The Astrophysical Journal*, *681*(1), Article#680.

Asplund, M. (2005). New light on stellar abundance analyses: departures from lte and homogeneity. *Annual Review of Astronomy and Astrophysics*, *43*, 481–530.

Asplund, M., Grevesse, N., Sauval, A. J., & Scott, P. (2009). The chemical composition of the sun. *Annual Review of Astronomy and Astrophysics*, *47*.

Bahcall, J. N., & Moeller, C. P. (1969). The ^{7}be electron-capture rate. *The Astrophysical Journal*, *155*, Article#511.

Bahcall, J. N., Pinsonneault, M., & Wasserburg, G. (1995). Solar models with helium and heavy-element diffusion. *Reviews of Modern Physics*, *67*(4), Article#781.

Bahcall, J. N., Serenelli, A. M., & Basu, S. (2005). New solar opacities, abundances, helioseismology, and neutrino fluxes. *The Astrophysical Journal Letters*, *621*(1), Article#L85.

Balthasar, H., Vázquez, M., & Wöhl, H. (1986). Differential rotation of sunspot groups in the period from 1874 through 1976 and changes of the rotation velocity within the solar cycle. *Astronomy and Astrophysics*, *155*, 87–98.

Baraffe, I., Pratt, J., Goffrey, T., Constantino, T., Folini, D., Popov, M., ... Viallet, M. (2017). Lithium depletion in solar-like stars: effect of overshooting based on realistic multi-dimensional simulations. *The Astrophysical Journal Letters*, *845*(1), Article#L6.

Basu, S., & Antia, H. (1997). Seismic measurement of the depth of the solar convection zone. *Monthly Notices of the Royal Astronomical Society*, *287*(1), 189–198.

Basu, S., & Antia, H. (2013). Revisiting the issue of solar abundances. , *440*(1), Article#012017.

Baumann, P., Ramírez, I., Meléndez, J., Asplund, M., & Lind, K. (2010). Lithium depletion in solar-like stars: no planet connection. *Astronomy & Astrophysics*, *519*, Article#87.

Blatt, J. M., Weisskopf, V. F., & Dyson, F. (1953). Theoretical nuclear physics. *Physics Today*, *6*(3), Article#17.

Boesgaard, A., & Tripicco, M. (1986). Lithium in the hyades cluster. *The Astrophysical Journal*, *302*, L49–L53.

Boesgaard, A. M., Stephens, A., & Deliyannis, C. P. (2005). Lithium and lithium depletion in halo stars on extreme orbits. *The Astrophysical Journal*, *633*(1), Article#398.

Böhm-Vitense, E. (1958). Über die wasserstoffkonvektionszone in sternen verschiedener effektivtemperaturen und leuchtkräfte. mit 5 textabbildungen. *Zeitschrift fur Astrophysik*, *46*, Article#108.

Bohm-Vitense, E., & Nelson, G. D. (1976). About the proper choice of the characteristic length in the convection theory. *The Astrophysical Journal*, *210*, 741–749.

Bonaca, A., Tanner, J. D., Basu, S., Chaplin, W. J., Metcalfe, T. S., Monteiro, M. J., . . . others (2012). Calibrating convective properties of solar-like stars in the kepler field of view. *The Astrophysical Journal Letters*, *755*(1), Article#L12.

Bonanno, A., Küker, M., & Paternò, L. (2007). Seismic inference of differential rotation in procyon a. *Astronomy & Astrophysics*, *462*(3), 1031–1037.

Bouvier, J. (2008). Lithium depletion and the rotational history of exoplanet host stars. *Astronomy & Astrophysics*, *489*(3), L53–L56.

Brajša, R., Ruždjak, D., & Wöhl, H. (2006). Temporal variations of the solar rotation determined by sunspot groups. *Solar Physics*, *237*(2), 365–382.

Brown, T. M., & Morrow, C. A. (1987). Depth and latitude dependence of solar rotation. *The Astrophysical Journal*, *314*, L21–L26.

Caballero Navarro, R., García Hernández, A., Ayala, A., & Suárez, J. (2020). Study of the effects of magnetic braking on the lithium abundances of the sun and solar-type stars. *Monthly Notices of the Royal Astronomical Society*, *496*(2), 1343–1354.

Carlos, Marília, Nissen, Poul E., & Meléndez, Jorge. (2016). Correlation between lithium abundances and ages of solar twin stars. *A&A*, *587*, Article#100. Retrieved from `https://doi.org/10.1051/0004-6361/201527478`

Charbonneau, P., & MacGregor, K. (1993). Angular momentum transport in magnetized stellar radiative zones. ii. the solar spin-down. *The Astrophysical Journal*, *417*, Article#762.

Charbonnel, C., & Balachandran, S. C. (2000). The nature of the lithium rich giants. mixing episodes on the rgb and early-agb. *arXiv preprint astro-ph/0005280*.

Chen, Y., Nissen, P., Benoni, T., & Zhao, G. (2001). Lithium abundances for 185 main-sequence stars-galactic evolution and stellar depletion of lithium. *Astronomy & Astrophysics*, *371*(3), 943–951.

Chen, Y., & Zhao, G. (2006). A comparative study on lithium abundances in solar-type stars with and without planets. *The Astronomical Journal*, *131*(3), Article#1816.

Choi, J., Dotter, A., Conroy, C., Cantiello, M., Paxton, B., & Johnson, B. D. (2016). Mesa isochrones and stellar tracks (mist). i. solar-scaled models. *The Astrophysical Journal*, *823*(2), Article#102.

Christensen-Dalsgaard, J., Proffitt, C., & Thompson, M. (1993). Effects of diffusion on solar models and their oscillation frequencies. *The Astrophysical Journal*, *403*, L75–L78.

Ćiprijanović, A. (2016). Galactic cosmic-ray induced production of lithium in the small magellanic cloud. *Astroparticle Physics*, *85*, 24–28.

Covey, K. R., Agüeros, M. A., Law, N. M., Liu, J., Ahmadi, A., Laher, R., ... Surace, J. (2016). Why are rapidly rotating m dwarfs in the pleiades so (infra) red? new period measurements confirm rotation-dependent color offsets from the cluster sequence. *The Astrophysical Journal*, *822*(2), Article#81.

Cox, J. P., & Giuli, R. T. (1968). *Principles of stellar structure. vol. 1: Physical principles*. New York.

Cyburt, R. H., Amthor, A. M., Ferguson, R., Meisel, Z., Smith, K., Warren, S., ... others (2010). The jina reaclib database: its recent updates and impact on type-i x-ray bursts. *The Astrophysical Journal Supplement Series*, *189*(1), Article#240.

Dantona, F., & Mazzitelli, I. (1984). Lithium depletion in stars-pre-main sequence burning and extra-mixing. *Astronomy and Astrophysics*, *138*, 431–442.

Delgado Mena, E., Israelian, G., González Hernández, J., Sousa, S., Mortier, A., Santos, N., . . . others (2014). Li depletion in solar analogues with exoplanets. extending the sample. *A&A*, *562*, Article#92.

Demarque, P., & Robinson, F. J. (2003). Stellar convection. *Astrophysics and Space Science*, *284*(1), 193–204.

Fossat, E., Boumier, P., Corbard, T., Provost, J., Salabert, D., Schmider, F., . . . others (2017). Asymptotic g modes: Evidence for a rapid rotation of the solar core. *Astronomy & Astrophysics*, *604*, Article#40.

Gallet, F., & Bouvier, J. (2015). Improved angular momentum evolution model for solar-like stars-ii. exploring the mass dependence. *Astronomy & Astrophysics*, *577*, Article#98.

Ghezzi, L., Cunha, K., Smith, V., & de La Reza, R. (2010). Lithium abundances in a sample of planet-hosting dwarfs. *The Astrophysical Journal*, *724*(1), Article#154.

Grevesse, N., Asplund, M., Sauval, J., & Scott, P. (2013). Why gn93 should not be used anymore. , *43*, Article#01004.

Grevesse, N., & Sauval, A. (1998). Standard solar composition. *Space Science Reviews*, *85*(1-2), 161–174.

Grossman, S. A. (1992). The theory and numerical simulation of non-local mixing-length convection.

Grossman, S. A., Narayan, R., & Arnett, D. (1993). A theory of nonlocal mixing-length convection. i-the moment formalism. *The Astrophysical Journal*, *407*, 284–315.

Gruyters, P., Lind, K., Richard, O., Grundahl, F., Asplund, M., Casagrande, L., . . . Korn, A. J. (2016). Atomic diffusion and mixing in old stars-vi. the lithium content of m30. *Astronomy & Astrophysics*, *589*, Article#61.

Henyey, L., Vardya, M., & Bodenheimer, P. (1965). Studies in stellar evolution. iii. the calculation of model envelopes. *The Astrophysical Journal*, *142*, Article#841.

Herwig, F. (2000). The evolution of agb stars with convective overshoot. *arXiv preprint astro-ph/0007139*.

Herwig, F., Blöcker, T., Schönberner, D., & Eid, M. E. (1997). Stellar evolution of low and intermediate-mass stars. iv. hydrodynamically-based overshoot and nucleosynthesis in agb stars. *arXiv preprint astro-ph/9706122*.

Holweger, H. (2001). Photospheric abundances: Problems, updates, implications. , *598*(1), 23–30.

Howe, R. (2009). Solar interior rotation and its variation. *Living Reviews in Solar Physics*, *6*(1), 1–75.

Howe, R., Christensen-Dalsgaard, J., Hill, F., Komm, R., Larsen, R., Schou, J., . . . Toomre, J. (2000). Deeply penetrating banded zonal flows in the solar convection zone. *The Astrophysical Journal Letters*, *533*(2), Article#L163.

Iben Jr, I., & MacDonald, J. (1985). The effects of diffusion due to gravity and due to composition gradients on the rate of hydrogen burning in a cooling degenerate dwarf. i-the case of a thick helium buffer layer. *The Astrophysical Journal*, *296*, 540–553.

Israelian, G., Santos, N., Mayor, M., & Rebolo, R. (2004). Lithium in stars with exoplanets. *Astronomy & Astrophysics*, *414*(2), 601–611.

Javaraiah, J., Bertello, L., & Ulrich, R. (2005). Long-term variations in solar differential rotation and sunspot activity. *Solar Physics*, *232*(1), 25–40.

Joyce, M., & Chaboyer, B. (2018). Not all stars are the sun: empirical calibration of the mixing length for metal-poor stars using one-dimensional stellar evolution models. *The Astrophysical Journal*, *856*(1), Article#10.

Karlsson, T., Bromm, V., & Bland-Hawthorn, J. (2013). Pregalactic metal enrichment: The chemical signatures of the first stars. *Reviews of Modern Physics*, *85*(2), Article#809.

Kippenhahn, R., Weigert, A., & Weiss, A. (1990). *Stellar structure and evolution* (Vol. 192). Springer.

Küker, M., Rüdiger, G., & Kitchatinov, L. (2011). The differential rotation of g dwarfs. *Astronomy & Astrophysics*, *530*, Article#48.

Langer, N., Heger, A., Wellstein, S., & Herwig, F. (1999). Mixing and nucleosynthesis in rotating tp-agb stars. *arXiv preprint astro-ph/9904257*.

Lodders, K. (2019). Solar elemental abundances. *arXiv preprint arXiv:1912.00844*.

López-Valdivia, R., Hernández-Águila, J., Bertone, E., Chávez, M., Cruz-Saenz de Miera, F., & Amazo-Gómez, E. (2015). Lithium abundance in a sample of solar-like stars. *Monthly Notices of the Royal Astronomical Society*, *451*(4), 4368–4374.

Maeder, A. (1975). Stellar evolution. iv-evolution of a star of 1.5 solar masses from the main-sequence to the red-giant branch with and without overshooting from convective core. *Astronomy and Astrophysics*, *43*, 61–69.

Meech, K. J., Weryk, R., Micheli, M., Kleyna, J. T., Hainaut, O. R., Jedicke, R., ... others (2017). A brief visit from a red and extremely elongated interstellar asteroid. *Nature*, *552*(7685), 378–381.

Mestel, L., & Weiss, N. (1987). Magnetic fields and non-uniform rotation in stellar radiative zones. *Monthly Notices of the Royal Astronomical Society*, *226*(1), 123–135.

Morel, P., & Thévenin, F. (2002). Atomic diffusion in star models of type earlier than g. *Astronomy & Astrophysics*, *390*(2), 611–620.

Pace, G., Castro, M., Meléndez, J., Théado, S., & do Nascimento Jr, J.-D. (2012). Lithium in m 67: From the main sequence to the red giant branch. *Astronomy & Astrophysics*, *541*, Article#150.

Paczynski, B. (1977). Helium shell flashes. *The Astrophysical Journal*, *214*, 812–818.

Palguta, J., Schubert, G., & Travis, B. J. (2010). Fluid flow and chemical alteration in carbonaceous chondrite parent bodies. *Earth and Planetary Science Letters*, *296*(3-4), 235–243.

Pasquini, L., Liu, Q., & Pallavicini, R. (1994). Lithium abundances of nearby solar-like stars. *Astronomy and Astrophysics*, *287*, 191–205.

Paxton, B., Bildsten, L., Dotter, A., Herwig, F., Lesaffre, P., & Timmes, F. (2010a). Mesa: Modules for experiments in stellar astrophysics. *Astrophysics Source Code Library*.

Paxton, B., Bildsten, L., Dotter, A., Herwig, F., Lesaffre, P., & Timmes, F. (2010b). Modules for experiments in stellar astrophysics (mesa). *The Astrophysical Journal Supplement Series*, *192*(1), Article#3.

Paxton, B., Marchant, P., Schwab, J., Bauer, E. B., Bildsten, L., Cantiello, M., . . . others (2015). Modules for experiments in stellar astrophysics (mesa): Binaries, pulsations, and explosions. *The Astrophysical Journal Supplement Series*, *220*(1), Article#15.

Pinsonneault, M. (2009). Rotational mixing and lithium depletion. *Proceedings of the International Astronomical Union*, *5*(S268), 375–380.

Proffitt, C. R., & Michaud, G. (1991). Gravitational settling in solar models. *The Astrophysical Journal*, *380*, 238–250.

Roxburgh, I. (1978). Convection and stellar structure. *Astronomy and Astrophysics*, *65*, 281–285.

Ryan, S. G. (2000, 08). The host stars of extrasolar planets have normal lithium abundances. *Monthly Notices of the Royal Astronomical Society*, *316*(3), L35-L39. Retrieved from `https://doi.org/10.1046/j.1365-8711.2000.03777.x`

Sandage, A. R., & Schwarzschild, M. (1952). Inhomogeneous stellar models. ii. models with exhausted cores in gravitational contraction. *The Astrophysical Journal*, *116*, Article#463.

Schlattl, H., & Weiss, A. (1999). On an overshooting approach to the solar li problem. *Astronomy and Astrophysics*, *347*, 272–276.

Serenelli, A. M., Basu, S., Ferguson, J. W., & Asplund, M. (2009). New solar composition: the problem with solar models revisited. *The Astrophysical Journal Letters*, *705*(2), Article#L123.

Sestito, P., Randich, S., Mermilliod, J.-C., & Pallavicini, R. (2003). The evolution of lithium depletion in young open clusters: Ngc 6475. *Astronomy & Astrophysics*, *407*(1), 289–301.

Shaviv, G., & Salpeter, E. E. (1973). Convective overshooting in stellar interior models. *The Astrophysical Journal*, *184*, 191–200.

Song, N., Alexeeva, S., Sitnova, T., Wang, L., Grupp, F., & Zhao, G. (2020). Impact of the convective mixing-length parameter α on stellar metallicity. *Astronomy & Astrophysics*, *635*, Article#176.

Sousa, S., Santos, N., Israelian, G., Delgado Mena, E., Fernandes, J., Mayor, M., ... Randich, S. (2011). Lithium depletion in solar type stars: Lithium and planet presence. , *448*, Article#81.

Spiegel, E. A. (1963). A generalization of the mixing-length theory of turbulent convection. *The Astrophysical Journal*, *138*, Article#216.

Spite, M., & Spite, F. (1981). Lithium abundance in two halo stars. *Comptes Rendus des Seances de l'Academie des Sciences. Serie 2*, *293*(4), 299–302.

Spruit, H. (2002). Dynamo action by differential rotation in a stably stratified stellar interior. *Astronomy & Astrophysics*, *381*(3), 923–932.

Stanley, J., G. R., Cochran, W. D., & Sneden, C. (1998, December). Exploration of the Lithium-Star-Planet Connection in Solar-Type Systems. , *193*, 45.14.

Swenson, F. J., & Faulkner, J. (1992). Lithium dilution through main-sequence mass loss. *The Astrophysical Journal*, *395*, 654–674.

Tassoul, M., & Tassoul, J.-L. (1984). Meridional circulation in rotating stars. vii-the effects of chemical inhomogeneities. *The Astrophysical Journal*, *279*, 384–393.

Taylor, S. R. (2001). *Solar system evolution: A new perspective*. Cambridge University Press.

Thompson, M., Toomre, J., Anderson, E., Antia, H., Berthomieu, G., Burtonclay, D., ... others (1996). Differential rotation and dynamics of the solar interior. *Science*, *272*(5266), 1300–1305.

Thompson, M. J., Christensen-Dalsgaard, J., Miesch, M. S., & Toomre, J. (2003). The internal rotation of the sun. *Annual Review of Astronomy and Astrophysics*, *41*(1), 599–643.

Thoul, A. A., Bahcall, J. N., & Loeb, A. (1993). Element diffusion in the solar interior. *arXiv preprint astro-ph/9304005*.

VandenBerg, D. A., Richard, O., Michaud, G., & Richer, J. (2002). Models of metal-poor stars with gravitational settling and radiative accelerations. ii. the age of the oldest stars. *The Astrophysical Journal*, *571*(1), Article#487.

Xiong, D., & Chen, Q. (1992). A nonlocal convection model of the solar convection zone. *Astronomy and Astrophysics*, *254*, Article#362.

Xiong, D., & Deng, L. (2001). The structure of the solar convective overshooting zone. *Monthly Notices of the Royal Astronomical Society*, *327*(4), 1137–1144.

Yi, S., Demarque, P., & Oemler Jr, A. (1997). On the origin of the uv upturn in elliptical galaxies. i. sensitivity of uv population synthesis to various input parameters. *The Astrophysical Journal*, *486*(1), Article#01.

Zhang, Q.-S., Li, Y., & Christensen-Dalsgaard, J. (2019). Solar models with convective overshoot, solar-wind mass loss, and pms disk accretion: Helioseismic quantities, li depletion, and neutrino fluxes. *The Astrophysical Journal*, *881*(2), Article#103.